2015

The Effect of Chronic Hypertension on Neuropathology in the TGSWDI Mouse Model of Alzheimer's Disease

Anna Kruyer

THE EFFECT OF CHRONIC HYPERTENSION ON NEUROPATHOLOGY IN THE TGSWDI MOUSE MODEL OF ALZHEIMER'S DISEASE

A Thesis Presented to the Faculty of

The Rockefeller University

in Partial Fulfillment of the Requirements for

the degree of Doctor of Philosophy

by

Anna Kruyer

June 2015

THE EFFECT OF CHRONIC HYPERTENSION ON NEUROPATHOLOGY IN THE TGSWDI MOUSE MODEL OF ALZHEIMER'S DISEASE

Anna Kruyer, Ph.D.

The Rockefeller University 2015

Numerous epidemiological studies link vascular disorders, such as hypertension, diabetes and stroke, with Alzheimer's disease. Hypertension, specifically, is an important modifiable risk factor for late onset Alzheimer's disease. Despite the abundance of clinical data connecting these conditions, animal studies investigating the connection between the two are lacking.

To examine the link between midlife hypertension and the onset of Alzheimer's disease later in life, chronic hypertension was induced in the TgSwDI mouse model of Alzheimer's disease in early adulthood using long-term administration of the eNOS inhibitor, Nω-Nitro-L-arginine methyl ester hydrochloride (L-NAME). L-NAME treatment accelerated cognitive deficits, microvascular deposition of the amyloid-beta peptide, vascular inflammation, blood brain barrier leakage, and pericyte loss in these mice.

Though lysosomal markers were increased in hypertensive TgSwDI mice relative to all other groups, autophagic structures appeared to be increased in both hypertensive TgSwDI mice, as well as hypertensive WT mice. The increased

presence of these structures altered cellular morphology at the neurovascular unit and compromised the blood brain barrier in hypertensive mice.

Additionally, midlife hypertension induced hippocampal neurodegeneration at an early age in TgSwDI mice. Neuronal loss is a defining characteristic of pathology in Alzheimer's disease, but is not replicated in many mouse models of the disease. Therefore, this may be a useful research model of Alzheimer's disease with mixed vascular and amyloid pathologies and may display classical features of the disease missing in more canonical mouse models.

To Jason Morris and, of course, to Mom.

ACKNOWLEDGEMENTS

I am grateful for the support, encouragement and guidance of Sid Strickland and Erin Norris. Together, they have created a warm work environment where new ideas are embraced and mistakes are seen as opportunities to learn; they have made the lab a truly joyful place to work. I am also grateful to my committee members, Cori Bargmann and Shai Shaham, for pushing me to think for myself and to never settle for less than a well-thought out and carefully designed experiment.

I am grateful to the kind and hard-working members of the Strickland lab, past and present, especially Zulin, who taught me how to perfuse and helped me get acquainted with the lab when I first joined. Dasha and Emily served as scientific sounding boards, teachers and trusted friends. They have made each day lovely, whether or not the data were. I am also very appreciative to Hiro and Dee of the EMRC, for always being generous with their time, advice and enthusiasm.

I am deeply grateful for the support of my family and close friends. Emily, Gabby, Jane and Monica have carried me through difficult times. My mom, dad and brother have always supported and never doubted me. I hear them cheering every time I walk into the lab.

Finally, I wouldn't be pursuing a career in biology if it weren't for the mentorship of Dr. Jason Morris. He taught me the value of persistence, resilience and hard work. He also taught me how to pipette. Thank you for showing me the way.

TABLE OF CONTENTS

LIST OF FIGURES

LIST OF TABLES

LIST OF SELECTED ABBREVIATIONS

3D-EM	three-dimension electron microscopy
Aβ	amyloid-beta peptide
AC	autophagic compartment
ACE	angiotensin-converting enzyme
AD	Alzheimer's disease
Ang-II	angiotensin-II
APP	amyloid precursor protein
AQP-4	aquaporin-4
ARB	angiotensin receptor blocker
AV	autophagic vacuole
BBB	blood brain barrier
BCA	bicinchoninic acid
BCLN2	beclin 2
BECN1	beclin 1
BP	blood pressure
BSA	bovine serum albumin
CA1	cornu ammonis area 1
CA2	cornu ammonis area 2
CA3	cornu ammonis area 3
CA4	cornu ammonis area 4
CAA	cerebral amyloid angiopathy
CATD	cathepsin D
CD31	cluster of differentiation 31
CNS	central nervous system
D	Dutch
DG	dentate gyrus
DS	dorsal subiculum
EM	electron microscopy
EMRC	Electron Microscopy Resource Center
eNOS	endothelial nitric oxide synthase

EOAD	early onset Alzheimer's disease
ER	endoplasmic reticulum
FUS	focused ultrasound
GFAP	glial fibrillary acidic protein
HMAR	heat-mediated antigen retrieval
HTN	hypertension
I	Iowa
ICH	intracerebral hemorrhage
IEM	immunoelectron microscopy
iNOS	inducible nitric oxide synthase
IP	intraperitoneal
IVF	*in vitro* fertilization
LAMP-1	lysosomal-associated membrane protein-1
L-NAME	Nω-Nitro-L-arginine methyl ester hydrochloride
LOAD	late onset Alzheimer's disease
MLB	multilamellar body
MVB	multivesicular body
nNOS	neuronal nitric oxide synthase
NO	nitric oxide
NOS	nitric oxide synthase
NVU	neurovascular unit
PCR	polymerase chain reaction
PDGF	platelet-derived growth factor
PFA	paraformaldehyde
PK	proteinase K
PS-1	presenilin-1
PS-2	presenilin-2
RAGE	receptor for advanced-glycation end products
Sw	Swedish
TAC	transverse aortic constriction
ThioS	Thioflavin S

Thy1	thymus cell antigen 1
WML	white matter lesion
WT	wild type

CHAPTER 1: INTRODUCTION

Alzheimer's disease (AD) is the most common form of dementia and there is no universal cause, prevention or treatment to delay or stop its progression. Familial forms of the disease often involve mutations in genes that result in overproduction of the amyloid-beta peptide (Aβ)[1], although this is not the cause of the disease in all cases. Such mutations affect the expression of the amyloid precursor protein (APP), which produces Aβ when cleaved. Mutations affecting production or function of presenilin-1 or 2 (PS-1 or -2), which function as part of the gamma-secretase intramembrane protease complex, can also result in production of the cleaved peptide[2]. These mutations result in early onset Alzheimer's disease (EOAD), with symptoms arising before the age of 65. Late onset AD (LOAD) often occurs without the contribution of known genetic risk factors, but results in symptoms similar to those of EOAD, including short term memory loss, confusion, irritability, mood swings and eventually long term memory loss[3, 4]. Individuals with AD exhibit deposition of Aβ as plaques in the brain as well as intraneuronal tangles of a highly soluble microtubule-associated protein known as tau[5]. Gradually the neuronal loss that characterizes this disease affects other bodily functions and results in death.

Cerebral Amyloid Angiopathy

Cerebral amyloid angiopathy (CAA), the deposition of Aβ along vessel walls in the central nervous system (CNS), is a common feature of AD present in up to 94% of AD patients[6]. The presence of Aβ in vessel walls in the brain has been proposed to

result from increased Aβ production of the brains in mouse models of the disease, as in humans with EOAD. However, in humans with LOAD, abnormal clearance of the peptide is often thought to be the cause[7]. Aβ can be endocytosed by astrocytes and microglia, support cells which function in clearing cell debris and pathogens in the CNS[8, 9]. These cells, as well as neurons, express enzymes, such as neprilysin and insulin-degrading enzyme, that allow Aβ to be degraded[10]. Specific clearance across the blood brain barrier (BBB) through molecules like LRP-1 as well as shuttling of Aβ-containing interstitial fluid along perivascular spaces have been shown to function in Aβ removal from the brain[11]. Abnormalities in these removal pathways may lead to increased CAA abundance in AD patients.

CAA has also been linked to the presence of brain microhemorrhage and even increased risk of hemorrhagic stroke[12, 13]. Though it is difficult to study the effects of CAA independent from symptoms of severe AD, as the two are often comorbid, some studies suggest a link between CAA and cognitive decline[6, 14]. While some have proposed that CAA specifically contributes to cognitive decline in AD, others support the view that CAA simply aggravates the cognitive decline already present due to AD[15].

Cerebrovascular Dysfunction in Alzheimer's Disease

More than 30% of AD cases exhibit cerebrovascular pathology in addition to the CAA, microvascular degeneration, and periventricular white matter lesions (WMLs) evident in almost all AD cases[16]. In fact, alterations in every cellular component of

the neurovascular unit (NVU), the tightly regulated network of cells involved in the coupling of neuronal energy demands to modulation of blood flow (Figure 1.1), have been observed in AD patients. Under normal conditions, endothelial cell tight junctions form the basis of the BBB (Figure 1.2), while pericytes regulate BBB formation and maintenance, vascular architecture, and capillary flow[17, 18]. In larger blood vessels, smooth muscle cell pulsation drives blood flow[19]. In AD, endothelial cells and pericytes degenerate in brain capillaries and smooth muscle cells are lost in larger arteries, leading to detrimental effects on neuronal perfusion and function[18, 20-24]. Astrocyte endfeet, which ensheath brain capillaries (Figures 1.1, 1.2), help regulate capillary blood flow, and maintain the extracellular milieu, are swollen in the presence of CAA[21, 22]. The direct cause of these cellular abnormalities has not been determined, though Aβ is toxic to neurons and other cell types *in vitro*[25]. Additionally, the presence of Aβ amongst the cells of the NVU could interfere with signaling between cell types, alter cellular health and function, and contribute to endothelial cell degeneration resulting in reduced flow-mediated dilation, an indicator of vessel reactivity, also observed in AD brains[26]. Thus, CAA may contribute to the reduced neurovascular coupling reported in multiple AD mouse lines[26-29]. Furthermore, the frequent co-incidence of stroke and AD suggests that the cerebrovascular changes that occur during AD progression compromise vascular integrity and function[30].

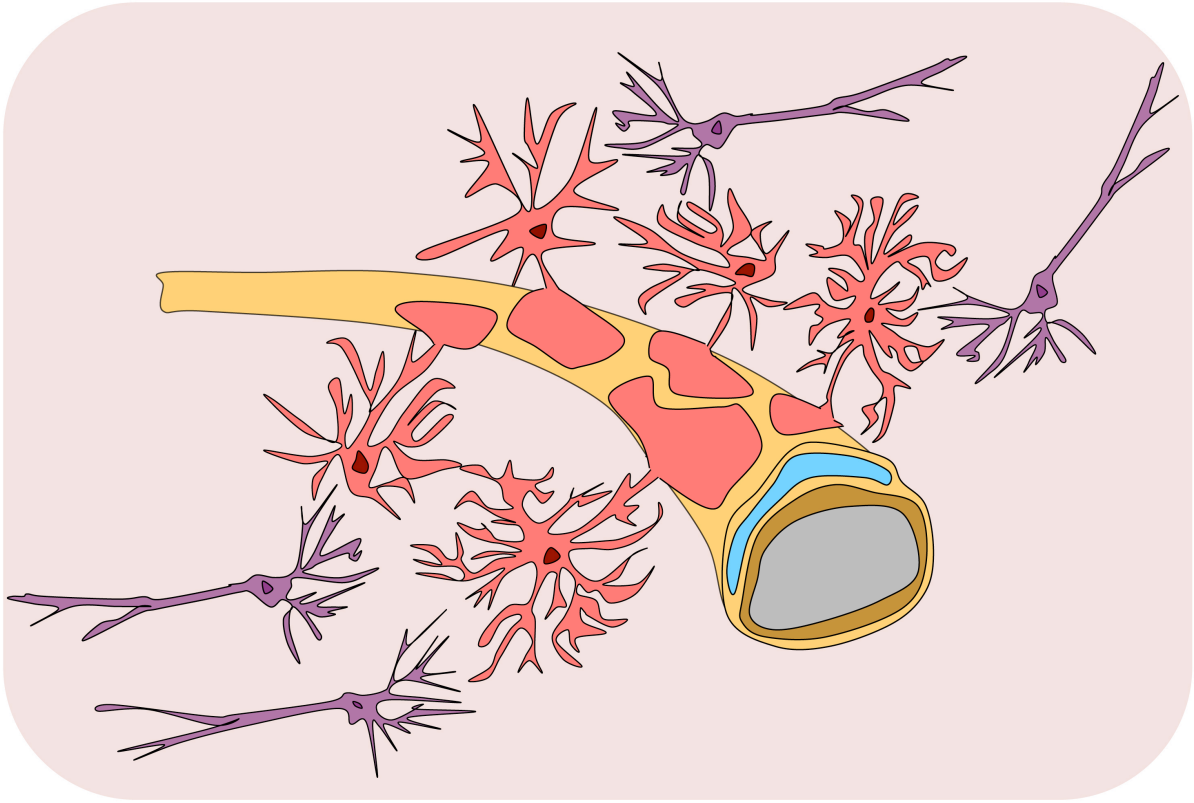

Figure 1.1. Structure and function of the NVU. The NVU is the tightly regulated network of cells involved in the coupling of neuronal energy demands to modulation of blood flow. Endothelial cell (brown) tight junctions form the basis of the BBB and keep blood components in the lumen (gray) from entering into the brain (light pink). The basement membrane (yellow), a protein matrix composed of collagen, fibrillin, laminin, integrins, entactins and dystroglycans, surrounds the endothelial cell layer. Sandwiched within the basement membrane are pericytes (blue), which participate in BBB formation and maintenance and in the recruitment of capillary flow. Surrounding astrocytes (red) extend endfoot processes that serve as the outermost layer of the capillary and help regulate capillary flow, maintain the extracellular milieu and act as support cells for nearby neurons (purple).

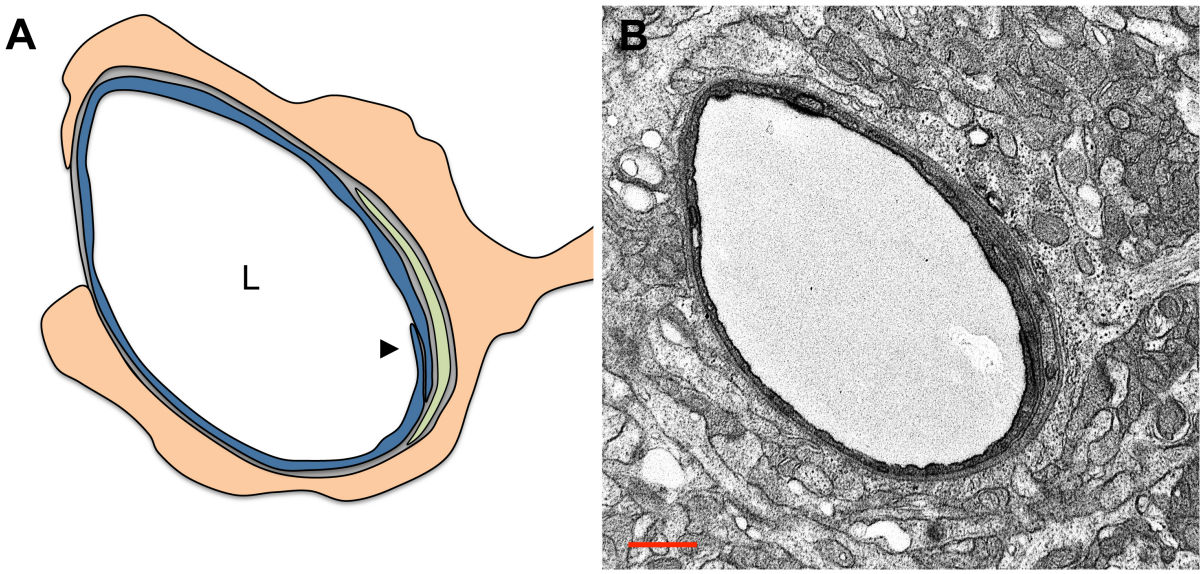

Figure 1.2. Ultrastructure of a normal brain microvessel. (A) A schematic of a normal WT capillary in cross-section (B) highlights important morphological features of the NVU. The endothelial cell (blue) serves as the first cell layer that separates brain tissue from blood components. The endothelial cell tight junction is composed of two closely associated areas of membrane that join directly due to the interaction of transmembrane proteins. Tight junctions make the endothelial cell layer virtually impermeable to fluid under normal circumstances and prevent blood components within the vessel lumen (L) from entering the brain. A layer of basement membrane (gray), a protein matrix that allows capillary cells to adhere to one another, surrounds the endothelial cell. The pericyte (green) is sandwiched within the basement membrane layer. The astrocyte endfoot (peach) is a cellular process that ensheathes the capillary, providing support for NVU cells as well as aiding in regulation of capillary flow (scale bar = 1 μm).

Cardiovascular Disease and Alzheimer's disease

Clinical evidence suggests that cardiovascular risk factors including atherosclerosis, atrial fibrillation, heart disease, diabetes, and hypertension are linked to AD onset[16]. In non-AD individuals, hypertension induces pathological changes in the brain such as impaired cerebral autoregulation, vascular remodeling, cerebral microbleeds, WMLs, lacunar infarcts, and cerebral atrophy[31-34]. Though midlife hypertension is a significant risk factor for AD and treatment alleviates this risk[32, 33], dramatic reduction in blood pressure (BP) often occurs at later stages of AD, after which point antihypertensive use is deleterious to cognitive function[34, 35]. It is possible that elevated BP during midlife compromises vascular integrity and leads to cellular, basement membrane, and/or BBB damage. However, after onset of AD symptoms, low BP may aggravate brain hypoperfusion already present in AD due to other types of vascular damage.

Given the vasoactive properties of Aβ[36], it is unclear whether midlife hypertension is an early symptom of the vascular pathology present in AD or if it contributes to the onset of the disease, though there is evidence to support both views. Surgically induced hypertension in wild type (WT) mice is sufficient to induce subtle increases in cerebral Aβ deposition after 10 weeks[37]. This Aβ deposition has been shown to result from upregulation of the receptor for advanced-glycation end products (RAGE) at the NVU, which allows transport of Aβ from the circulation into the brain[38]. Alternatively, Aβ has been shown to be vasoactive and may itself contribute to the onset of hypertension[39].

Autophagy in Alzheimer's Disease

Macroautophagy, referred to herein as "autophagy", is the process by which unnecessary or dysfunctional cytoplasmic components are degraded by lysosomes[40]. Under normal conditions, autophagy is a very efficient process and autophagosomes, containing cellular debris, or amphisomes, containing endocytosed extracellular material, are rapidly cleared by fusion with lysosomes[41] (Figure 1.3). For this reason, active autophagy is scarcely observed in tissues like the brain[42]. Given that AD is a disease of excessive protein accumulation, it is not surprising that autophagy has been found to be increased in brains of AD patients[43]. Autophagy plays a central role in the pathophysiology of AD and dysfunction of this process is deleterious to neuronal function. Interestingly, mice overexpressing human APP and also null for the autophagy-related gene 7 (Atg7) exhibit reduced parenchymal Aβ deposition due to inhibited Aβ secretion from cells[44]. However, this reduction in Aβ deposition corresponds with increased intracellular Aβ-load and consequent cellular damage.

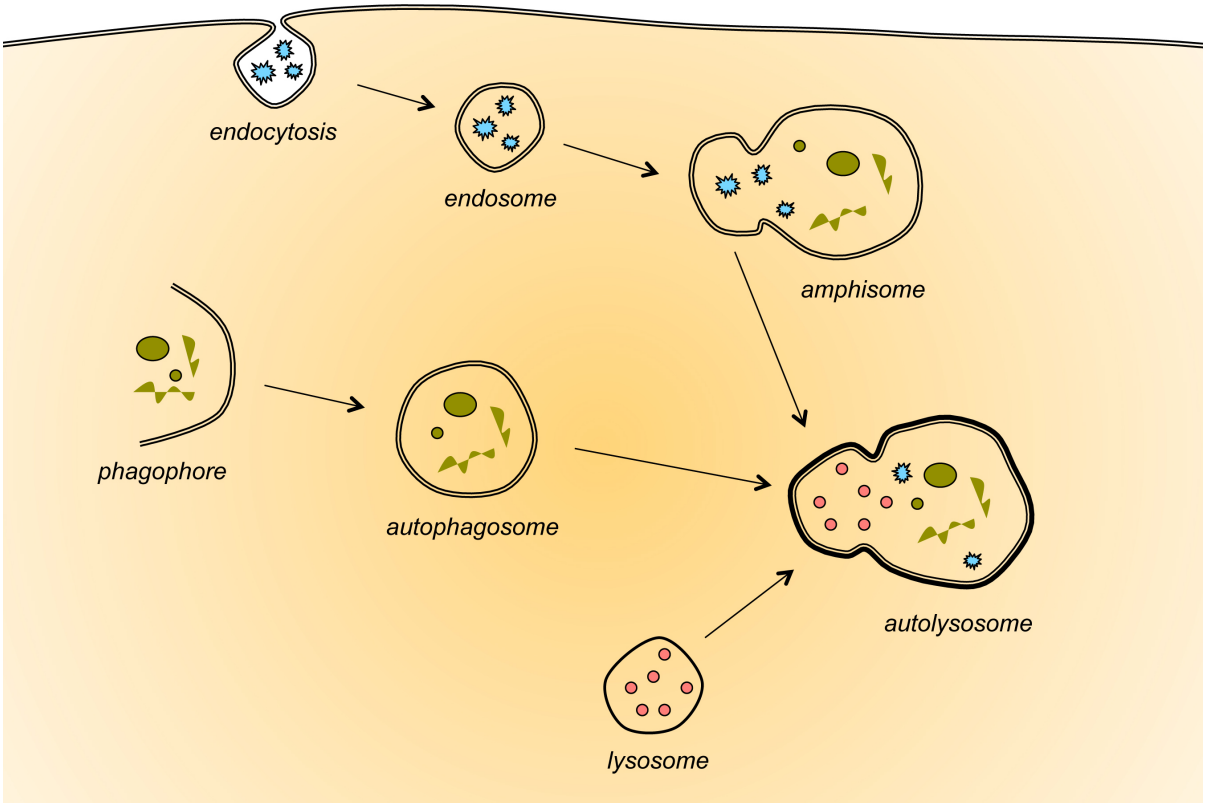

Figure 1.3. Degradation of intracellular and extracellular components by lysosomes. Autophagy is the basic catabolic mechanism for degradation of unnecessary or dysfunctional cellular components. Target cytoplasmic constituents are isolated from the cytoplasm by a double-membraned vesicle known as the autophagosome. An autolysosome, or autophagic vacuole, is formed when the autophagosome fuses its external membrane with the membrane of the lysosome. Endosomes, containing extracellular components imported for degradation, mature to form multivesicular bodies (MVBs) that fuse either directly with the lysosome or with a late autophagosome to form an amphisome. After lysosome fusion, degradation of autophagosome, endosome or amphisome components are mediated by acidic lysosomal hydrolases. Permeases on autolysosomal membranes allow diffusion of degraded components back into the cytoplasm.

Though changes in lysosomal function occur with age[41], it has been proposed that Aβ is itself the substrate of dysfunctional autophagy in AD and is also the cause[45]. Autophagic vacuoles (AV), intracellular membrane-bound components bound for fusion with lysosomes, are abundant in AD neurons[46], leading some to propose that early autophagic processes are functional in AD, but fusion with lysosomes and/or post-autophagic clearance mechanisms are impaired[42]. One proposed barrier to autophagic efficiency in AD is that autophagosomes form in synapses where misfolded tau aggregates. Autophagosomes must undergo retrograde transport to the cell soma, where lysosomes are most abundant, for degradation. When neurites become damaged due to disruption of tau microfilaments, this retrograde transport is impaired and AVs accumulate in swollen dystrophic and degenerating neurites[47]. Thus the necessity for increased lysosome activity in AD paired with defective lysosomal clearance mechanisms create conditions favorable for protein aggregation and cellular damage.

Alzheimer's Disease Mouse Models

Mouse models have been instrumental to the progress made in understanding and attempting to treat AD. The identification of APP mutations in families with EOAD led to the understanding that misprocessing of this protein was linked to disease onset. Homologous recombination was ultimately used to insert the human APP gene, containing known AD-causing mutations identified in EOAD families, into the mouse genome, leading to the development of numerous mouse models and a more aggressive study of AD *in vivo*. The first mouse model available for widespread use

was the PDAPP model, which expressed transgenic human APP carrying the Indiana mutation (V717F) under the platelet-derived growth factor (PDGF) promoter, leading to expression of transgenic APP in neurons[48]. Researchers found that 40 copies of transgenic APP had integrated into the mouse genome, resulting in an 18-fold elevation of APP RNA and a 10-fold elevation of human APP protein expression compared to mouse APP[49]. Similar corresponding changes were observed when levels of Aβ peptide were quantified. Furthermore, these mice exhibited Aβ plaque deposition, neuroinflammation, learning deficits and synapse loss in an age-dependent manner, all consistent with pathological changes observed in human AD patients.

The Arctic, Australian, Austrian, Belgian, Dutch, English, Flemish, Florida, French, German, Indiana, Iowa, Iranian, Leuven, London, Osaka, Swedish, Taiwanese and Tottori mutations are all named after geographic locations of families carrying specific mutations in APP that result in EOAD. Different combinations of these and PS-1 and -2 mutations have been inserted into the genomes of mice in order to generate models with different pathological characteristics comparable to what is observed in humans with both EOAD and LOAD.

TgSwDI Mouse Model

Many AD mouse models have been generated since the introduction of the PDAPP mouse model to research, each presenting with different features of AD that are of interest to researchers. The TgSwDI mouse model is unique among other AD mouse

models, since it represents the first model of CAA. Other AD mouse models exhibit CAA, especially during later stages of pathological progression, but TgSwDI mice display dramatically increased microvascular Aβ deposits relative to parenchymal deposits in the brain [50]. This mouse line carries a human APP transgene containing three sets of EOAD mutations driven by the thymus cell antigen 1, theta (Thy1) promoter that leads to predominant expression of transgenic APP in neurons and some glia in the striatum and hippocampus. The Swedish mutation (Sw) results in two adjacent amino acid substitutions (K670M/N671L) and sits at the β-secretase cleavage site of APP, likely leading to increased cleavage of APP and thus increased Aβ production[50] (Figure 1.4). The Dutch (D) and Iowa (I) mutations (E693Q and D694N, respectively) refer to adjacent amino acid substitutions that likely increase deposition of Aβ along vessels rather than within in the brain parenchyma (Figure 1.4). This mouse model exhibits dramatically increased capillary CAA in parts of the hippocampus and the thalamus, but decreased plaque deposition relative to other models. Additionally, the CAA in this mouse model yields neuroinflammation and cognitive decline consistent with AD.

The TgSwDI mouse model was generated by the Van Nostrand group at Stony Brook University and its pathology has been well characterized by members of the group[50-52]. They have observed Aβ deposition in the subiculum, hippocampus and cortex of these mice at 3 months-of-age and widespread deposition in the forebrain by 12 months-of-age. Researchers from this group report that early microvascular Aβ deposits are largely Aβ40 in composition. In fact Aβ40 is ten times more

abundant in the brains of these mice than Aβ42. The length of the Aβ peptide, typically 37-43 residues, is determined by the gamma secretase protein complex, which cleaves Aβ at its C-terminal end[53]. Aβ40 is produced more readily than Aβ42 and is abundant in CAA; Aβ42 has been shown to be more fibrillogenic and more toxic than Aβ40[54, 55]. Microvascular Aβ accumulation in TgSwDI mice is mostly fibrillar and Aβ is 13-fold more abundant near microvessels than in the parenchyma. In fact, 50% of forebrain vessels exhibit CAA. This group cites both increased production as well as decreased clearance of mutant Aβ as the cause for increased CAA in TgSwDI mouse brains.

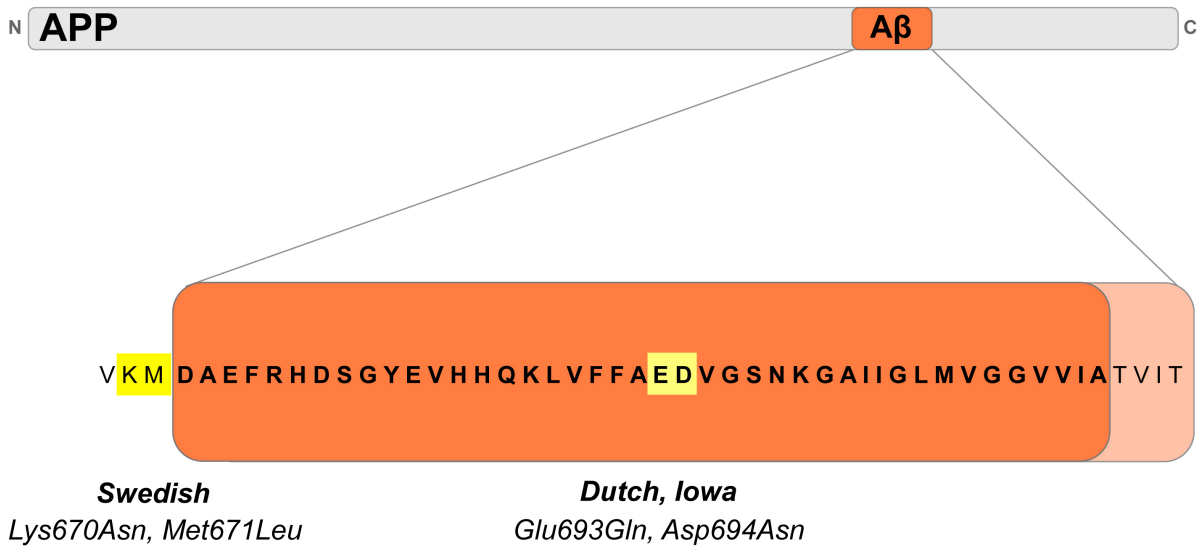

Figure 1.4. APP mutations expressed by the transgenic TgSwDI mouse line. The TgSwDI mouse model of AD carries a human APP transgene, driven by the neuronal Thy1 promoter, with mutations all near or within the region cleaved to form the Aβ peptide (orange rectangle). All of the mutations in the inserted transgene were found to be expressed by different families with EOAD. The Swedish mutation refers to two adjacent amino acid substitutions, K670M and N671L, which lie at the β-secretase cleavage site of APP. These mutations likely lead to increased production of the Aβ peptide. The Dutch and Iowa mutations are adjacent substitutions (E693Q and D694N, respectively) that increase the likelihood that the resulting Aβ peptide will be deposited along vessels in the brain rather than in the brain parenchyma.

Given the largely vascular Aβ pathology in the TgSwDI mouse model and my interest in studying the link between vascular dysfunction and AD onset, I examined TgSwDI mice for potential effects of CAA on AD progression. I also induced chronic hypertension in TgSwDI mice and examined behavioral, cellular, and ultrastructural changes in order to better understand the impact of chronic hypertension on AD pathogenesis.

CHAPTER 2: MATERIALS AND METHODS

Animal Use

TgSwDI +/+ and C57Bl6J mice were purchased from The Jackson Laboratory and bred in house to generate the mice used for experiments described in Chapter 3. TgSwDI +/- and -/- littermates were generated using *in vitro* fertilization (IVF) at the Transgenic Services Laboratory at The Rockefeller University and were used to conduct the experiments described in Chapter 6. Both TgSwDI +/+ and +/- animals as well as either C57Bl6J or TgSwDI -/- controls were used for experiments described in Chapters 4 and 5. For this reason, a Table listing the genotypes of AD and WT groups for each set of experiments described herein has been included for reference (Table 2.1). Genotypes were determined by PCR on tail samples taken before weaning. TgSwDI +/+ or +/- mice were considered AD animals, and C57Bl6J or TgSwDI -/- mice were used as WT controls. When described, TgCRND8 +/- and Tg6799 +/- were also considered AD and TgCRND8 -/- and Tg6799 -/-, respectively, were used as WT controls. All mice were maintained on a 12-hour light/dark cycle with food and water provided *ad libitum* and mice of both sexes were used in approximately equal ratios for all experiments, except when otherwise specified (Table 2.1). All animal procedures were approved by the Institutional Animal Care and Use Committee at The Rockefeller University.

Table 2.1. AD and WT cohort details by experiment.

Chapter	Subsection	AD Cohort	WT Cohort	Sex
3	Cognitive Decline	TgSwDI +/+	C57Bl6J	Both
3	Amyloid Deposition	TgSwDI +/+	C57Bl6J	Both
3	Gliosis	TgSwDI +/+	C57Bl6J	Both
3	BBB Breakdown	TgSwDI +/+	C57Bl6J	Both
3	Autophagy	TgSwDI +/+	C57Bl6J	Both
3	Differences in Depressiveness, Anxiety and Locomotion in TgSwDI Mice	TgSwDI +/+	C57Bl6J	Both
3	TgSwDI Background Characterization	TgSwDI +/+	C57Bl6J	Both
4	Ang-II and L-NAME-Induced Hypertension in AD Mouse Models	TgSwDI +/+	C57Bl6J	Both
4	Ang-II and L-NAME-Induced Hypertension in AD Mouse Models	Tg6799 +/-	Tg6799 -/-	Both
4	Ang-II and L-NAME-Induced Hypertension in AD Mouse Models	TgCRND8 +/-	TgCRND8 -/-	Both
4	L-NAME-Induced Hypertension	TgSwDI +/-	C57Bl6J	Male
5	Cognitive Decline	TgSwDI +/-	TgSwDI -/-	Both
5	Vascular Amyloid Deposition	TgSwDI +/-	TgSwDI -/-	Both
5	Microgliosis	TgSwDI +/-	TgSwDI -/-	Both
5	BBB Integrity	TgSwDI +/-	TgSwDI -/-	Both
5	Astrocyte Alterations	TgSwDI +/-	C57Bl6J	Both
5	Pericyte Loss	TgSwDI +/-	TgSwDI -/-	Both
5	Neuronal Loss	TgSwDI +/-	TgSwDI -/-	Both
6	Autophagy at the NVU	TgSwDI +/-	TgSwDI -/-	Both
6	Effect of Autophagy on Astrocyte Endfoot Morphology	TgSwDI +/-	TgSwDI -/-	Both
6	Clearance of Autophagic Remnants Through the BBB	TgSwDI +/-	TgSwDI -/-	Both
6	Lysosomal Protein Expression	TgSwDI +/-	TgSwDI -/-	Both

Genotyping

The presence of the TgSwDI transgene was assessed in DNA preparations from tail samples of TgSwDI +/- and -/- using primers against the transgene and an internal control gene (oIMR5260, 0IMR5261, oIMR1544, oIMR3580; The Jackson Laboratory) and the following polymerase chain reaction (PCR) conditions: 3 minutes at 94°C; 30 seconds at 94°C, 1 minute at 52°C, and 1 minute at 72°C, repeated for 35 consecutive cycles; 2 minutes at 72°C.

Statistics

All numerical data are presented as mean ± standard error of the mean. Statistical significance of data collected over time (BP, Barnes maze performance curves) was determined using a two-way ANOVA with a Bonferroni *post-hoc* correction. In all other cases, statistical significance was determined using a 2-tailed Student's *t*-test comparing different experimental groups. *p*-values <0.05 were considered significant.

Y-maze

Mice were allowed to freely explore an open-armed Y-shaped maze for 5 minutes in low lighting (50 lux). The order of arm entry was scored and alternation was determined by dividing the number of arm entry triads (all three arms visited subsequently) by the total number of arm visits minus 2[56]. Percent alternation was compared between groups. For this and all subsequent behavior tests described,

scoring was conducted by an experimenter who was blind to the genotype and to the treatment and age (when relevant) of all animals.

Barnes Maze

The Barnes maze apparatus (TAP Plastics) consisted of a white circular platform 92 cm in diameter with 20 equally spaced holes, each 5 cm in diameter and 7.5 cm apart. Of these holes, 19 were blocked with black plastic and 1 (target hole) was routed to a black escape box that was secured below the surface of the table. Distal visual cues consisting of black and white geometric shapes were placed throughout the testing room, and ambient lighting was kept high (1500 lux) to motivate animals to find and enter the escape box. During training, mice were allowed to search the maze for the target hole for 2 minutes, after which time they were guided to the target hole. Training consisted of 1 trial per day for each mouse for 4 consecutive days. On the fifth day, a probe trial was carried out to assess spatial memory of the mice (24-hr probe trial) [57]. The target hole was blocked off with black plastic, and the mice were allowed to explore the maze for 90 seconds while their behavior was recorded. An extended probe trial was held five days later (5-d probe trial). All trials were recorded and scored for latency to find the target hole (first nose poke) as well as latency to enter the target hole using Ethovision software (Noldus). Velocity, distanced traveled, and number of entries into the area around the target hole were determined and compared between groups.

Contextual Fear Conditioning

Fear conditioning experiments were run in a conditioning chamber (MedAssociates) equipped with a light and an overhead video camera and all trials were recorded for subsequent scoring. On the first day of the test, mice were placed in a conditioning chamber that had been cleaned with 70% ethanol and were allowed to habituate to the chamber for 2 minutes. Animal behavior during these first 2 minutes was used to assess baseline freezing behavior. Mice then received 2 foot shocks (0.7 mA for 2 seconds each), one minute apart. Mice were removed from the chamber 30 seconds after the last foot shock. After 24 hours, each mouse was placed into the same chamber in which it received foot shocks the previous day and allowed to explore the chamber for 5 minutes while its movements were recorded. Freezing behavior for all trials was scored in 5-second bins and was taken to indicate a mouse's memory of the foot shocks from the previous day[58].

Porsolt Swim Test

Each mouse was placed in a 4-L transparent beaker filled to 80% capacity with room temperature water. The final water level was 5 cm below the mouth of the beaker, so mice were not able to attempt escape. Mobility of each mouse in the water was observed for 6 minutes and all trials were video recorded for later analysis[59]. Animal movement was scored manually every 5 seconds and immobility was defined as lack of movement, except for that which was required to keep the animal afloat. The total time spent immobile over the course of the trial was compared between groups.

Fixed Immunohistochemistry

Mice were heavily anesthetized by IP injection of 1 mL 2.5% tribromoethanol and perfused with 5 mL 0.9% saline followed by 15-30 mL 4% paraformaldehyde (PFA) according to body weight. Brains were post-fixed overnight in 4% PFA and cryoprotected for 24 hours in 30% sucrose in 0.1 M phosphate buffer at 4°C. Brains were then frozen on powdered dry ice and sliced into 30-micron coronal sections using a microtome. Sections were collected into freezing medium (30% glycerol, 30% ethylene glycol, 40% 0.1 M phosphate buffer) and stored at -20°C until use. Hippocampus-containing free-floating brain sections were mounted on glass slides using a gelatin-based mounting medium and dried overnight at room temperature.

Slides were rinsed upright in 1X PBS for 5 minutes before undergoing antigen retrieval. Antigen retrieval conditions were determined for each antibody (Table 2.2) and included no treatment, incubation in Proteinase K (Dako) and/or boiling in sodium citrate buffer (10 mM sodium citrate, 0.05% Tween 20 in ddH_2O, pH 6.0). Slides were rinsed 3 times for 5 minutes each in 1X PBS and blocked in 3% normal donkey serum with 0.3% Triton X-100 in 1X PBS for 1 hour at room temperature. Antibodies were diluted in blocking buffer at concentrations ranging from 1:100-1:10,000 and sections were incubated in primary antibody solution for 12-18 hours at room temperature and then washed in 1X PBS 3 times for 5 minutes each. Sections were incubated in fluorescently-labeled secondary antibody (Alexa Fluor, donkey anti-host species, 1:200) for 1-2 hours at room temperature, then washed and

covered using ProLong Gold antifade reagent (Life Technologies) and microscope cover glass (Fisher).

Sections were visualized using an Axiovert 200 inverted epifluorescence microscope or an LSM510 laser scanning confocal microscope (Carl Zeiss, Inc.). All sections were imaged at 20x-40x magnification. Exposure time and gain were consistent for each stain between all sections from all animals.

Table 2.2. Antibodies used for immunohistochemical studies.

Antibody	Vendor	Host Species	Reactivity	Fixation	Antigen Retrieval	Concentration
anti-α-SMA	Sigma-Aldrich	FITC-labeled	Many, including mouse	PFA perfusion	none	1:500
G2-10 anti-Aβ40	Millipore	Mouse	Human	15' EtOH at 4C	2' in 25% PK	1:100
6E10 anti-Aβ40 and 42	Covance	FITC-labeled	Human	PFA perfusion	5' PK	1:100
BA3-9 anti-Aβ42	Covance	Rabbit	Human	15' EtOH at 4C	2' in 25% PK	1:500
anti-albumin	Abcam	Chicken	Mouse, Rat, Human	30' PFA at RT	none	1:100
anti-AQP-4	Santa Cruz	Rabbit	Mouse, Rat, Human	PFA perfusion	5' PK	1:100
anti-CATD	R.A. Nixon	Rabbit	not tested	PFA perfusion	5' PK	1:10,000
anti-CD31	BD Pharmingen	Rat	Mouse	10' PFA at RT	none	1:100
anti-collagen IV	Fitzgerald	Rabbit	Many, including mouse	PFA perfusion	15' HMAR + 5' PK	1:100
anti-GFAP	Santa Cruz	Goat	Many, including mouse	PFA perfusion	5' PK	1:200
anti-Iba-1	Wako	Rabbit	Mouse, Rat, Human	PFA perfusion	15' HMAR	1:100
1D4B anti-LAMP-1	DSHB	Rat	Mouse	PFA perfusion	5' PK	1:100
anti-NeuN	Millipore	Rabbit	Mouse, Rat	15' PFA at RT	none	1:200
anti-PDGFRβ	Abcam	Rabbit	Mouse, Rat, Human	PFA perfusion	none	1:100

Fresh Immunohistochemistry

Mice were heavily anesthetized by IP injection of 1 mL 2.5% tribromoethanol and perfused with 15-30 mL 0.9% saline according to body weight. After perfusion, brains were removed and immediately covered in powdered dry ice. Brains were stored at -80°C until slicing into 30-micron coronal sections using a cryostat. Tissue sections were thaw-mounted directly onto glass slides and stored at -80°C until use. Staining was carried out as in "Fixed Immunohistochemistry", but with brief fixation using 4% PFA or ethanol (Table 2.2) and without antigen retrieval.

Thioflavin S Staining

Hippocampus-containing fixed free-floating coronal brain sections were mounted onto glass slides using a gelatin-based mounting medium and dried overnight at room temperature. Slides were rinsed in 1X PBS and immersed in Thioflavin S (ThioS) solution (0.02% Thioflavin S dissolved in ddH_2O and filtered, Sigma-Aldrich) for 30 minutes at room temperature. Slides were then immersed in 70% ethanol for 15 minutes, washed and covered using ProLong Gold antifade reagent (Life Technologies) and microscope cover glass. Z-stacks containing 5 images, each 1 μm apart, were collected for each hippocampal subregion at 25X magnification using an inverted LSM510 laser scanning confocal microscope (Carl Zeiss, Inc.). Exposure time and gain were consistent between all sections from all animals.

Evans Blue Extravasation Assay

A solution of 2% Evans blue (Sigma-Aldrich) in 0.9% saline was injected (10 mL/kg body weight) intraperitoneally (IP) into each mouse. 24 hours after injection, mice were heavily anesthetized by IP injection of 1 mL 2.5% tribromoethanol and perfused transcardially with 0.9% saline to remove the intravascular dye. Brains were frozen immediately on powdered dry ice and kept at -80C until sectioning. Brains were sectioned coronally at 30 microns using a cryostat and Evans blue extravasation was assessed directly by analysis of fluorescence in hippocampal subregions at 20x-40x magnification.

L-NAME-Induced Hypertension

Mice were weighed and divided into cages according to treatment type. Water consumption per cage was quantified over a 7-day period and Nω-Nitro-L-arginine methyl ester hydrochloride (L-NAME, Sigma-Aldrich) was diluted into drinking water so that each mouse consumed approximately 100 mg/kg body weight per day. Treatment was initiated at 3-4 months-of-age and continued for 3 or 6 months.

Angiotensin-II and L-NAME-Induced Hypertension

Mice were anesthetized by IP injection of 2.5% tribromoethanol (500 mg/kg body weight) and atropine (0.04 mg/kg body weight) and osmotic infusion pumps (Alzet) were implanted subcutaneously at the scruff of the neck to deliver 1 μg/kg body weight per minute angiotensin II (Ang-II, Sigma-Aldrich) dissolved in sterile 0.9% saline. Surgical incisions were stitched closed using 6-0 silk sutures (Harvard

Apparatus). Following surgery, mice were injected IP with buprenorphine HCl (0.03 mg/kg body weight) and 500 μL sterile 0.9% saline and allowed to recover on a heating pad. Additionally, L-NAME was delivered as described in "L-NAME-induced Hypertension".

Tail Cuff Plethysmography

BP was measured one week prior to and every week during Ang-II and/or L-NAME treatment by tail cuff plethysmography according to the manufacturer's instructions (Kent Scientific). Mice were placed in a restrainer and rested on top of a heating pad to keep body temperature around 37°C. Three BP readings were obtained and averaged for each animal.

Stereology

Images of hippocampal subregions (Figure 2.1), the dentate gyrus (DG), the dorsal subiculum (DS), cornu ammonis 1 (CA1) and cornu ammonis 3 (CA3), from immunostained tissue were quantified using NIH Image J software. Hippocampus subregions were identified and outlined. Stained images were split into their component red, green and blue color channels, and the channel containing signal was selected for further processing. Images were thresholded manually to yield intensity in the areas containing apparent signal but not in background. Signal value was normalized to the size of the area from which it was extracted. For "vessel coverage" quantifications, stretches containing pixels of both the marker of interest and a vascular marker were selected using the line selection tool, added and

normalized to the size of the region quantified. Signal intensity, item number and pixel length was analyzed for each subregion and then compared between groups.

Figure 2.1. Anatomical map of hippocampal subregions. The hippocampus coordinates memory consolidation and spatial navigation and is one of the first regions in the brain to suffer damage in humans with AD and in the TgSwDI mouse model of AD. Hippocampal subregions are depicted here in a schematic of a coronal section through the hippocampus. The DG (green) receives excitatory inputs from the entorhinal cortex (not shown) and projects to pyramidal cells in the CA3 (light blue) via the mossy fiber tract. The DG is thought to be involved in pattern separation, as it converts similar inputs to substantially different outputs. Behaviorally, it contributes to the formation of new episodic memories and spontaneous exploration of novel environments. Additionally, the neurogenesis that happens in the DG contributes to spatial memory formation. Schaffer collaterals connect the CA3 to the CA1 (dark blue). The CA1 has been proposed to perform match-mismatch roles in the hippocampus, comparing memory retrieval with sensory input. CA1 cells synapse in the subiculum (dorsal subiculum, red) for relay out of the hippocampus. The subiculum is implicated in working memory and processing of spatial relationships, as well as the spread of Aβ to other hippocampal and non-hippocampal brain regions in AD.

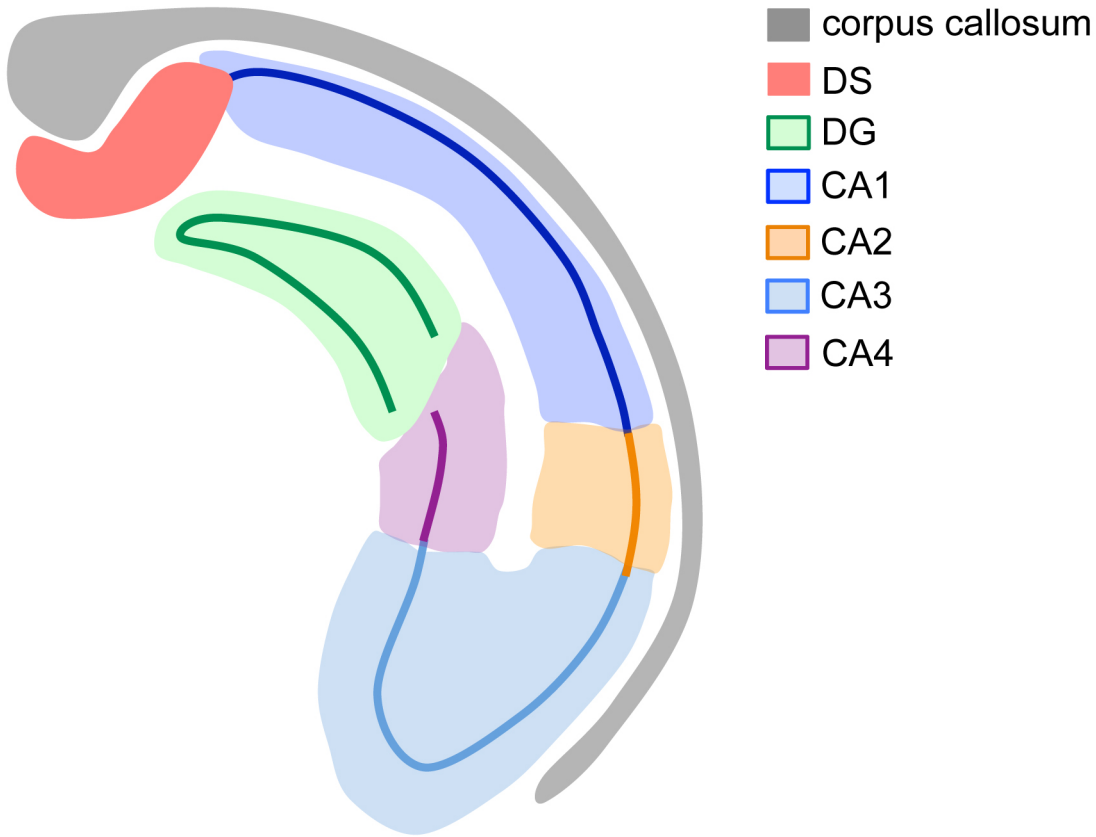
corpus callosum
DS
DG
CA1
CA2
CA3
CA4

Immunoelectron Microscopy

Mice were heavily anesthetized by IP injection of 2.5% tribromoethanol and were perfused with 0.9% saline followed by 15-30 mL 4% PFA according to body weight at slow speed. Brains were removed, immersed in 4% PFA, and sliced into 50-μm sections using a Leica VT 1000S vibrating blade microtome. The dorsal subiculum was removed and frozen in liquid nitrogen under high pressure using a Leica EM PACT2. Freeze substitution was performed using a Leica AFS2 automatic freeze substitution unit[60]. Tissue was sectioned at 90 nm onto carbon-coated copper mesh grids. After drying, grids were rinsed in 20 mM HEPES, pH 7.5, blocked with 3% bovine serum albumin (BSA) and 0.1% saponin in 20 mM HEPES, pH 7.5 for 2 hours at room temperature and incubated in primary antibody (1:900-1:32,000) at 4°C overnight (Biosource). Grids were then washed, incubated in blocking solution for 5 minutes, and incubated in 12-nm gold anti-host species secondary antibody (Jackson ImmunoResearch) in a solution containing 0.5% BSA, 0.1% saponin, and 20 mM HEPES, pH 7.5, for 1 hour at room temperature. After washing and fixing in 2.5% glutaraldehyde for 3 minutes, tissue sections were imaged using a JEOL 100CX transmission electron microscope at 80 kV. All post-perfusion steps were conducted at The Rockefeller University Electron Microscopy Resource Center (EMRC).

Transmission Electron Microscopy

Mice were heavily anesthetized by IP injection of 2.5% tribromoethanol and were perfused with 0.9% saline followed by 15-30 mL 4% PFA according to body weight

at a slow speed. Brains were removed and sliced using a brain matrix into 1-mm thick coronal sections. Sections were then immersed in 2.5% glutaraldehyde in 0.1 M sodium cacodylate buffer with 2 mM $CaCl_2$ at 4°C for 24 hours. Sections were immersed in 0.1 M sodium cacodylate buffer at 4°C for 24 hours and the dorsal subiculum was isolated. Tissue was post-fixed with 1% osmium tetroxide and 0.5-1.5% potassium ferrocyanide in 0.1 M sodium cacodylate buffer for 1 hour on ice. Tissue was washed once in 0.1 M sodium cacodylate buffer and twice in ddH_2O and stained in 1% uranyl acetate for 30 minutes at room temperature. Tissue was then quickly washed in water and dehydrated in increasing concentrations of ethanol (70%, 80%, 95%, 100%, 100%, 100%), followed by propylene oxide for 10 minutes each at room temperature. Propylene oxide was replaced with two exchanges of EMbed812 resin and tissue was placed under vacuum for 24 hours at room temperature. The resin was exchanged three more times over the following 24 hours and kept under vacuum before samples were cured in resin for 48 hours at 60°C. The tissue was sliced at 60-80 nm using a Leica Ultracut E and visualized using a JEOL 100CX transmission electron microscope at 80 kV. All post-perfusion steps were conducted at the Rockefeller University EMRC.

3View

Mice were heavily anesthetized by IP injection of 1 mL 2.5% tribromoethanol and perfused with 5 mL 0.9% saline followed by 15-30 mL 4% PFA according to body weight at slow speed. Brains were removed, immersed in 4% PFA, sliced into 100-µm sections using a Leica VT 1000S vibrating blade microtome and the dorsal

subiculum was removed and immersed in 4% PFA and 2.5% glutaraldehyde in 0.1 M sodium cacodylate buffer with 2 mM $CaCl_2$ overnight. The tissue was washed and incubated in 1.5% potassium ferrocyanide, 2% osmium tetroxide in 0.1 M sodium cacodylate buffer with 2 mM $CaCl_2$ for 1 hour on ice. Tissue was then washed with room temperature ddH_2O and incubated in filtered 0.1% thiocarbohydrazide solution in ddH_2O for 20 minutes. After rinsing, the tissue was re-exposed to 2% osmium tetroxide for 30 minutes, washed and incubated in aqueous 1% uranyl acetate for 12-18 hours. The tissue was stained in aqueous 20 mM lead nitrate and 30 mM aspartic acid, pH 5.5, at 60C for 30 minutes. After washing, the tissue was dehydrated in increasing concentrations of ethanol (20%, 50%, 75%, 100%, 100%, 100%) in a Pelco Biowave at 10C and 150 watts for 40 seconds each, then placed in ice-cold acetone for 10 minutes, followed by room temperature acetone for 10 minutes. Increasing concentrations of durcupan resin in acetone was infiltrated into samples using a Pelco Biowave (25%, 50%, 75%, 100%, 100%) and left to infiltrate under vacuum overnight. Samples were embedded between sheets of aclar and cured at 60°C for 48 hours. After mounting, blocks were trimmed and sputter coated for 120 seconds using gold/palladium (Denton). The tissue surface was imaged every 50 nm for 25 μm using a MERLIN scanning electron microscope (Carl Zeiss, Inc.) and processed using Gatan 3View System software.

Western Blotting

Fresh hippocampi or dorsal subiculum samples were dissected on ice and homogenized in lysis buffer (25 mM Tris-HCl, pH 7.6; 150 mM NaCl, 1% NP-40, 1%

sodium deoxycholate, 0.1% SDS) with protease and phosphatase inhibitors added (Sigma-Aldrich, Roche) and sonicated on ice. After large cellular debris was removed from samples by centrifugation, protein concentration was determined by spectrophotometry using a bicinchoninic acid (BCA) kit (Thermo Scientific) according to the manufacturer's instructions. Loading dye with β-mercaptoethanol was added to the samples, which were then boiled for 5 minutes at 100C. 20-30 µg of protein were loaded per lane and samples were run on a denaturing 8% Tris-Glycine gel, transferred to a nitrocellulose membrane and blocked in a 5% milk and 3% BSA solution dissolved in Tris-buffered saline with 0.5% Tween 20. Blots were probed with antibodies (1:1000-1:2000) in blocking buffer at 4°C overnight and washed. Blots were then incubated with the appropriate HRP-labeled secondary antibody (1:5000-1:10,000) in blocking buffer, washed again, incubated in chemiluminescent reagent (PerkinElmer) and exposed to film. Band intensity was quantified using NIH ImageJ software and normalized to actin from the same blot.

Hypoxyprobe Detection

A solution of 60 mg/kg body weight pimonidazole HCl (dissolved in sterile 0.9% saline, Hypoxyprobe) was injected IP into each mouse. 60 minutes after injection, the mice were heavily anesthetized by IP injection of 1 mL 2.5% tribromoethanol and perfused transcardially with 15-30 mL 0.9% saline according to body weight. Brains were removed and frozen immediately on powdered dry ice and kept at -80°C until sectioning. Brains were sectioned coronally at 30 microns onto glass slides using a cryostat and stored at -80°C until use. Slides were then incubated in FITC-MAb1

according to the manufacturer's instructions. Hippocampal subregions within stained sections were imaged at 20-40x magnification.

CHAPTER 3: CHARACTERIZATION OF ALZHEIMER'S NEUROPATHOLOGY IN THE TGSWDI MOUSE MODEL

Cognitive Decline

Cognitive decline was examined in TgSwDI mice by a variety of behavioral tests. Given that previous publications reported cognitive decline in TgSwDI mice at 3 months-of-age[52], but had not yet tested younger mice (W. Van Nostrand, personal communication), TgSwDI mice were tested for learning and memory impairments at 2, 3 and 6 months-of-age. Though 2-, 3- and 6-month-old TgSwDI mice exhibited no differences in spontaneous alternation using the Y-maze test or expression of learned fear after fear conditioning, 6-month-old TgSwDI mice did exhibit a reduced preference for the target hole (Figure 3.1A) during the 5-d probe trial in the Barnes maze, a test of spatial learning and memory[57], when compared to age-matched WTs (Figure 3.1B). Thus the earliest detectable indication of cognitive decline in this colony of TgSwDI mice occurred at 6 months-of-age.

Figure 3.1. TgSwDI mice exhibit cognitive deficits at 6 months-of-age. (A) The Barnes maze tests spatial learning and memory. Mice were trained to find the location of a target hole (red) that led to a hidden escape box (blue) based on visual cues around the maze and were tested for their learned preference for the area near the target hole after training. (B) At 6 months-of-age, TgSwDI mice exhibited no preference for the target hole during the 5-d probe trial, compared to WT mice ($p<0.05$). TgSwDI also exhibited reduced preference for the hole adjacent to the target hole (hole number 20) compared to controls ($p<0.05$).

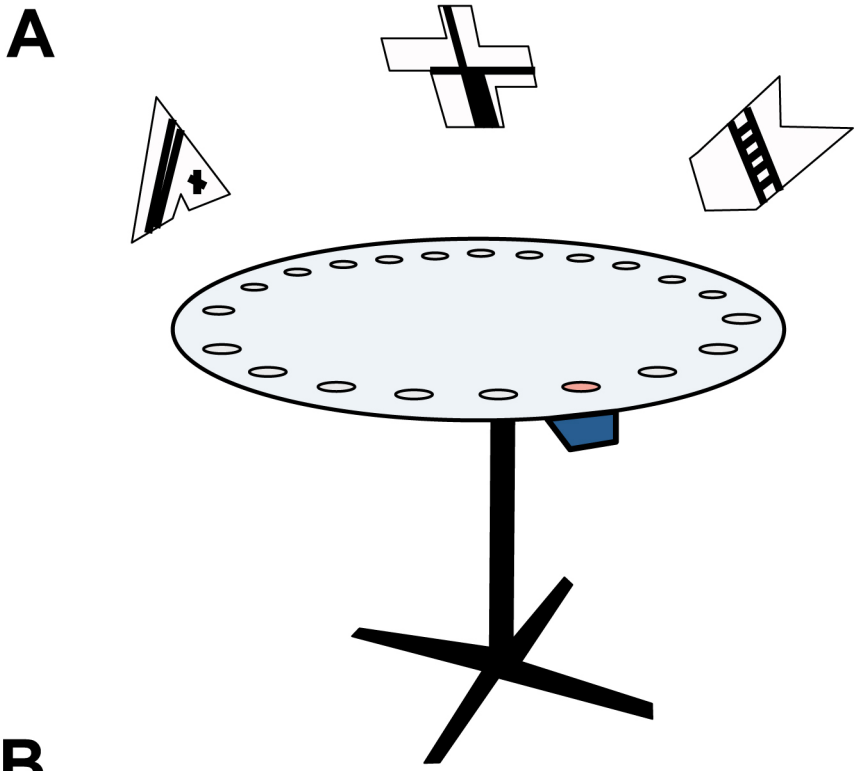
A

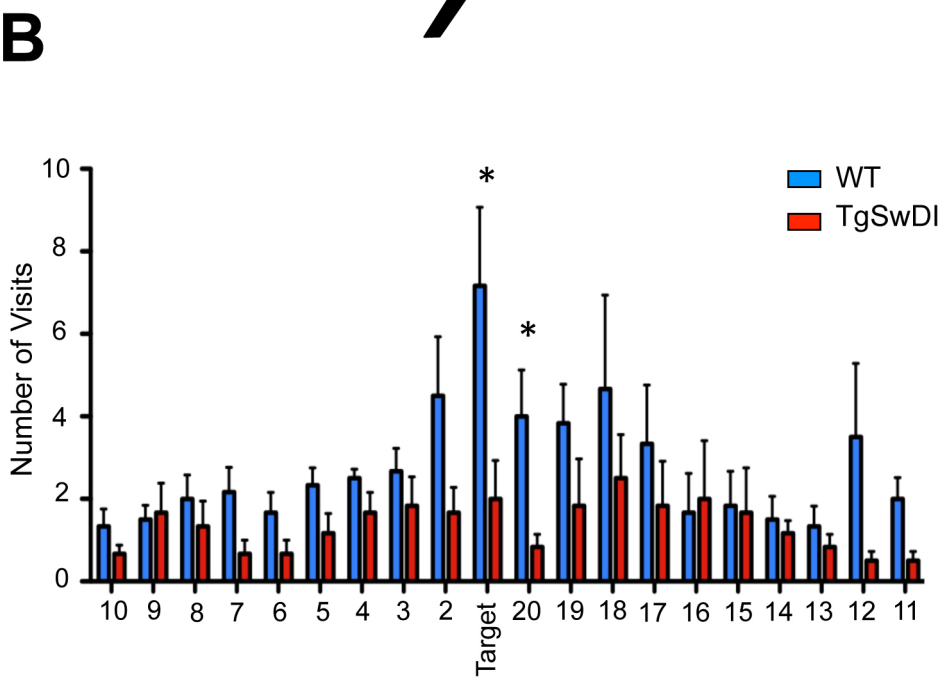
B
WT
TgSwDI
Number of Visits
0
2
4
6
8
10
*
*
10 9 8 7 6 5 4 3 2 Target 20 19 18 17 16 15 14 13 12 11

Amyloid Deposition

Compared to WT mice and 2-month-old TgSwDI mice, which exhibited no Aβ deposition in the brain by ThioS staining, TgSwDI mice exhibited more Aβ in the hippocampus starting at 3 months-of-age (Figure 3.2). TgSwDI mice exhibited a small amount of Aβ in the DS and DG regions of the hippocampus at 3 months-of-age, though the deposition appeared in small plaque-like patches (Figure 3.2B). By 6 months-of-age, ThioS staining revealed abundant CAA and decreased presence of parenchymal plaques relative to earlier time points (Figure 3.2C vs. 3.2A,B).

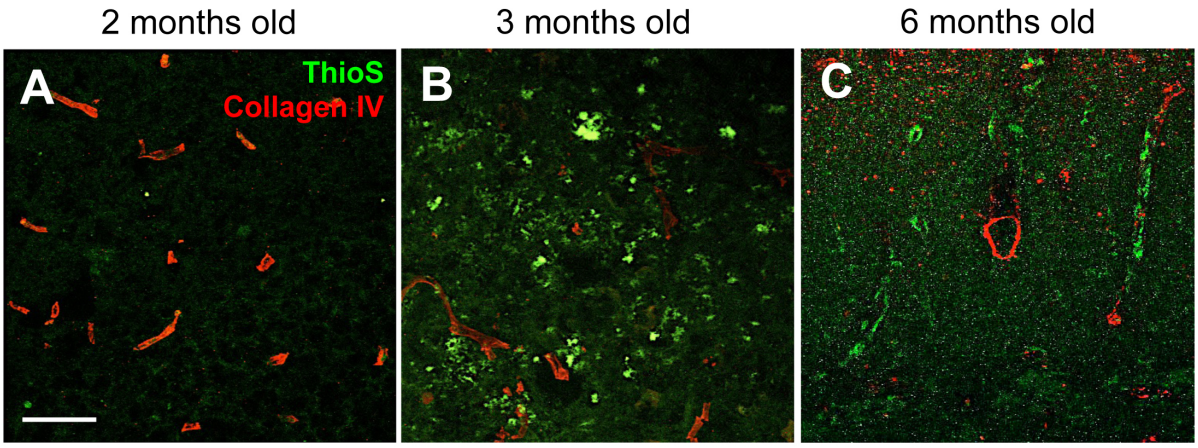

Figure 3.2. Pattern of Aβ deposition over time in TgSwDI mice. Deposition of Aβ in the DS was examined in 2- (A), 3- (B), and 6-month-old (C) TgSwDI mice by ThioS staining (green). Anti-collagen IV co-staining (red) was used to identify capillaries. At 2 months-of-age, TgSwDI mice exhibited little-to-no ThioS-positive signal in the DS (A), whereas small diffuse plaques were observed by 3 months-of-age (B). At 6 months-of-age, parenchymal plaque-load was reduced and Aβ was abundant along capillaries in the brain (C; scale bar = 50 μm).

Gliosis

Microglia activation in TgSwDI mice was determined by abundance of microglia compared to WT (Figure 3.3). Microglia were stained using a fluorescently-labeled tomato isolectin, a sugar-binding glycoprotein with specific affinity for poly-N-acetyl lactosamine residues present on the surface membranes of microglia and endothelial cells[61]. Positive signal was determined to be microglial rather than endothelial based on morphology of stained cells. TgSwDI mice (Figure 3.3D-F) exhibited more microglia-like staining at 2, 3 and 6 months-of-age in the DG and DS compared to WT mice that exhibited no observable microgliosis at these ages (Figure 3.3A-C). Importantly, this result demonstrates that microgliosis preceded both Aβ deposition as plaques, which occurred at 3 months-of-age in TgSwDI mice, and as CAA, which occurred at 6 months-of-age (Figure 3.2).

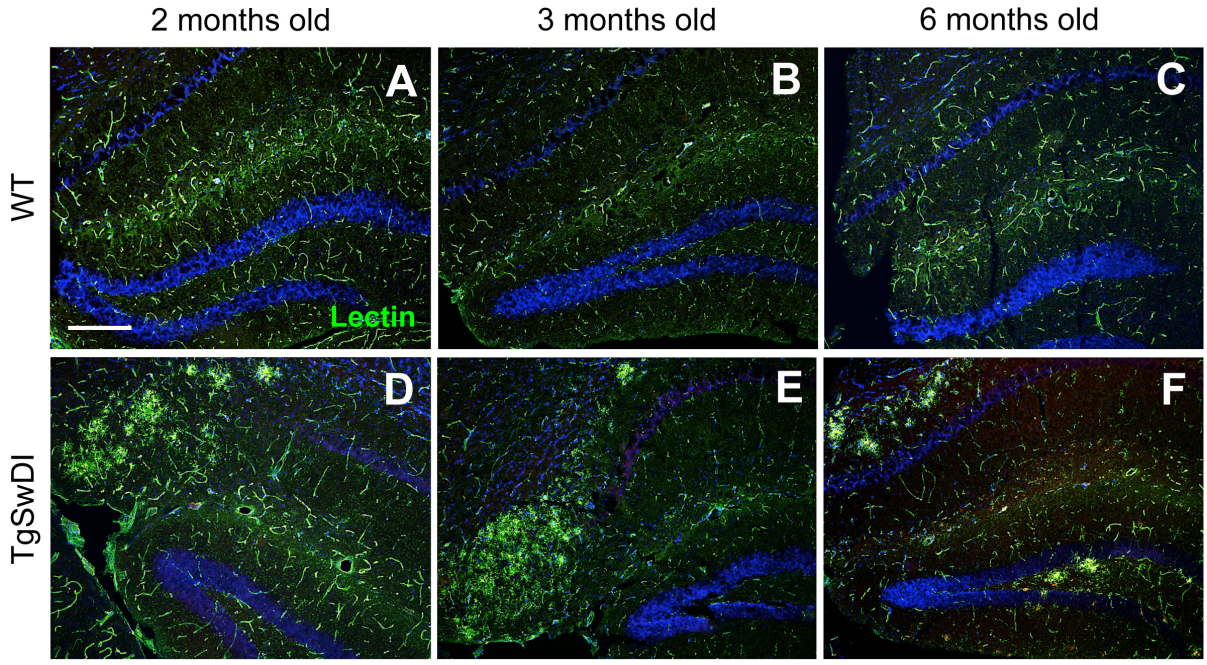

Figure 3.3. Microgliosis precedes Aβ deposition in TgSwDI mouse brains. Fluorescently-labeled tomato isolectin (green) is a sugar-binding glycoprotein with specific affinity for sugar residues on microglial and endothelial cell surfaces. Stained endothelial cells and microglia are morphologically distinct; capillary endothelial cells were present in all images and appeared as thin streaks, while microglia appeared as large patches of dense signal. The increased appearance of microglia in the DS of 2- (D), 3- (E), and 6-month-old (F) TgSwDI mice compared to WT mice of the same ages (A, 2-months; B, 3-months; C, 6-months-old) indicate that microglia were activated in TgSwDI brains as early as 2 months-of-age. Microgliosis becomes apparent in the DG of TgSwDI mice around 6 months-of-age, later than in the DS (F vs. D, scale bar = 100 μm).

BBB Integrity

The Evans blue injection model was used to determine the age at which TgSwDI mice first exhibited BBB breakdown (Figure 3.4). When injected IP, the azo dye Evans blue (red) enters the blood stream and binds to albumin with high affinity. Under normal conditions, the plasma protein albumin (65 kDa) is too big to cross the BBB and is removed during perfusion along with the associated Evans blue. In the case of a leaky BBB, however, albumin carries Evans blue into the brain parenchyma where it can be detected by fluorescence microscopy. After injection, Evans blue was detected in the cortex and hippocampus of 3-month-old TgSwDI mice (Figure 3.4B), but not in 2-month-old TgSwDI mice (not shown) or WT mice at any age examined (up to 12 months; Figure 3.4A). By 12 months-of-age, Evans blue leakage in the brains of TgSwDI mice was prominent (Figure 3.4D).

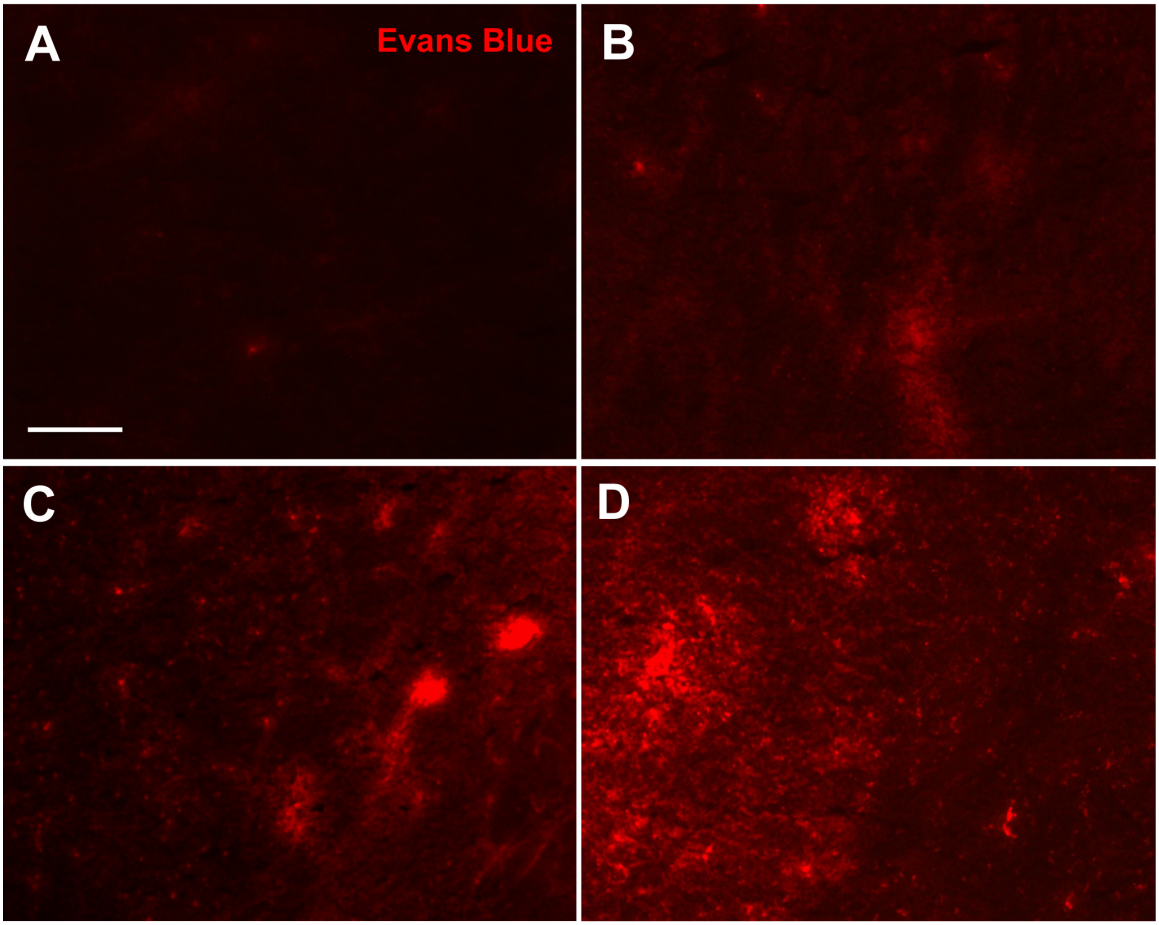

Figure 3.4. TgSwDI mice exhibit early BBB breakdown. Evans blue was injected into TgSwDI and WT mice of different ages (A-D). 18 hours after injection, mice were perfused with saline and their brains removed. Imaging revealed the presence of Evans blue in the DS of TgSwDI mice as early as 3 months-of-age (B). Evans blue leakage was severe at 6 (C) and 12 months-of-age (D) in TgSwDI mice compared to WT mice at 12 months-of-age (A), where little-to-no signal was observed (scale bar = 50 μm).

Autophagy

Lysosomal-associated membrane protein-1 (LAMP-1) was used as an autophagic marker since it is present on both lysosomal and endosomal membranes[62] (Figure 3.5). LAMP-1 is often increased at dysfunctional synapses in AD, as AVs are known to build up in dystrophic neurites in the brain[46]. LAMP-1 signal was evident in the DS of TgSwDI mice as early as 3 months-of-age (Figure 3.5B), the earliest age examined. By 6 months-of-age, LAMP-1 staining was evident in the DS and DG (Figure 3.5C) as well as the thalamus (not shown), suggesting that pathology was not only more severe at this age, but also more extensive. Though LAMP-1 immunostaining is typically used to indicate synaptic dysfunction in AD mice, it is possible that other cell types in the brain were responsible for the observed increase in LAMP-1 staining, as no cell type-specific co-stain was used. LAMP-1 signal became more diffuse in the DS at 6 months-of-age, possibly coincident with the transition from Aβ deposition as plaques to CAA (Figure 3.2).

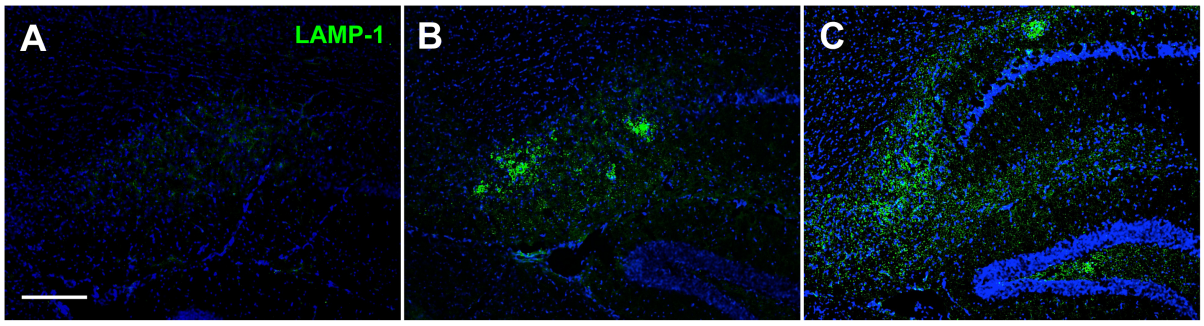

Figure 3.5. TgSwDI mice display evidence of increased autophagy. LAMP-1, a protein present on lysosomal and endosomal membranes, was examined in TgSwDI and WT brain tissue using an anti-LAMP-1 antibody (A-C). At 6 months-of-age, no LAMP-1 was detectable in the hippocampus of WT mice (A). In TgSwDI mice at 3 months-of-age, LAMP-1 appeared as small clusters in the DS of the hippocampus (B). LAMP-1 staining was also present as clumps in the DG and CA1 in TgSwDI mice at 6 months-of-age (C). The LAMP-1 signal in the DS at this time point was more widespread, though large patches were no longer apparent (scale bar = 100 μm).

Differences in Depressiveness, Anxiety and Locomotion in TgSwDI Mice

Researchers who generated the TgSwDI mouse line report early cognitive deficits, but no changes in balance, locomotion or anxiety[52]. However, TgSwDI mice from the colony I examined exhibited significant differences in defecation, an indication of anxiety level in mice, in a number of behavioral tests during testing for onset of cognitive decline (Figure 3.6). During Barnes maze testing, TgSwDI mice exhibited increased defecation at all ages (Figure 3.6A-C), a finding that was similar during fear conditioning (Figure 3.6D). TgSwDI mice also exhibited increased learned helplessness at 3 months-of-age on the Porsolt swim test (Figure 3.6E). Together, these findings suggest differences in emotionality in TgSwDI mice compared to WT mice, independent of cognitive decline, which was only detectable at 6 months-of-age (Figure 3.1).

Figure 3.6. TgSwDI mice exhibit increased anxiety- and depressive-like behaviors. (A-C) During Barnes maze training, TgSwDI mice defecated more than age-matched WT control mice at 2 (A), 3 (B) and 6 months-of-age (C; *p<0.05, **p<0.01). Defecation is an indication of anxiety in mice and decreased gradually over the course of Barnes maze training in most groups. (D) During fear conditioning, defecation decreased with age in WT mice, but remained elevated in TgSwDI mice at 2, 3 and 6 months-of-age (*p<0.05, **p<0.01). (E) The Porsolt swim test is used to examine depressive-like behavior in mice. A reduced latency to immobility is known as “learned helplessness”, a behavioral output that is similar to some features of depression in humans. TgSwDI exhibited shorter latencies to immobility at 3 months-of-age compared to age-matched WT controls (E, *p<0.05). This trend persisted at 6 months-of-age (not shown).

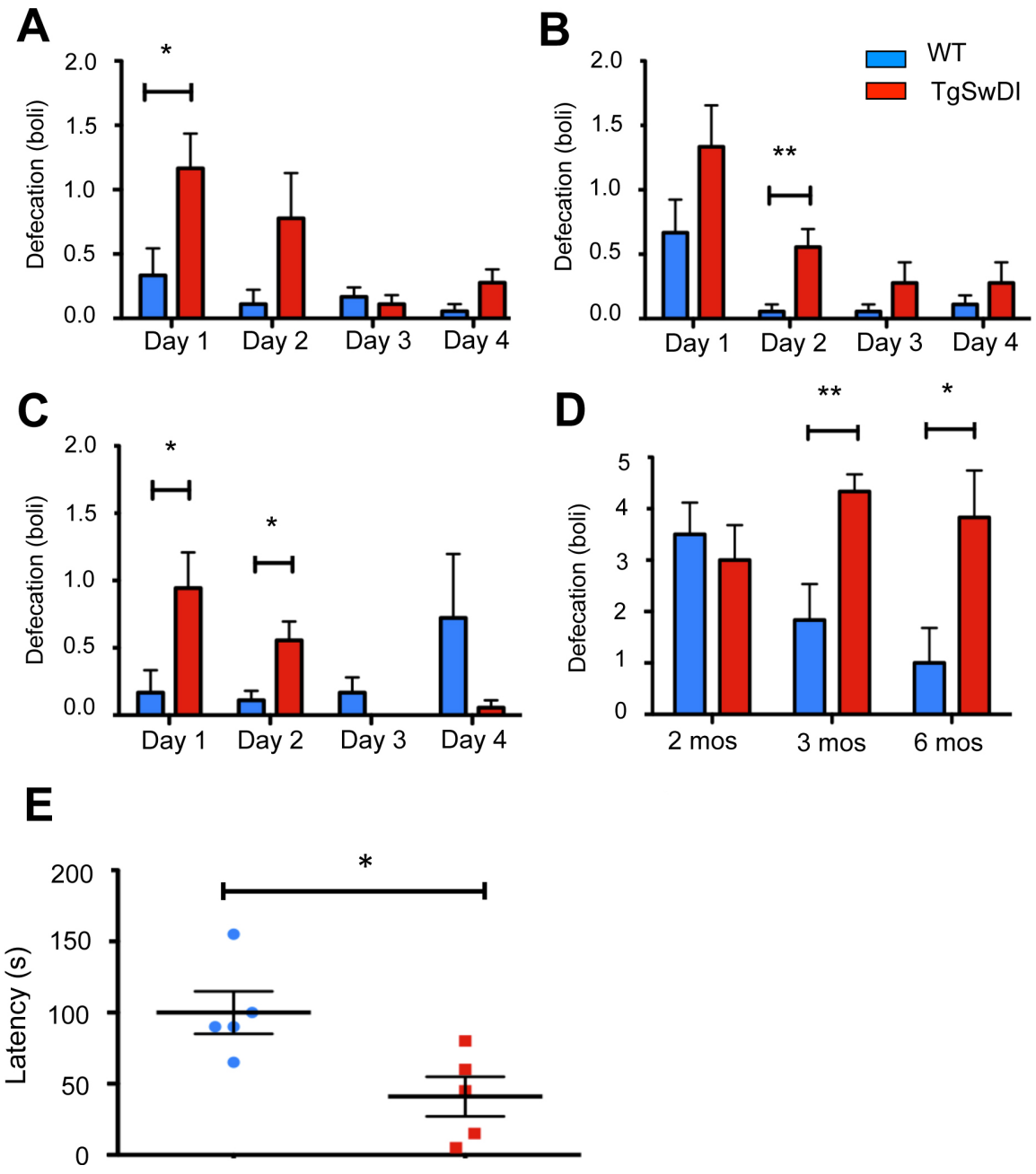
A
B
C
D
E
Defecation (boli)
Day 1
Day 2
Day 3
Day 4
WT
TgSwDl
2 mos
3 mos
6 mos
Latency (s)
*
**

TgSwDI mice also exhibited reduced mobility in multiple behavioral tests relative to WT mice (Figure 3.7). During Y-maze testing, TgSwDI mice were consistently less mobile than WTs at 2, 3 and 6 months-of-age (Figure 3.7A). During Barnes maze testing, TgSwDI mice exhibited an age-dependent reduction in mobility (Figure 3.7B). Given these results, it is unclear whether the decreased latency to immobility observed in TgSwDI mice at 3 months-of-age during the Porsolt swim test (Figure 3.6E) represents increased depressiveness in the animals or is an artifact of their reduced locomotion.

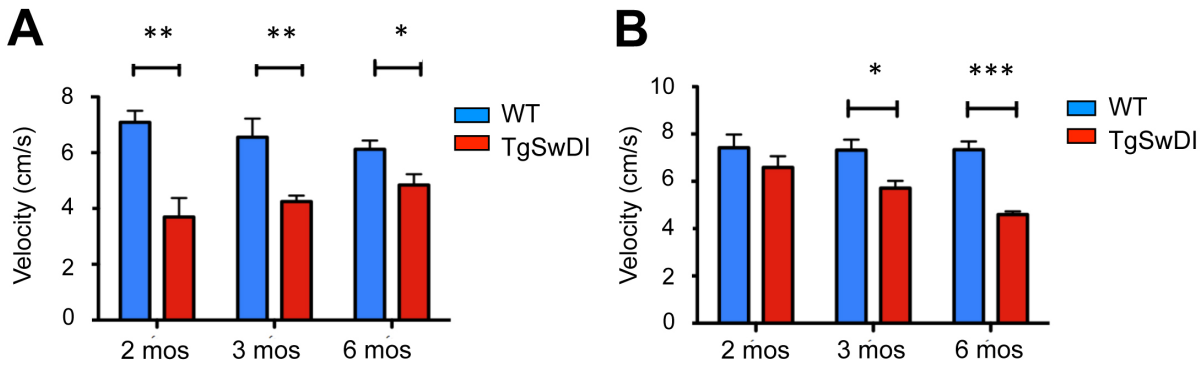

Figure 3.7. TgSwDI mice exhibit reduced mobility. During behavioral testing for cognitive decline, TgSwDI mice demonstrated reduced mobility in the Y-maze (A) and Barnes maze (B) tests compared to age-matched WT controls. Mobility was reduced in this mouse line at both 3 and 6 months-of-age using both tests (A,B; *p<0.05, **p<0.01, ***p<0.001). At 2 months-of-age, TgSwDI mice only exhibited reduced locomotion during Y-maze testing. Given that increased latency to immobility was observed at 3 months-of-age during the Porsolt swim test, it is possible that the Porsolt swim test result is suggestive of motor differences, rather than a depressive-like phenotype in TgSwDI mice.

TgSwDI Background Characterization

Since the TgSwDI mouse model was generated on a pure C57Bl6J background[50], C57Bl6J mice were initially used as controls. This method was beneficial, since frequent genotyping and separation of mice were not required during breeding. Additionally, TgSwDI mice were used as homozygotes and two copies of the transgene resulted in earlier and more severe pathology and both TgSwDI and C57Bl6J mice could be ordered to supplement experiments if breeding was slow. However, after establishing that the behavior of this colony of TgSwDI mice was inconsistent with published reports[52] (Figures 3.1, 3.6, 3.7), DNA samples from two of eight colony founder mice were sent for background characterization to determine if C57Bl6J was the correct control based on the background of the TgSwDI mice from this colony.

An initial 384 SNP background strain characterization test (Charles River) indicated that both founder animals were mostly C57Bl6J (99.73% and 99.61%). However, both animals were found to be heterozygous for a marker on chromosome 10 in a region polymorphic between C57Bl6J and C57Bl6N substrains, indicating that the TgSwDI mice from this colony had a mixed C57Bl6 background.

Though C57Bl6 substrains arose from the same mouse line, decades of breeding in separate facilities have resulted in subtle genomic divergence[63]. Two spontaneous mutations have arisen in coding sequence DNA since the two lines have been bred separately. The Crb1 gene contains a 1bp deletion in C57Bl6N mice compared to

C57Bl6J and a deletion in the Nnt gene can now be found in C57Bl6J mice. Though these differences are seemingly inconsequential, other groups have reported behavioral differences between C57Bl6J and N substrains[64]. Further analysis on colony founder DNA involved the examination of 15 microsatellite markers showing polymorphism between C57Bl6 substrains (Charles River). Microsatellite marker testing showed that both founder mice had slightly more C57Bl6J in their genetic backgrounds than C57Bl6N (62.5% and 65.62%). The unique differences between the founders at these microsatellite sites are listed in Table 3.1. The importance of the D2Mit277, D6Mit116, D11Mit71, and D18Mit49 loci, which were different in the two founders, are not known, as these regions have not been studied in detail. The Nnt gene, which was polymorphic between the two founders, encodes a mitochondrial NAD(P) transhydrogenase. This integral inner mitochondrial membrane protein couples hydride transfer between NAD(H) and NADP(+) to proton translocation across the inner mitochondrial membrane. The importance of this polymorphism is unclear, since the effect of each polymorphism on gene product production and function is not known.

Table 3.1. Mixed background of TgSwDI mice.

Marker	Chromosome	Position (cM)	Founder A	Founder B
RD8 (Crb1)	1	73.0	N	N
D2Mit1	2	1.0	J	J
D2Mit277	2	69.0	N	N / J
D3Nds6	3	19.2	N	N
D3Mit22	3	33.7	N	N
D6Mit116	6	5.5	N / J	N
D6Mit300	6	59.2	J	J
D9Mit90	9	9.0	J	J
D11Mit71	11	1.1	N / J	J
D11Mit134	11	16.0	N	N
D11Mit285	11	52.0	J	J
Nnt	13	67.2	N	J
D14Mit185	14	54.0	J	J
D18Mit49	18	49.0	J	N
DXMit144	X	40.0	J	J
DXMit64	X	45.0	J	J
DXMit186	X	69.0	J	J
C57BL6J (%)			**62.5**	**65.62**

Use of Homozygotes vs. Heterozygotes

Due to the mixed background observed in the colony of TgSwDI mice being studied and the potential effects of strain background on behavioral characteristics in mice, TgSwDI mice were crossed with C57Bl6J mice to generate TgSwDI +/- and -/- for future use. Though the background would still be mixed for these mice, the background would be similarly mixed in the littermates used as controls.

Importantly, preliminary studies conducted on this mouse line (Figures 3.1-3.7) employed TgSwDI homozygotes. The new breeding and genotyping scheme would require the use of heterozygotes. The onset and severity of pathology is likely to vary between homozygotes and heterozygotes and previously published reports on this mouse line describe experiments done with homozygotes. Thus findings in heterozygotes are likely to be less severe at any given time point due to expression of one copy of transgenic APP rather than two.

CHAPTER 4: INDUCING HYPERTENSION IN TGSWDI MICE

Assessment of Methods for Inducing Hypertension in Mice

Surgical, genetic and chemical techniques have been developed to induce hypertension in rodent models for research. Surgical models entail the ligation of the renal artery or abdominal aorta, or removal of one kidney. All of these techniques result in reduced kidney function. Since the kidneys regulate the amount of fluid in the body as well as arterial constriction and damaged kidneys often overproduce renin, these techniques increase arterial constriction and result in high BP. The transverse aortic constriction (TAC) model has also been used for studying the effects of hypertension on the brain and heart[65]. TAC, which involves ligation of the transverse aorta, causes increased BP and blood volume in the vasculature leading up to the point of constriction, which includes the right carotid artery as well as the heart.

Ultimately, surgical techniques for inducing hypertension were avoided, because wounds resulting from surgical techniques are susceptible to infection or injury. Wounded mice often require single-housing so that they are protected from fighting with other mice as well as easily monitored while they heal. Social isolation in mice in turn results in altered behavior in a number of behavior tests and has even been shown to exacerbate AD pathology[66-68]. Thus, surgically-induced hypertension was likely to result in experimental artifacts based on housing conditions and/or a smaller experimental cohort.

Genetic models of hypertension involve overexpression of WT or transgenic renin, resulting in increased circulating Ang-II. Ang-II stimulates vascular smooth muscle cells and results in their contraction[69]. Ang-II also stimulates ion exchange in the kidneys resulting in increased blood volume, BP and blood pH[70]. In fact, Ang-II is so effective at increasing BP that angiotensin converting enzyme (ACE), the enzyme required for production of Ang-II, is the target of a major group of antihypertensive drugs, the ACE inhibitors[71]. Angiotensin receptor blockers (ARBs) or Sartans, another group of commonly used antihypertensive drugs, are effective due to their action in preventing Ang-II binding to receptors[72]. Genetic models to induce hypertension were not ideal, since AD mouse models can be weak when crossed to other strains. Often the mixture of the genetic background is important to the survival of a strain when a deleterious transgene, such as mutated APP, is inserted into the genome. Changing the background of a strain can result in changes in litter size, pup survival and birth rates. Also, generating a double-transgenic mouse colony often requires many months to achieve cohorts large enough for experimentation, even when adjusting the genetic background of the strain has no impact on reproduction and survival of the mice.

Finally, chemical models of hypertension involve administration of chemical components of the pathway that regulates BP endogenously and/or chemicals that regulate the production of pathway components. Direct Ang-II administration is one example of this. Ang-II treatment can be paired with administration of L-NAME to provide a two-pronged approach to increasing BP[73]. Chemical models are useful

since treatment can be adjusted to yield more or less severe hypertension. Treatments are also often easy to administer or withhold from mice at different time points, depending on experimental requirements, which is not true for surgical or genetic models.

Ang-II and L-NAME-Induced Hypertension in AD Mouse Models

Ang-II is a component of the endogenous renin-angiotensin system, which controls BP in mammals. The serum globulin angiotensinogen is produced in the liver and released into the circulation, where it becomes activated by renin to form angiotensin I. Angiotensin I is converted to Ang-II by ACE. Ang-II is a potent vasoactive peptide and, because it causes vasoconstriction, it can independently raise BP when delivered subcutaneously.

L-NAME supplementation of Ang-II treatment has been described as a useful technique for inducing hypertensive intracerebral hemorrhage (ICH) in rodents[73]. L-NAME is an endothelial cell nitric oxide synthase (eNOS) inhibitor. Nitric oxide synthases (NOS) catalyze the production of nitric oxide (NO) from L-arginine endogenously. NO is an important cellular signaling molecule and also modulates vascular tone, insulin secretion, peristalsis, angiogenesis and neural development[74]. It also functions in the brain as a retrograde neurotransmitter[75]. Three forms of NOS are produced endogenously: eNOS, which is produced by endothelial cells; nNOS, which is produced by neurons; and iNOS, or inducible NOS, which increases levels of NO as an immune defense against pathogens. L-NAME causes vasoconstriction

by selective inhibition of eNOS, which is produced by the vascular endothelium to induce vasodilation. Therefore, L-NAME directly inhibits the ability of the endothelium to dilate and relieve spikes in BP caused by physiological changes, such as increased levels of Ang-II.

Ang-II infusion along with L-NAME administration were used in early attempts to increase BP in 3 different mouse models of AD used in the lab: TgSwDI, Tg6799 and TgCRND8. However, Ang-II and L-NAME administration together resulted in seizures and increased mortality shortly after initiation of treatment in all three mouse lines (Figure 4.1A). Additionally, the use of this model for induction of ICH by other groups was worrisome[73], since this would be a potential limitation on treatment duration. For this reason, no further experiments were conducted using this technique.

Figure 4.1. Effect of treatments to induce hypertension on long-term survival in AD mouse lines. L-NAME and Ang-II were used to induce hypertension in the TgSwDI, Tg6799 and TgCRND8 AD mouse lines. After the start of treatment (Day 0), mortality increased in all three mouse lines (A). TgCRND8 mice exhibited the most extreme drop in survival during treatment, followed by TgSwDI and Tg6799 mice. Frequent seizures were observed in L-NAME and Ang-II-treated mice of each strain. No increase in mortality was observed in untreated mice. (B) Given this drop in survival following combined L-NAME and Ang-II treatment, TgSwDI and WT mice were treated with L-NAME alone. Both groups exhibited an increase in BP from baseline levels (Day -2) without any associated increase in mortality (not shown) despite the extended duration of treatment.

A

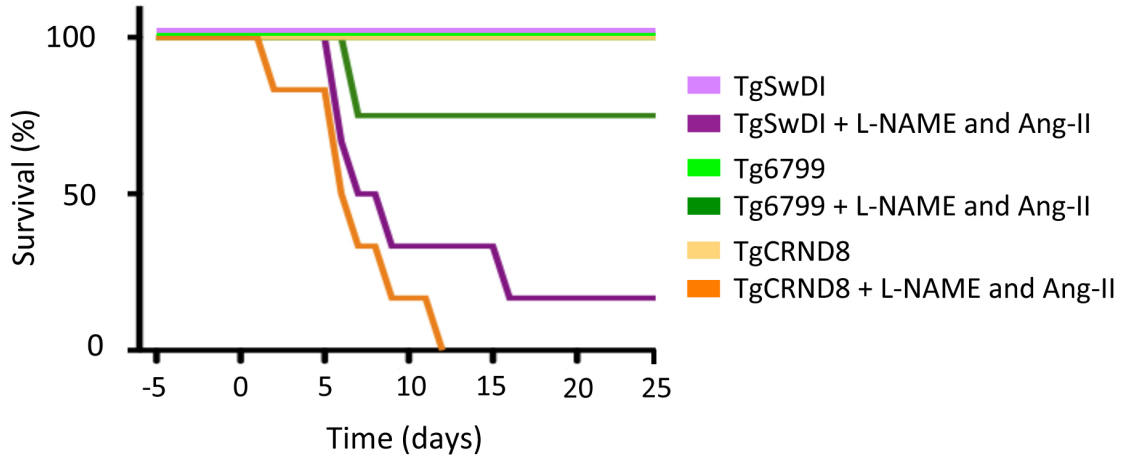
100
50
0
Survival (%)
-5
0
5
10
15
20
25
Time (days)
TgSwDI
TgSwDI + L-NAME and Ang-II
Tg6799
Tg6799 + L-NAME and Ang-II
TgCRND8
TgCRND8 + L-NAME and Ang-II

B

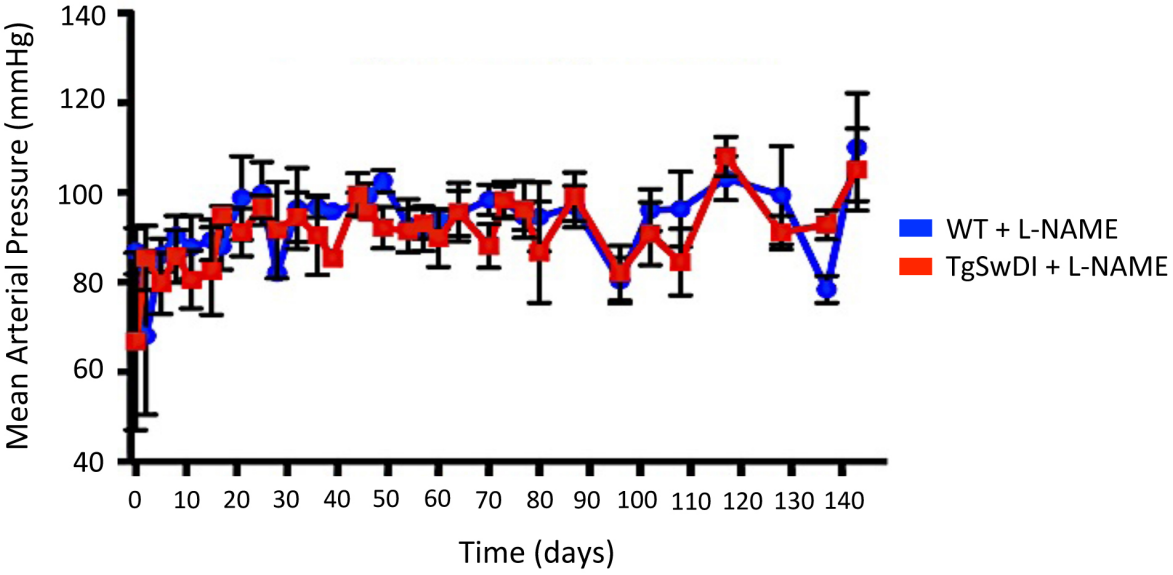
140
120
100
80
60
40
Mean Arterial Pressure (mmHg)
0
10
20
30
40
50
60
70
80
90
100
110
120
130
140
Time (days)
WT + L-NAME
TgSwDI + L-NAME

L-NAME-Induced Hypertension

Due to the increased mortality observed in AD mice following Ang-II and L-NAME administration (Figure 4.1A), L-NAME treatment alone was examined for its effects on BP (Figure 4.1B). Administration of L-NAME increased BP in both TgSwDI and WT mice (Figure 4.1B). BP rose gradually after initiation of treatment (Day 0) and remained elevated after the first 3-4 weeks of treatment. Additionally, treatment of mice for up to 5 months resulted in no increase in mortality in either genotype (not shown).

One benefit of this method relative to other treatment types was that the amount of L-NAME administered could be adjusted easily since L-NAME was delivered in the drinking water of the mice. Additionally, no surgical incisions were required for L-NAME administration. Even if AD mice could tolerate Ang-II treatment alone for an extended duration, Ang-II was infused through a subcutaneous pump that required a small incision on the back of each mouse for insertion. Additionally, the infusion pump used for Ang-II delivery required replacement once contents were expelled every 2-4 weeks. Thus, the duration of treatment would have been limited by the cost of the pumps and the number of times animals could be anesthetized and operated on before suffering extensive surgical trauma. Since long-term L-NAME administration could best mimic chronic human hypertension, which can last decades, it was selected as the method for inducing hypertension in TgSwDI mice.

CHAPTER 5: EFFECTS OF HYPERTENSION ON ALZHEIMER'S NEUROPATHOLOGY IN TGSWDI MICE

Cognitive Decline

L-NAME was used to chemically induce hypertension in TgSwDI and WT mice (Figure 5.1). This protocol was designed to mimic the pattern of hypertension that predisposes humans to LOAD, which occurs in individuals with midlife hypertension prior to indications of cognitive decline[34, 76, 77]. Since TgSwDI mice are predisposed to AD, hypertension was induced at 3-4 months-of-age, which corresponds to early adulthood in humans, but is before AD-related cognitive decline was observed in this mouse line (Figure 3.1). Mice were treated for 3 or 6 months and were 6-7 or 9-10 months during testing and analysis, respectively. L-NAME-treated WT and TgSwDI mice exhibited a significant increase in BP compared to water-treated animals, which stabilized after the first four weeks of treatment (Figure 5.2A). There were no differences in levels of CD31 or α-smooth muscle actin between normotensive and hypertensive groups throughout treatment (not shown), suggesting that hypertension did not affect the overall number of vessels in brain tissue in these animals. The Barnes maze was used to compare the cognitive abilities of normotensive and hypertensive WT and TgSwDI mice. After 3 months of L-NAME treatment, TgSwDI mice performed significantly worse during the 5-day probe trial compared to water-treated TgSwDI mice and all WT mice (Figure 5.2B), indicating that chronic hypertension impacted cognition after only 3 months, well before significant cognitive impairment was evident from the transgene alone. Following 6 months of treatment, hypertensive TgSwDI mice performed worse during Barnes maze training, taking

significantly longer to find the escape hole compared to all other groups (Figure 5.2C). Unlike the homozygote cohort (Figure 3.7), there were no differences in baseline locomotor activity between any of the groups when heterozygotes and littermate controls were tested (not shown). Interestingly, this cohort of water-treated TgSwDI mice (9-10 months-of-age) did not have cognitive deficits relative to WT mice in this test, though chronic hypertension was able to induce significant cognitive dysfunction.

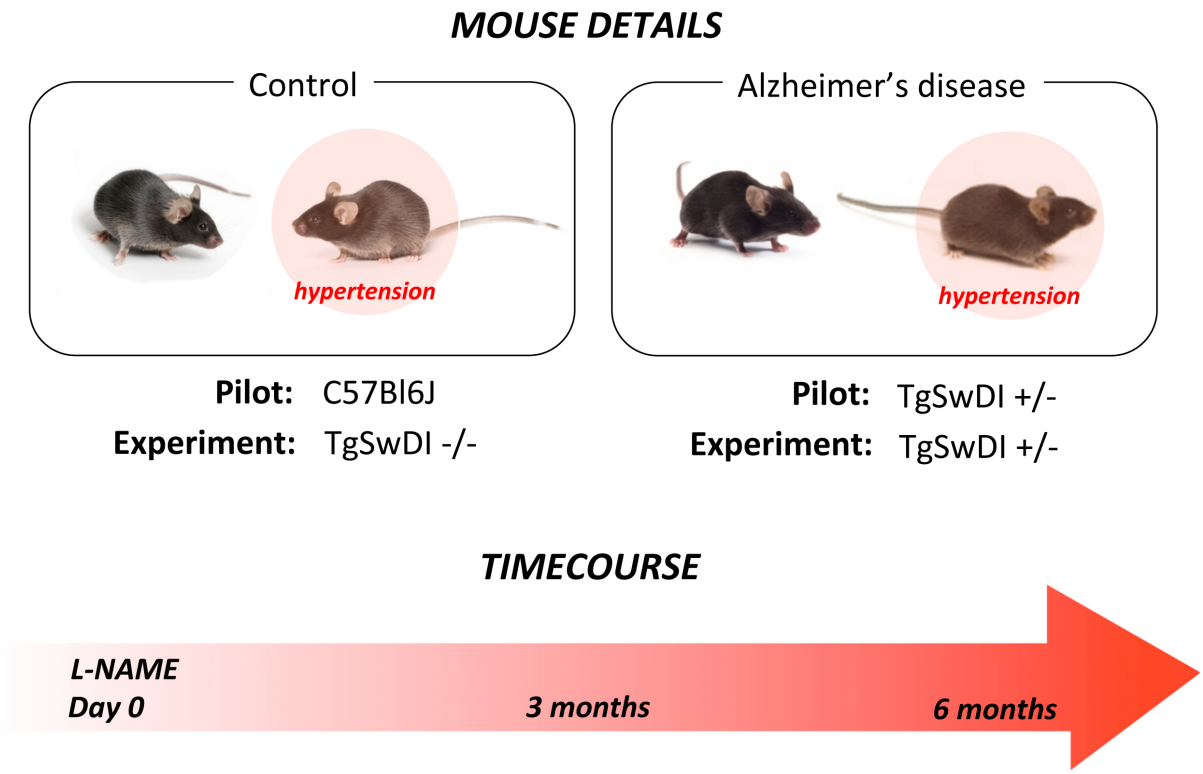

Figure 5.1. L-NAME-induced chronic hypertension experimental setup. IVF was used to generate a cohort of TgSwDI +/- mice from TgSwDI +/+ and C57Bl6J mice. The males from this cross and age-matched C57Bl6J males were used to test the experimental paradigm (pilot group). When they reached 3-4 months-of-age, half of the mice of each genotype were treated with L-NAME (hypertensive) for 3 or 6 months, at which time they were sacrificed. The rest of the cohort was treated with water. At 8 weeks of age, the female TgSwDI +/- mice generated from the first cross were subsequently crossed with C57Bl6J male mice using IVF to generate a new cohort of TgSwDI +/- and -/- mice (experimental group). Because they were generated by IVF, all members of the experimental cohort were age-matched and the controls were littermates. Mice of each genotype were treated with either L-NAME or water as described for the pilot group. After 3 or 6 months, behavioral experiments were conducted and mice were sacrificed for tissue analysis.

Figure 5.2. Chronic L-NAME treatment induces hypertension in WT and TgSwDI mice and accelerates AD-related cognitive decline. (A) WT and TgSwDI mice administered L-NAME in their drinking water exhibited significantly elevated BP compared to water-treated groups (***$p<0.001$ for effect of treatment for each genotype). Mice treated with water maintained constant BP. Treatments started on day 0, after baseline BP was measured. (B) TgSwDI mice treated with L-NAME for 3 months exhibited cognitive deficits in the Barnes maze relative to untreated TgSwDI and WT groups. During the probe trial carried out 5 days after training, hypertensive TgSwDI mice approached the target hole less frequently than normotensive TgSwDI (*$p<0.05$) and WT ($p<0.05$) mice. There was no effect of hypertension on cognitive function in WT mice. (C) Long-term hypertension, induced by L-NAME treatment for 6 months, affected learning in TgSwDI mice, which exhibited extended latencies to find the target hole during training compared to normotensive TgSwDI mice (***$p<0.001$), an effect not observed after 3 months of L-NAME treatment [not shown; n=8-12/group (A), 10-12/group (B,C)].

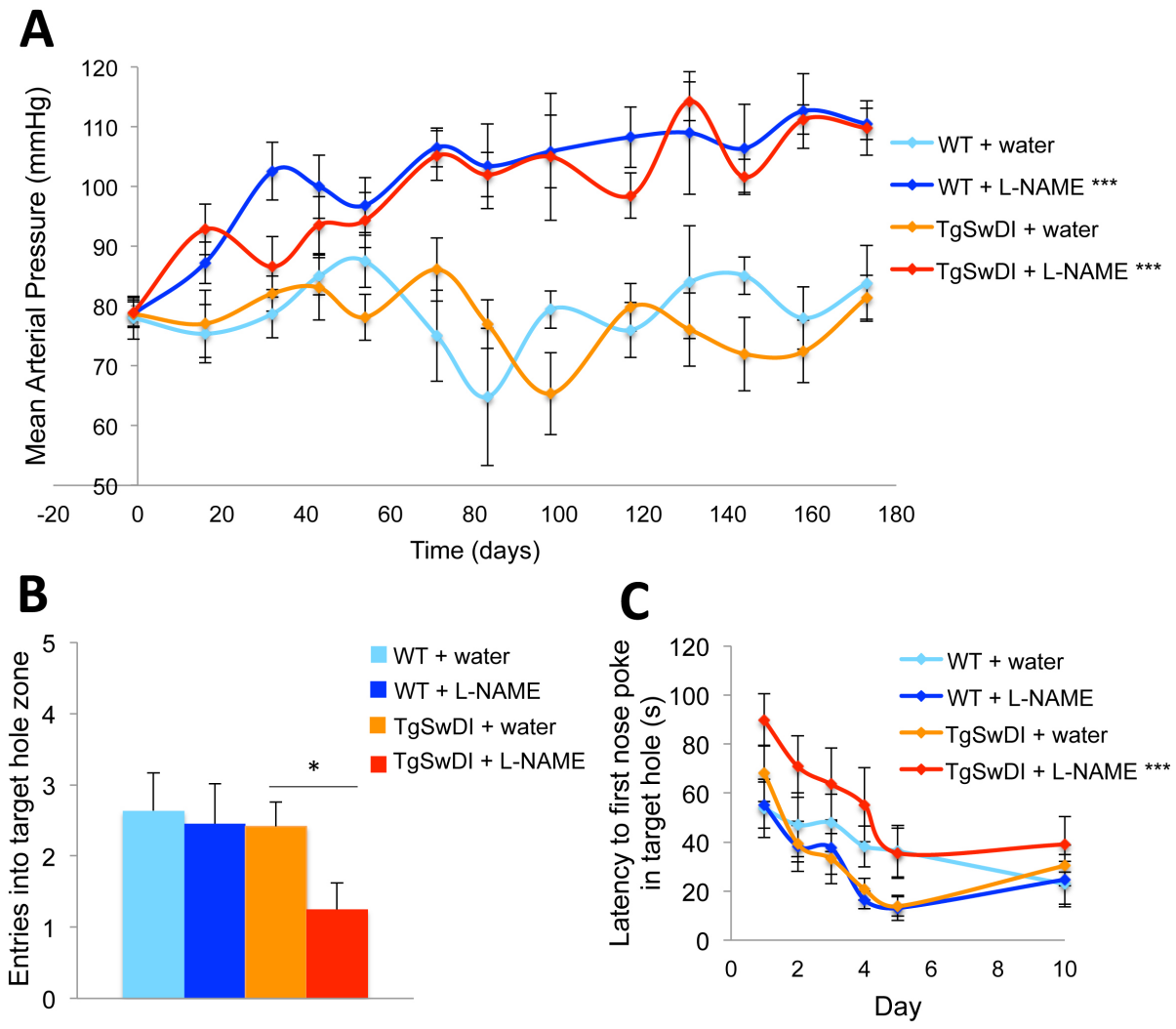
A
Mean Arterial Pressure (mmHg)
120
110
100
90
80
70
60
50
-20
0
20
40
60
80
100
120
140
160
180
Time (days)
WT + water
WT + L-NAME ***
TgSwDI + water
TgSwDI + L-NAME ***
B
Entries into target hole zone
5
4
3
2
1
0
*
WT + water
WT + L-NAME
TgSwDI + water
TgSwDI + L-NAME
C
Latency to first nose poke in target hole (s)
120
100
80
60
40
20
0
0
2
4
6
8
10
Day
WT + water
WT + L-NAME
TgSwDI + water
TgSwDI + L-NAME ***

Vascular Amyloid Deposition

To determine if increased levels of Aβ in the hippocampus were responsible for the cognitive deficits observed in hypertensive TgSwDI mice, ThioS was used to detect fibrillar Aβ. Sections were co-stained with an anti-collagen IV antibody, which recognizes the basement membrane of capillaries. After quantifying the total length of capillaries stained by collagen IV in the DS of each mouse, the length of vessels in the same sections that was stained by ThioS was quantified. These values were used to calculate the percent of DS capillaries with CAA. Aβ in the DS of normotensive TgSwDI mice was microvascular and parenchymal (Figure 5.3A, D). However, there were fewer plaques observed in hypertensive TgSwDI mice and significantly more CAA (Figure 5.3B, E). These results demonstrated that this microvascular Aβ staining was increased in hypertensive mice compared to normotensive animals (Figure 5.3C, F), yet there was not an increase in overall Aβ levels (not shown), suggesting that hypertension increased the likelihood that Aβ would be deposited microvascularly. The small number of plaques observed in hypertensive TgSwDI mice (Figure 5.3E) could have been the result of new Aβ production and/or deposition, since plaque-like deposits of Aβ were observed in earlier stages of disease before microvascular Aβ deposits were observed (Figure 3.2). Immunoelectron microscopy (IEM) analysis confirmed that the Aβ deposited in these mice was microvascular. Bundles of electron-dense finger-like clusters adhered to the basement membrane surrounding microvessels and stained positive with a pan-amyloid marker (Figure 5.3G).

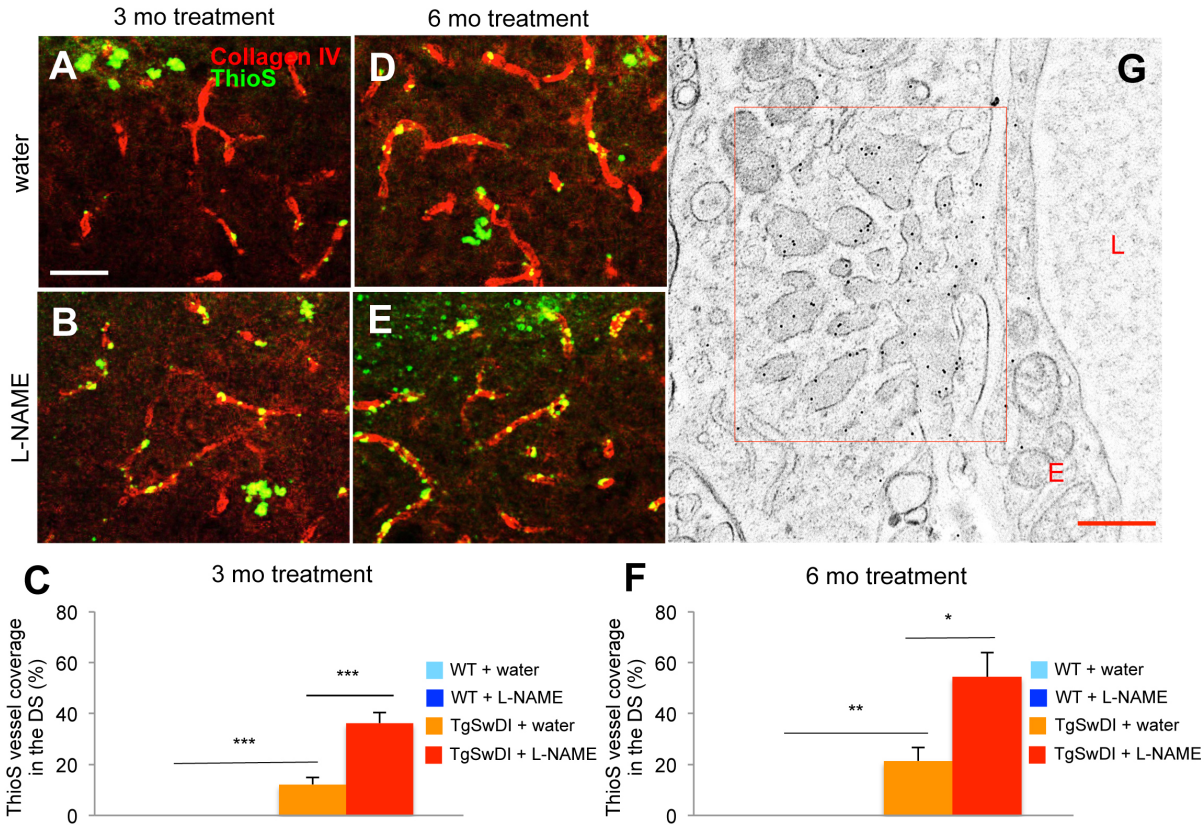

Figure 5.3. Hypertensive TgSwDI mice exhibit increased microvascular Aβ deposition. ThioS (green) and an anti-collagen IV antibody (red) were used to determine levels of CAA in normotensive (A,D) and hypertensive (B,E) TgSwDI mice. CAA levels were significantly increased after 3 (B,C) and 6 (E,F) months of L-NAME treatment (***p<0.001 or **p<0.01 normotensive TgSwDI vs. normotensive WT; ***p<0.001 or *p<0.05 normotensive vs. hypertensive TgSwDI; scale bar=50 μm; n=7-8/group). (G) Microvascular Aβ deposition, observed by immunoelectron microscopy, appeared as dark finger-like projections adhering to the basement membrane of capillaries in hypertensive TgSwDI brains (L, lumen; E, endothelial cell; scale bar=500 nm).

Microgliosis

Since activated astrocytes and microglia are often abundant in tissue with Aβ deposition[78], glial markers were examined in normotensive and hypertensive TgSwDI and WT brains (Figure 5.4). Though levels of astrocyte markers were similar in normotensive and hypertensive TgSwDI mice (not shown), the microglial marker Iba-1 was upregulated in hippocampal subregions of hypertensive TgSwDI mice compared to those of normotensive mice (Figure 5.4 B,E vs. A,D). Iba-1 expression was significantly higher in water-treated TgSwDI mice compared to water-treated WT mice and was even higher in L-NAME-treated TgSwDI mice (Figure 5.4C,F). The pattern of Iba-1 staining in the DG appeared patchy (Figure 5.4B), likely due to the presence of larger parenchymal plaques in this region, compared to the DS, where the staining appeared vascular (Figure 5.4E). Due to the vascular appearance of Iba-1 in the DS, electron microscopy (EM) was used to examine Aβ-laden microvessels and confirm that CAA was often surrounded by infiltrating microglia (M in Figure 5.4G).

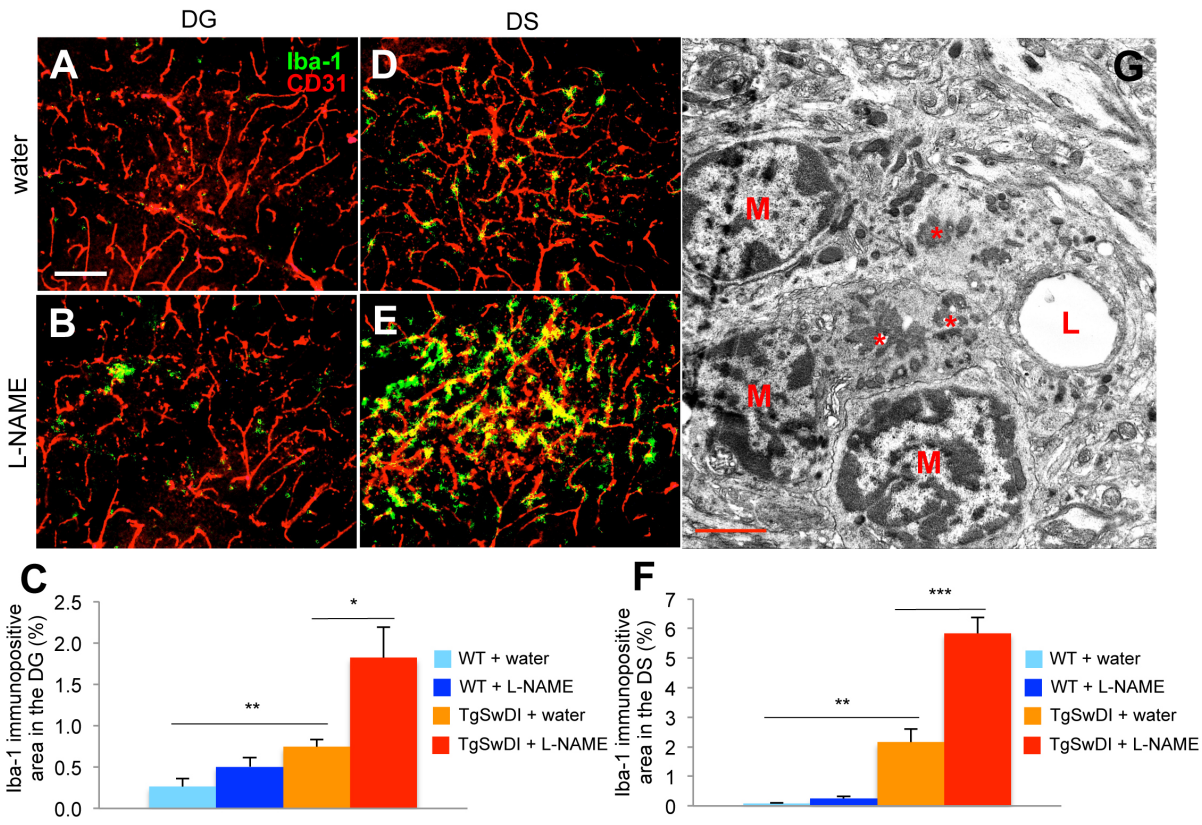

Figure 5.4. Hypertensive TgSwDI mice display increased vascular microgliosis. Microgliosis was examined in tissues using an anti-Iba-1 antibody (green) and vessels were stained with an endothelial cell-specific anti-CD31 antibody (red). Compared to water-treated TgSwDI (A,D) and WT (not shown) groups, the DG (B) and DS (E) of hypertensive TgSwDI brains exhibited significantly more Iba-1 staining after 6 months of treatment (C,F; **p<0.01 normotensive TgSwDI vs. normotensive WT; *p<0.05 or ***p<0.001 normotensive vs. hypertensive TgSwDI; scale bar=100 μm; n=6-9/group). (G) The infiltration of microglia was observed by EM of brain capillaries in hypertensive TgSwDI samples. Capillaries laden with Aβ (*) were surrounded by infiltrating microglial nuclei (M, microglia; L, lumen; scale bar=2 μm).

BBB Integrity

Since the BBB is disrupted in AD patients and mouse models[79-81], BBB integrity was examined to determine if hypertension affected this feature of AD pathology. Under normal conditions, tight junctions, which form the basis of the BBB[82], appear continuous and lay flat, preventing diffusion of blood components into the brain[83] (Figure 1.2, 5.5A). However, the tight junctions in samples from hypertensive TgSwDI mice appeared to be breaking off into the capillary lumen and lifting slightly from the endothelial cell layer (arrowheads in Figure 5.5B-D), providing an opportunity for BBB leakage. Given these structural alterations, tissue was examined for the presence of blood components that could enter the brain if BBB integrity were compromised. Albumin was elevated in the DS and DG of hypertensive TgSwDI brains when compared to normotensive TgSwDI brains after only 3 months of treatment, indicating that BBB integrity was compromised due to hypertension (Figure 5.5G,H).

Figure 5.5. Hypertensive TgSwDI mice have increased BBB disruption.

Compared to capillary structure in water-treated mouse vessels (A), capillaries in brains of hypertensive TgSwDI mice exhibited tight junction alterations (arrowheads in B-D). Compared to the structure of normal tight junctions (arrow in A), those of hypertensive TgSwDI mice were often lifting or fragmented (arrowheads in B-D). The plasma protein albumin, which was present at low levels in the DS of normotensive TgSwDI brains (E), was significantly enriched in the DS (F-H; *$p<0.05$) and DG (not shown) of hypertensive TgSwDI mice after 3 months of L-NAME treatment. Compared to normotensive WT mice, hypertensive WT mice also exhibited significant leakage of albumin from the vasculature into the DS after 3 months of L-NAME treatment (H, *$p<0.05$; scale bar in A=1 μm, E=20 μm; n=4-6/group).

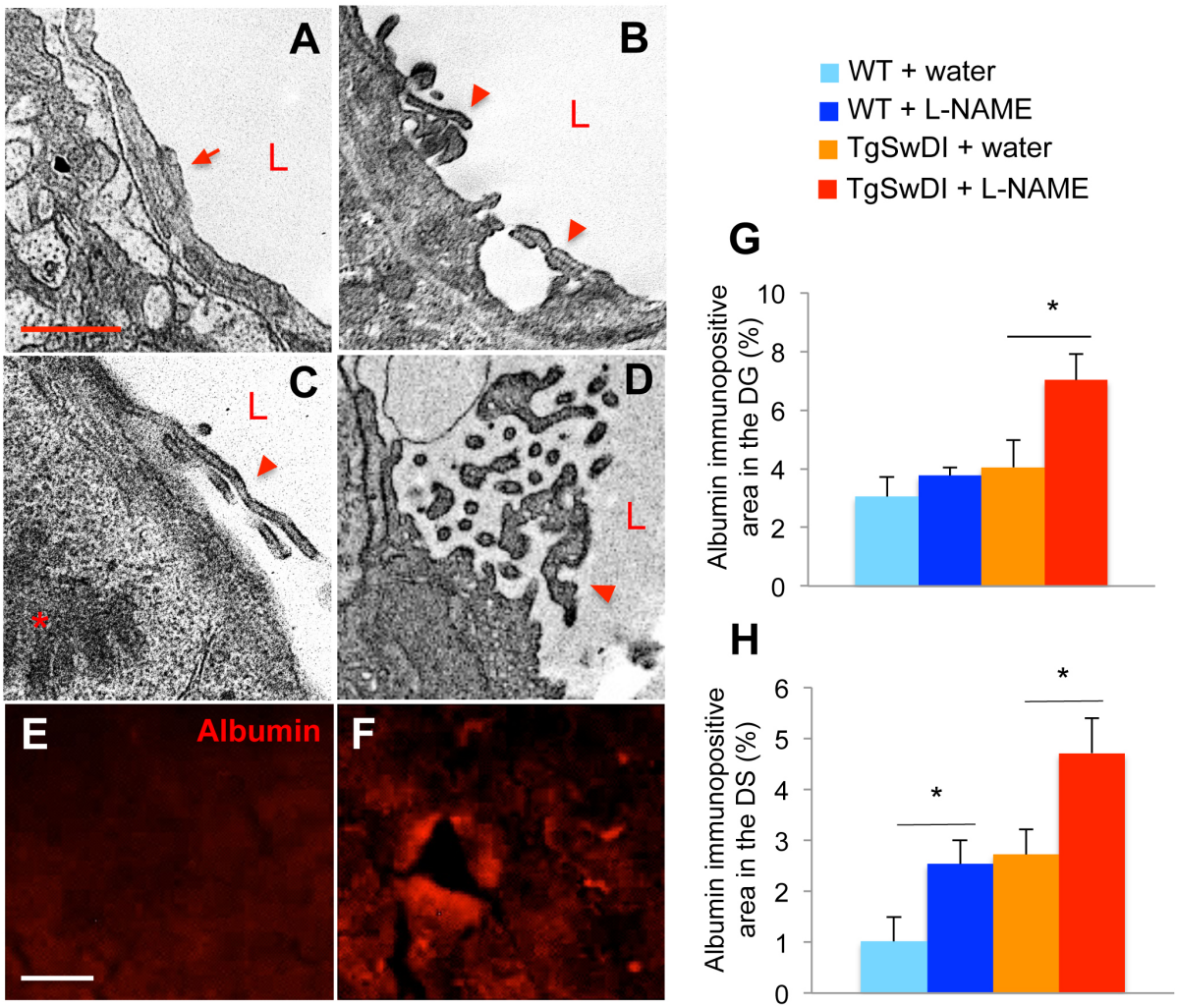
A
L
B
L
C
L
*
D
L
E
Albumin
F
WT + water
WT + L-NAME
TgSwDI + water
TgSwDI + L-NAME
G
Albumin immunopositive area in the DG (%)
0
2
4
6
8
10
*
H
Albumin immunopositive area in the DS (%)
0
1
2
3
4
5
6
*
*

Astrocyte Alterations

Though no changes were observed in levels of astrocyte markers examined in the experimental cohort (not shown) and despite similarities in microglial markers between the pilot and experimental cohorts (Figure 5.4, 5.6A,B), initial analysis of the pilot cohort revealed dramatic changes in astrocytic markers. Levels of glial fibrillary acidic protein (GFAP) were significantly increased in the hippocampi of hypertensive TgSwDI mice (Figure 5.6C,D).

Figure 5.6. Hypertensive TgSwDI mice from the pilot group exhibit increased microgliosis and astrocyte activation. The elevation in Iba-1 levels in the DS of hypertensive TgSwDI mice in the experimental group was also seen in hypertensive TgSwDI mice in the pilot group when examined using an anti-Iba-1 antibody (A, brown; B, ***p<0.001 normotensive TgSwDI vs. normotensive WT, **p<0.01 normotensive vs. hypertensive TgSwDI). However, the astrocyte marker GFAP, which was not differentially regulated in hypertensive TgSwDI mice compared to normotensive animals in the experimental group (not shown), was significantly increased in hypertensive TgSwDI mice (C) compared to normotensive mice (not shown) in the pilot group, as well as in hypertensive WT mice compared to normotensive control mice (D; **p<0.01 normotensive vs. hypertensive WT, ***p<0.001 normotensive TgSwDI vs. normotensive WT, *p<0.05 normotensive vs. hypertensive TgSwDI). GFAP (red) was observed as dense staining in the DG and DS (not shown) of hypertensive TgSwDI mice from the pilot group (C, scale bar = 100 μm).

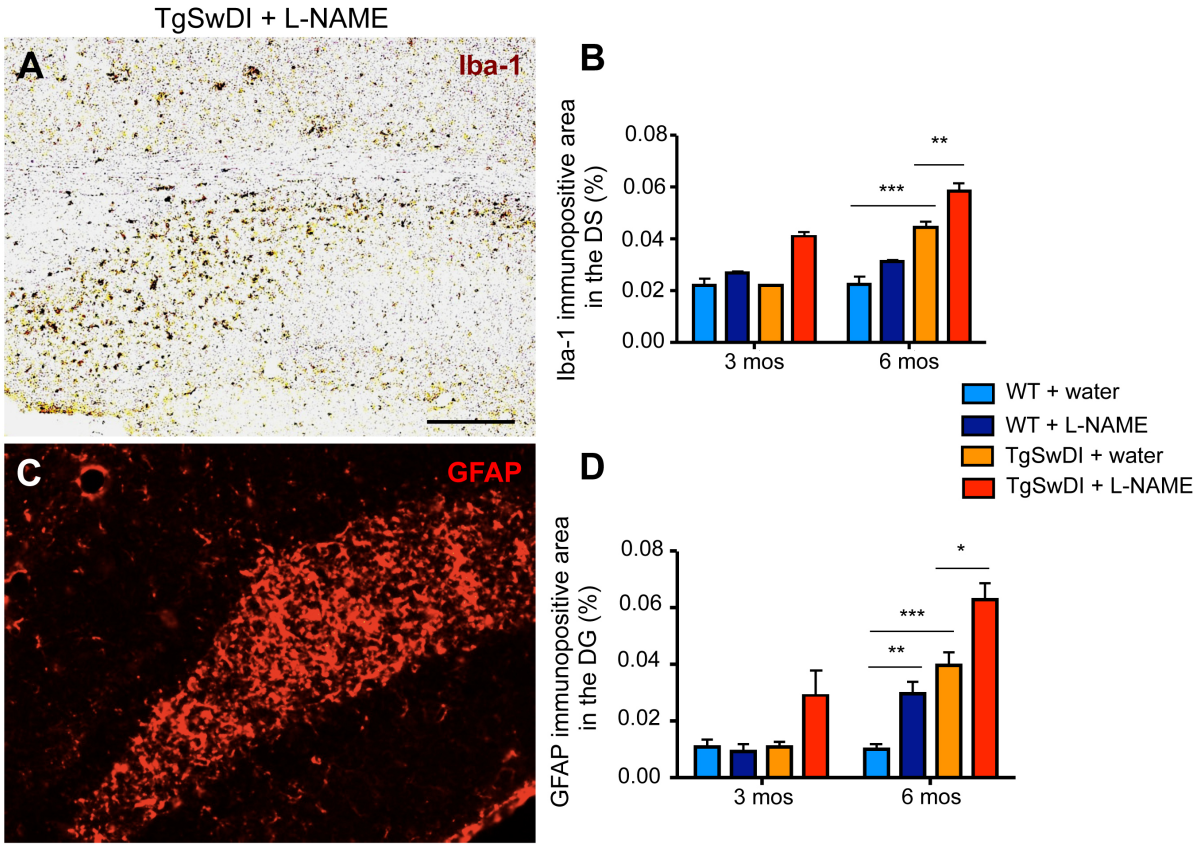
TgSwDI + L-NAME
A
Iba-1
B
Iba-1 immunopositive area in the DS (%)
0.08
0.06
0.04
0.02
0.00
3 mos
6 mos
**
***
WT + water
WT + L-NAME
TgSwDI + water
TgSwDI + L-NAME
C
GFAP
D
GFAP immunopositive area in the DG (%)
0.08
0.06
0.04
0.02
0.00
3 mos
6 mos
*
***
**

Additionally, levels of the water channel protein aquaporin-4 (AQP-4) appeared dramatically misregulated in hypertensive TgSwDI from the pilot group (Figure 5.7). Overall staining intensity was significantly increased in hypertensive TgSwDI mice (Figure 5.7D,J) relative to normotensive TgSwDI mice (Figure 5.7C,I), as well as nomortensive (A,G) and hypertensive WT mice (B,E,H,K). Despite this increase, localization of the endfoot marker along capillaries was largely absent (Figure 5.7F,L). These changes were subtle in normotensive TgSwDI, but severe in hypertensive TgSwDI mice. Importantly, hypertensive WT mice exhibited increased AQP-4 staining intensity as well as vessel coverage (Figure 5.7E,F,K,L), suggesting that the hypertension-induced alterations that occurred in WTs were misregulated in TgSwDI mice. Levels of α-syntrophin, an anchoring protein for AQP-4, were also reduced in the pilot cohort (not shown). Reduction in levels of this protein could contribute to AQP-4 mislocalization.

Figure 5.7. Hypertensive TgSwDI mice from the pilot group display mislocalized protein expression in astrocyte endfeet. The astrocyte endfoot marker AQP-4 was identified using an anti-AQP-4 antibody (red) in tissue from both the pilot and experimental cohorts. Despite seeing no differences in AQP-4 staining in mice from the experimental group (not shown), AQP-4 levels were increased in both the DG (A-D) and DS (G-J) of hypertensive TgSwDI mice (D, J) compared to normotensive TgSwDI mice (C, I) after 3 and 6 months of treatment. AQP-4 staining in normotensive (A,G) and hypertensive (B,H) WT animals showed what appeared to be vascular staining, consistent with the adherence of endfeet to capillaries. In hypertensive TgSwDI mice, staining was no longer localized to capillaries (F,L) and was dramatically upregulated (E,K), a pattern also observed in normotensive TgSwDI mice, but to a less dramatic extent. Notably, L-NAME treatment increased both AQP-4 staining intensity and vessel coverage in WTs, suggesting that the effect of hypertension on AQP-4 levels is misregulated in TgSwDI mice (*$p<0.05$, **$p<0.01$, ***$p<0.001$; scale bar = 50 μm).

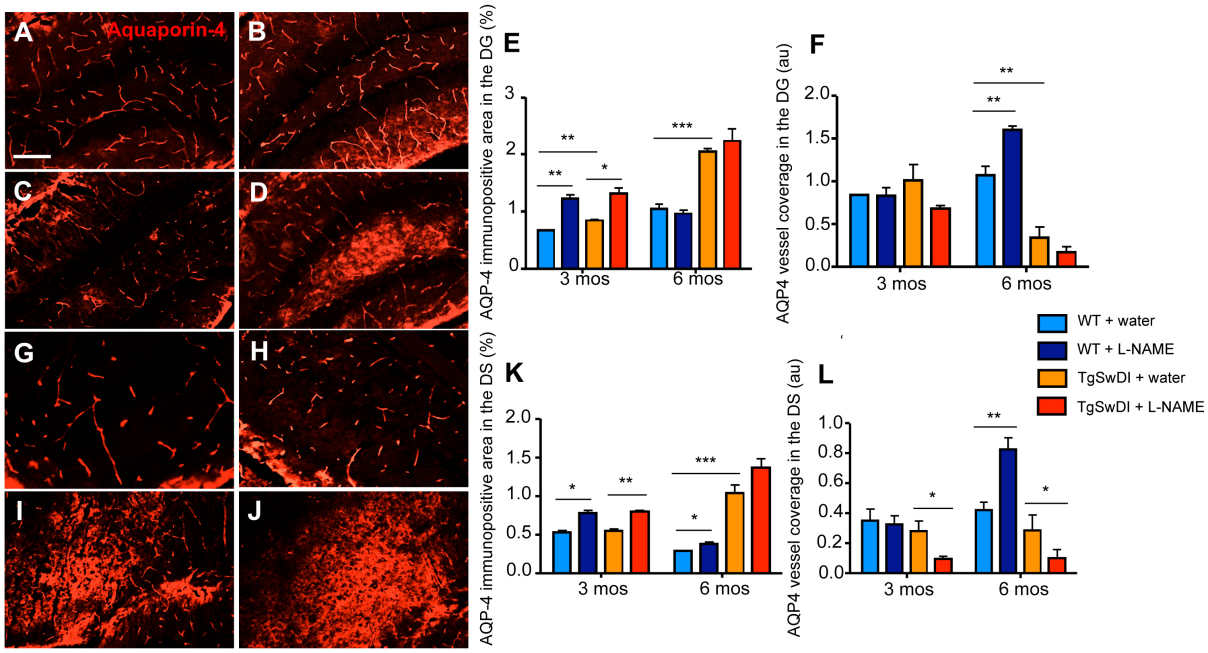
A
Aquaporin-4
B
C
D
G
H
I
J
E
AQP-4 immunopositive area in the DG (%)
3 mos
6 mos
F
AQP4 vessel coverage in the DG (au)
K
AQP-4 immunopositive area in the DS (%)
L
AQP4 vessel coverage in the DS (au)
WT + water
WT + L-NAME
TgSwDI + water
TgSwDI + L-NAME

Pericyte Loss

Pericyte loss occurs in severely affected AD patients[84] and in older TgSwDI mice[28], so levels of PDGFRβ were quantified to determine if the expression of this pericyte marker was altered in hypertensive groups. After 6 months of L-NAME treatment, hypertensive TgSwDI mice exhibited a significant decrease in PDGFRβ staining in both the DG and DS (Figure 5.8 A,D vs. B,E). Taken together, these results suggest that pericyte loss can occur at a much earlier age when there is concomitant hypertension.

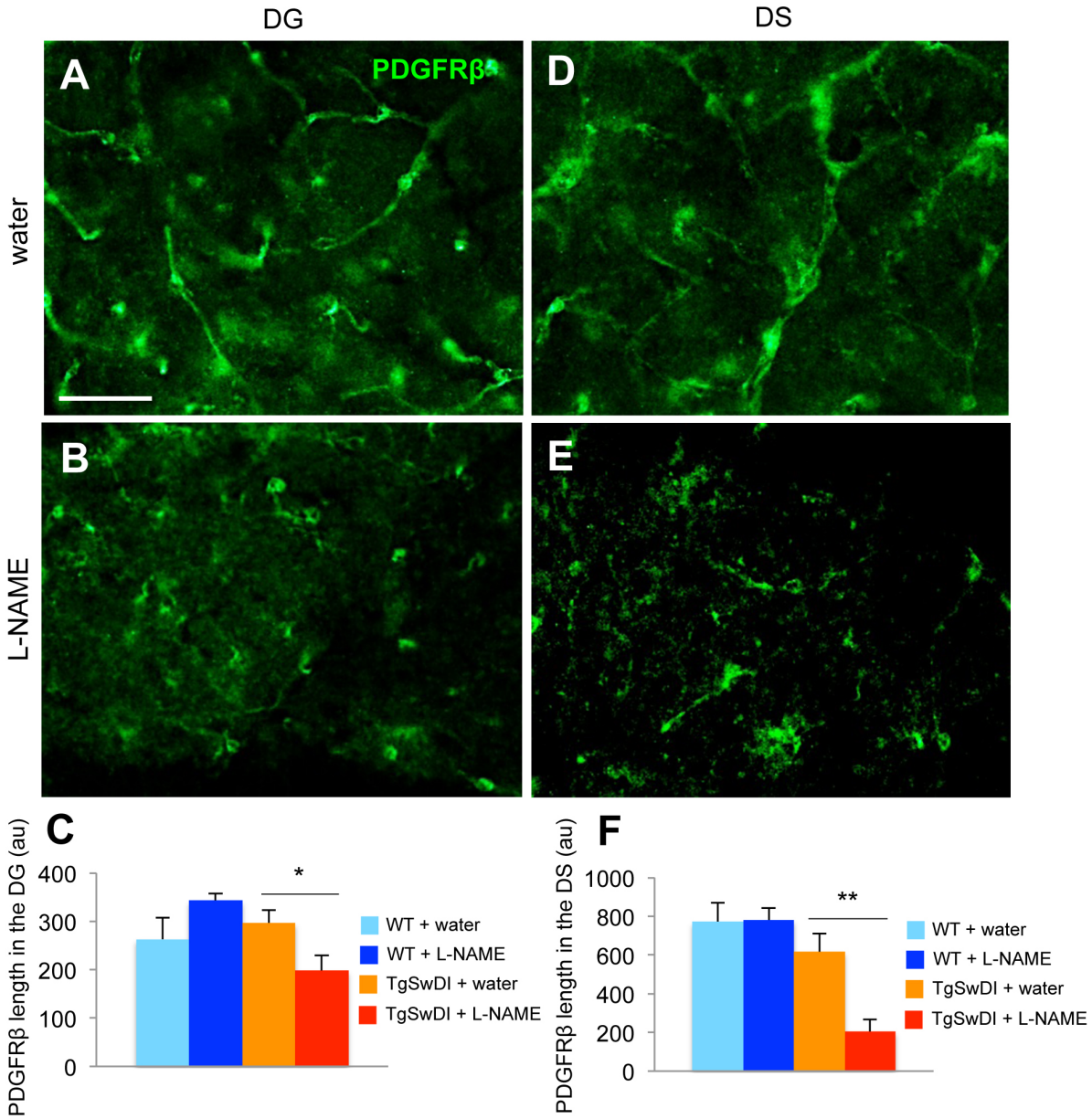

Figure 5.8. Hypertensive TgSwDI mice exhibit early pericyte loss. Anti-PDGFRβ antibody was used to examine pericyte coverage of vessels in normotensive (A,D) and hypertensive (B,E) TgSwDI mice. (C,F) PDGFRβ levels were significantly reduced in hypertensive TgSwDI mice in the DG and DS compared to control groups after 6 months of treatment (*p<0.05, **p<0.01; scale bar=50 μm; n=5-9/group).

Neuronal Loss

Neurodegeneration is a hallmark feature of AD, but many mouse models of this disease do not exhibit this pathology[83]. Under normal conditions, the TgSwDI mouse model also does not show signs of neuronal loss[85]. However, due to the accelerated timecourse of other pathologies in L-NAME-treated TgSwDI mice, the hippocampus was examined and exhibited significantly reduced neuronal staining in the DS (Figure 5.9). This degeneration occurred after short-term L-NAME treatment (3 months) and at only 6-7 months-of-age, when no neuronal loss was evident in normotensive TgSwDI mice (Figure 5.9 A-C). Normotensive TgSwDI mice at 9-10 months-of-age began to exhibit signs of neuronal loss (Figure 5.9D), making hypertension-induced cell death at this age less dramatic (Figure 5.9F).

Figure 5.9. Hypertensive TgSwDI mice exhibit early neuronal loss. Anti-NeuN antibody was used to identify neurons in the DS of normotensive (A,D) and hypertensive (B,E) TgSwDI mice. (C) Reduced NeuN intensity was observed in hypertensive TgSwDI mice after 3 months of L-NAME treatment (*$p<0.05$, n=3-9/group). (F) Since NeuN intensity was slightly decreased in normotensive TgSwDI animals after 6 months of treatment due to advanced age (9-10 months-of-age), there was no longer a significant difference between groups. Although NeuN intensity appeared reduced in the DS of hypertensive WT mice compared to normotensive WT mice after 3 and 6 months of treatment, neither change was significant (C,F; *$p<0.05$; scale bar=50 μm; n=5-9/group).

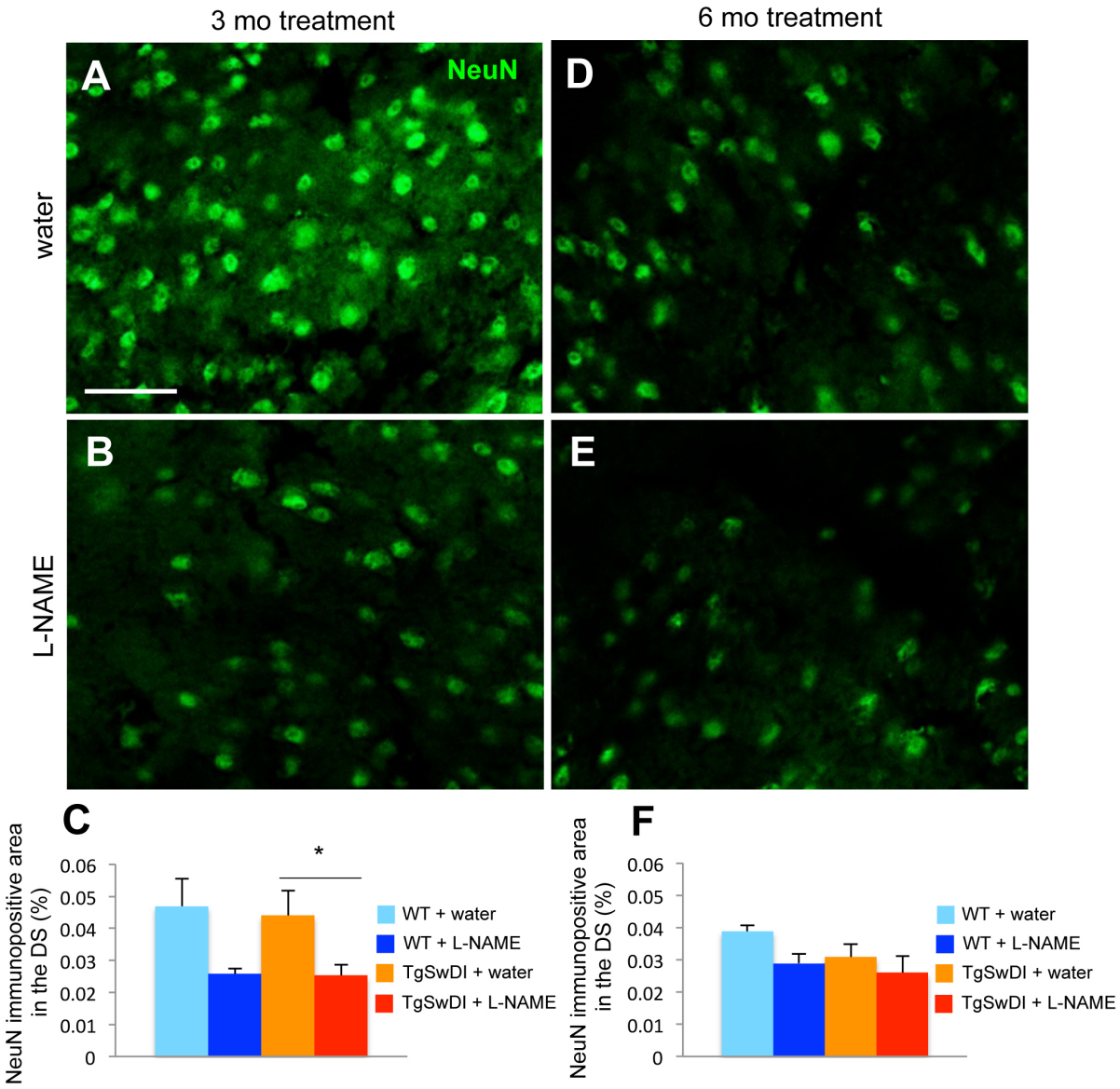
3 mo treatment
6 mo treatment
A
NeuN
D
water
B
E
L-NAME
C
F
NeuN immunopositive area in the DS (%)
0.06
0.05
0.04
0.03
0.02
0.01
0
*
WT + water
WT + L-NAME
TgSwDI + water
TgSwDI + L-NAME

Although the pericyte loss observed in hypertensive TgSwDI mice (Figure 5.8) has been reported in 18 month-old TgSwDI homozygote mice without hypertension[28], neuronal loss has never been reported in this mouse model at any age. This is an important finding, since neuronal loss is a widely accepted hallmark of AD, yet does not occur in many commonly used AD models[86].

CHAPTER 6: EFFECTS OF HYPERTENSION ON AUTOPHAGY IN TGSWDI MICE

Increased Autophagy in Hypertensive TgSwDI Mice at the NVU

Autophagy was first identified using EM techniques[87] and EM is still used to identify autophagic compartments morphologically [46]. EM has superior resolution compared to light microscopy and many antibodies used to identify autophagic compartments by immunofluorescence or light microscopy are unsuccessful. By EM, lysosomes appear as uniformly electron-dense intracellular spheres[87]. Endosomes and MVBs, which have been reported to carry Aβ into cells for degradation in AD[88], appear as round bodies containing smaller spheres of various electron densities[89].

Early ultrastructural observations of hypertensive TgSwDI brain tissue revealed abundant autophagic activity. Lysosomes and MVBs were often present near sites of CAA in hypertensive TgSwDI brain tissue processed for EM (Figure 6.1) and have been observed in all cellular components of the NVU, including microglia, pericytes, astrocytic endfeet and endothelial cells, within a narrow block of tissue at one time (not shown). This is unusual, since it is rare to see lysosomal activity in healthy brain tissue due to the rapid rate of autophagic flux[42]. Both microglia and astrocytes are known to take up and degrade Aβ deposited in AD[8, 90]. However, the participation of pericytes, endothelial cells and the endfeet of astrocytes in clearance of CAA has not been reported.

Figure 6.1. Lysosomes are present in multiple NVU cell types in hypertensive TgSwDI mice. (A-D) EM images showed the presence of lysosomes, which appeared as electron-dense spheres, in multiple cell types in hypertensive TgSwDI brain tissue. (A) Microglia nuclei (*) were present at the basement membrane of a capillary, likely due to the presence of Aβ nearby (not shown). The dark spheres within the microglia shared morphological characteristics with lysosomes (arrowhead), while the nearby round bodies containing spheres of different electron densities were morphologically similar to MVBs. Lysosomes and/or MVBs were also abundant in pericytes (B), astrocyte endfeet (C) and endothelial cells (D) in hypertensive TgSwDI mice (L, lumen; scale bar = 2 μm in A, 1 μm in B,C,D).

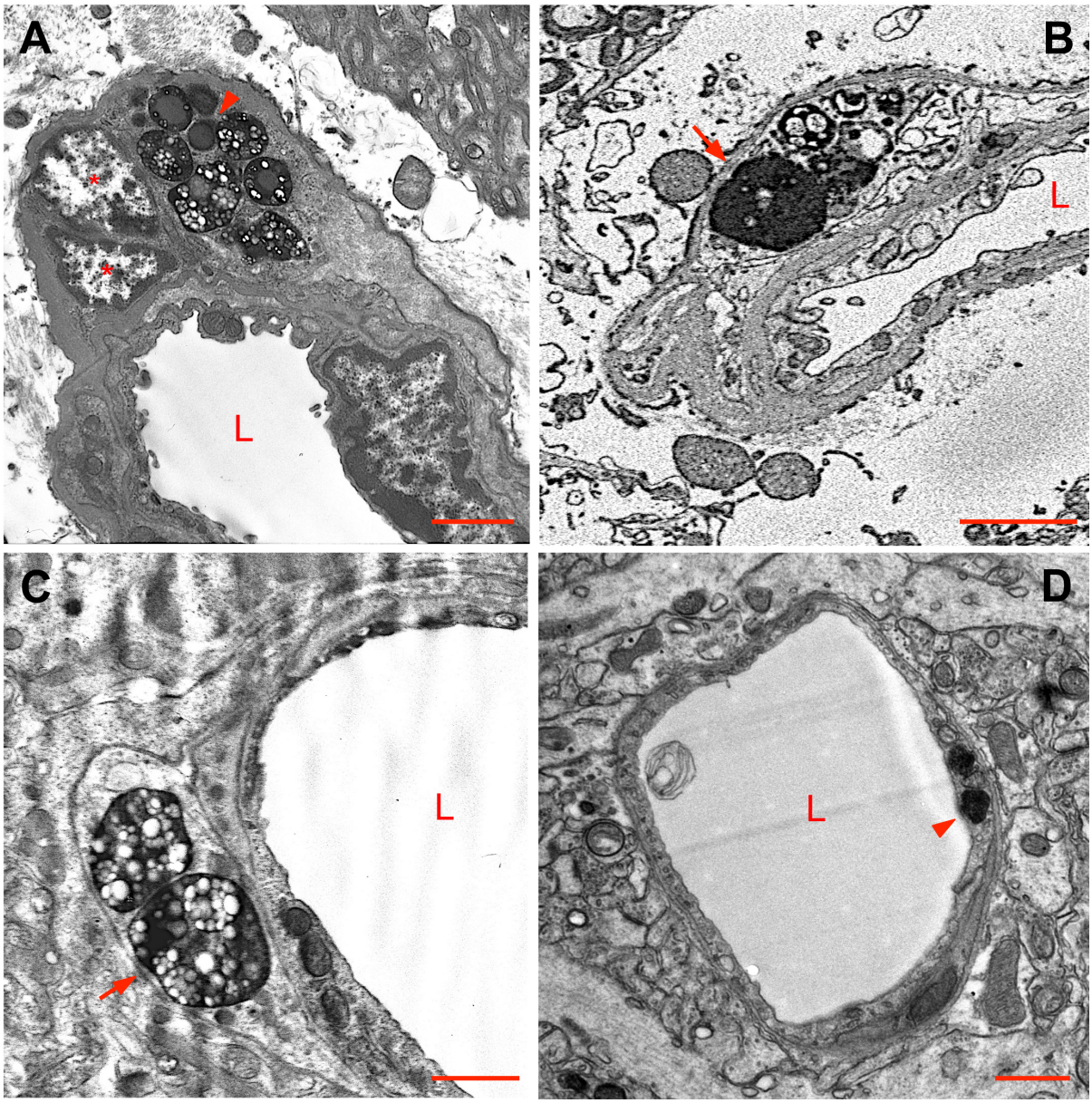
A
B
C
D
L
L
L
L
*
*

Lysosomal Protein Expression is Increased in Hypertensive TgSwDI Mice

Given the increased abundance of lysosomes observed in NVU cell types in hypertensive TgSwDI brains, levels of autophagic markers were examined in brain sections from these animals (Figure 6.2). LAMP-1 was used as a marker as previously described for the characterization of neuropathology in TgSwDI homozygous mice (Figure 3.5). Levels of LAMP-1 were significantly increased in hypertensive TgSwDI mice (Figure 6.2A,B). The staining pattern of LAMP-1 in the DS resembled that of microglia in the same mice (Figure 5.4E), consistent with the observation of lysosomes in microglia (Figure 6.1) as well as in other NVU cell types. Cathepsin D (CATD), a lysosomal aspartyl protease involved in degradation of proteins within lysosomes [91], was also increased in hypertensive TgSwDI mice (Figure 6.2 C,D) and showed a similar staining pattern to that of Iba-1 and LAMP-1 (Figure 5.4E, 6.2A). Microglial co-staining is required to confirm cell type-specific expression of these markers.

Figure 6.2. Levels of lysosomal markers are increased in hypertensive TgSwDI mice. Given the abundance of lysosomes observed by EM at the NVU in hypertensive TgSwDI mouse brains, tissue sections from hypertensive TgSwDI mice were examined for the presence of lysosomal markers. Levels of LAMP-1, a protein found on endosomal and lysosomal membranes, were increased in the DS of both normotensive (not shown) and hypertensive TgSwDI (A) groups relative to WT groups (B, ***p<0.001). Moreover, levels of LAMP-1 were significantly increased in hypertensive TgSwDI mice relative to normotensive TgSwDI mice (B, **p<0.01). Since LAMP-1 is not specific for lysosomes, levels of the lysosomal protease CATD were examined using an anti-CATD antibody. Again, both normotensive (not shown) and hypertensive TgSwDI (C) groups exhibited a significant increase in CATD levels relative to WT mice (D, **p<0.01). Elevated levels of CATD were also observed in hypertensive TgSwDI mice relative to normotensive TgSwDI mice (D, ***p<0.001), similar to what was observed with LAMP-1 staining (scale bar = 50 μm).

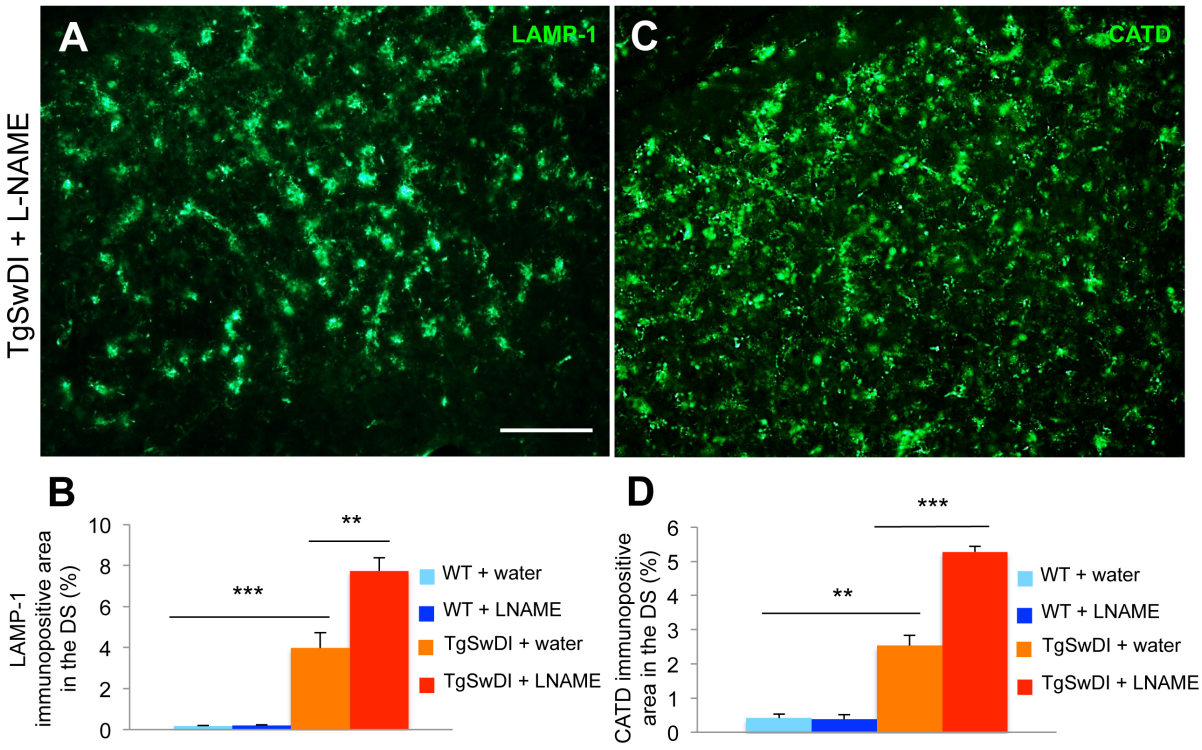
A
LAMR-1
C
CATD
TgSwDI + L-NAME
B
LAMP-1 immunopositive area in the DS (%)
10
8
6
4
2
0
***
**
WT + water
WT + LNAME
TgSwDI + water
TgSwDI + LNAME
D
CATD immunopositive area in the DS (%)
6
5
4
3
2
1
0
**
***
WT + water
WT + LNAME
TgSwDI + water
TgSwDI + LNAME

Effect of Hypertension on Astrocyte Endfoot Morphology

By EM, astrocyte endfeet appeared less electron-dense than surrounding cells (Figure 1.2). In normotensive WT mouse brains, lysosomes as well as vacuolar structures within astrocyte endfeet were occasionally observed (not shown). However, such vacuoles were abundant in astrocyte endfeet in both hypertensive WT (Figure 6.3A) and hypertensive TgSwDI mice (Figure 6.3B).

These vacuoles were morphologically similar to structures observed in primary cortical neuron cultures from rat pups after induction of autophagy by rapamycin treatment[42]. These structures are also morphologically similar to known autophagic structures: MVBs, AVs and multilamellar bodies (MLBs) (Figure 6.4). Thus, it is possible that the vacuolar structures observed in the endfeet of hypertensive TgSwDI and WT mouse brains were produced during autophagic flux. However, since the identity of these structures has not yet been confirmed by IEM analysis or by examination after induction or suppression of autophagy, they will be referred to as autophagic compartments (ACs) herein. In hypertensive TgSwDI and WT brain tissue, ACs are so abundant that they appear to cause dramatic swelling of the astrocyte endfeet (Figure 6.3).

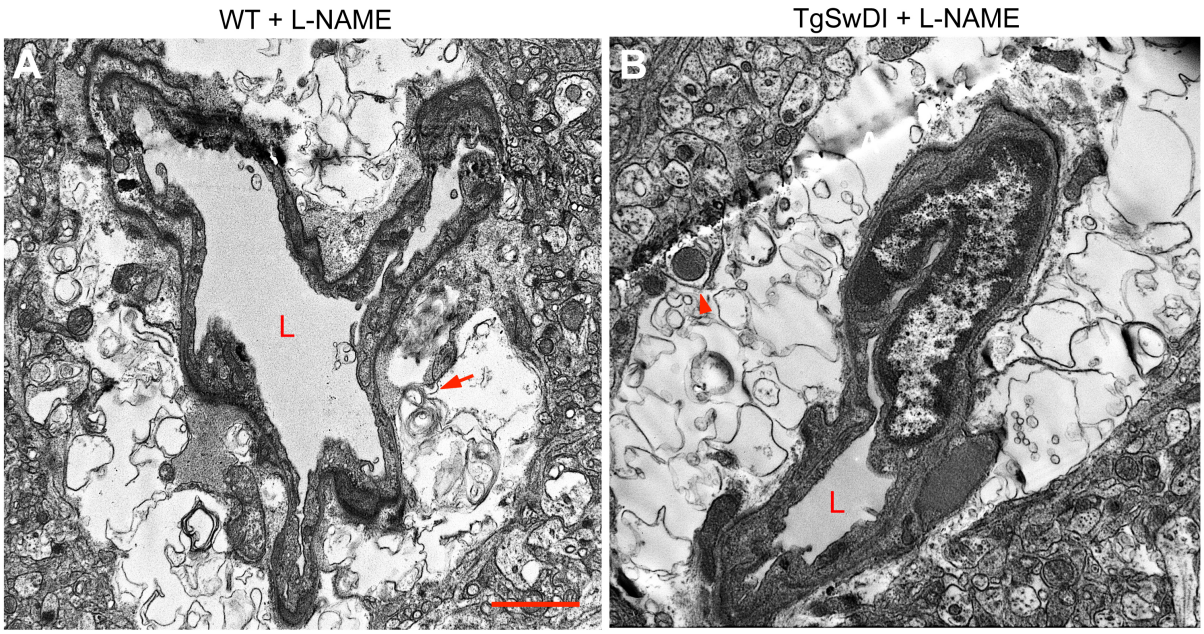

Figure 6.3. Hypertension causes buildup of ACs in swollen astrocyte endfeet. The buildup of ACs is most noticeable in the astrocyte endfeet of hypertensive WT (A) and TgSwDI (B) mouse brains. Astrocyte endfeet are typically more electron-dense than surrounding tissue (Figure 1.2). In hypertensive TgSwDI and WT mice, the accumulation of ACs resulted in a dramatic enlargement of these astrocytic processes. In (A), two MLBs (arrow) are observed amongst the ACs while in (B), a lysosome (arrowhead) can be observed (L, lumen; scale bar = 2 μm).

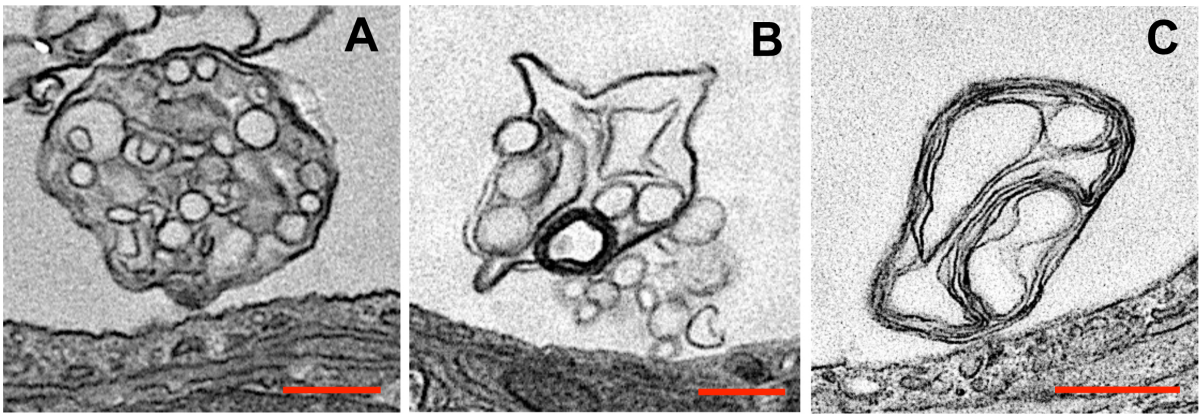

Figure 6.4. ACs in hypertensive mice share morphological features with autophagic structures. ACs observed using EM in hypertensive WT (A) and TgSwDI (B,C) mice resemble different autophagic structures. The round compartments and darker components contained within the membrane of the AC shown in A resemble features of an MVB. The structure in B is morphologically similar to an AV, which has membranes surrounding less electron-dense components. An AC that shared characteristics of an MLB can be observed in C. Due to their morphological similarities to a variety of different autophagic structures, ACs may refer to multiple entities, rather than one discrete type of autophagic body (scale bars = 500 nm).

Clearance of ACs Through the BBB

Further EM analysis revealed that ACs were often localized within tight junctions of endothelial cells in hypertensive TgSwDI and WT mice (Figure 6.5). The localization of ACs to tight junction structures may have altered the permeability of the BBB and contributed to the BBB leakage observed in hypertensive TgSwDI and WT mice (Figure 5.5).

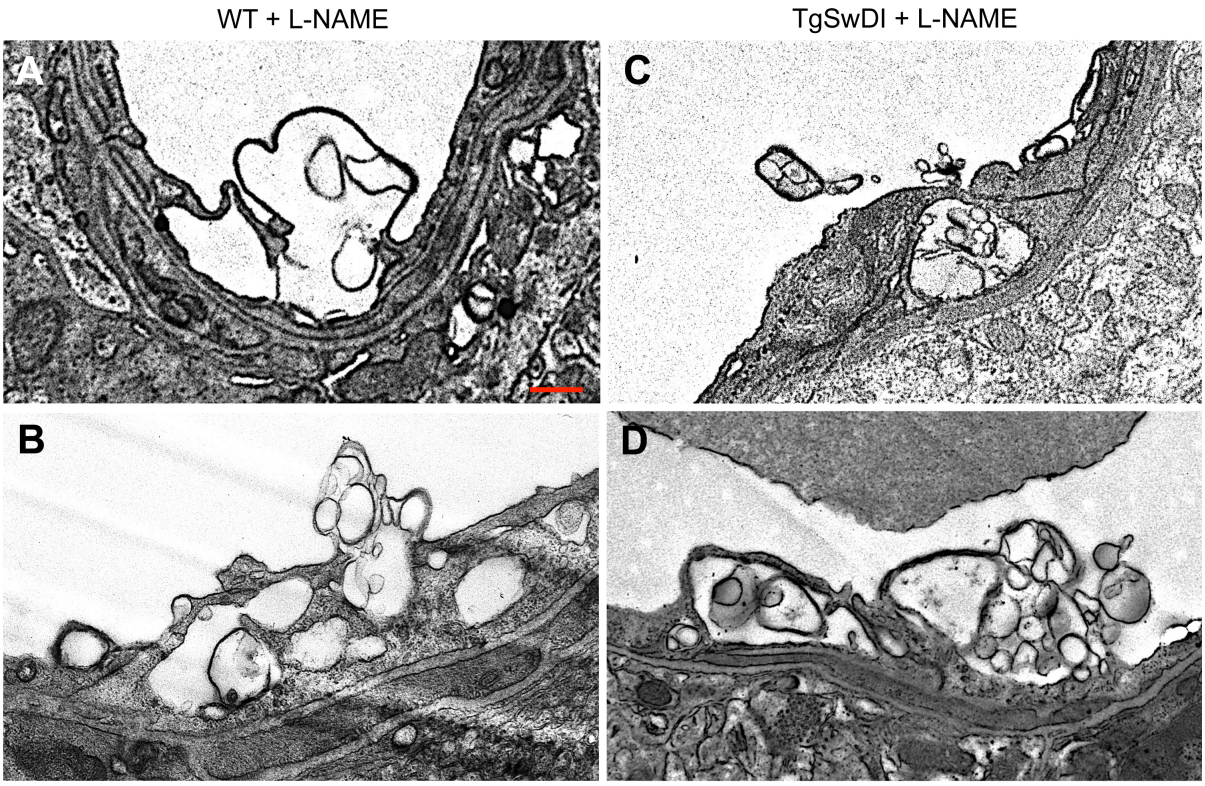

Figure 6.5. ACs are cleared through the BBB in hypertensive mice. ACs are often abundant within tight junction structures in hypertensive WT (A,B) and TgSwDI (C,D) mice, but never in normotensive WT or TgSwDI mice (not shown). Moderate (A,C) to severe (B,D) disruption of the tight junctions can be observed in the brains of hypertensive mice of both genotypes (scale bar = 500 nm). The disruption of tight junctions in hypertensive mice due to the presence of ACs may contribute to the reduced BBB integrity observed in these animals.

The frequent presence of ACs within the lumen of capillaries in hypertensive mice (Figure 6.6) suggests active clearance of these structures from the brain to the blood. Clearance of ACs could have occurred through endothelial tight junctions (Figure 6.5) or through exocytosis by endothelial cells (Figure 6.7). Clearance of autophagic structures into the blood has not been reported previously, so should be considered with caution. However, potentially similar mechanisms, such as receptor-mediated transcytosis, have been reported[92].

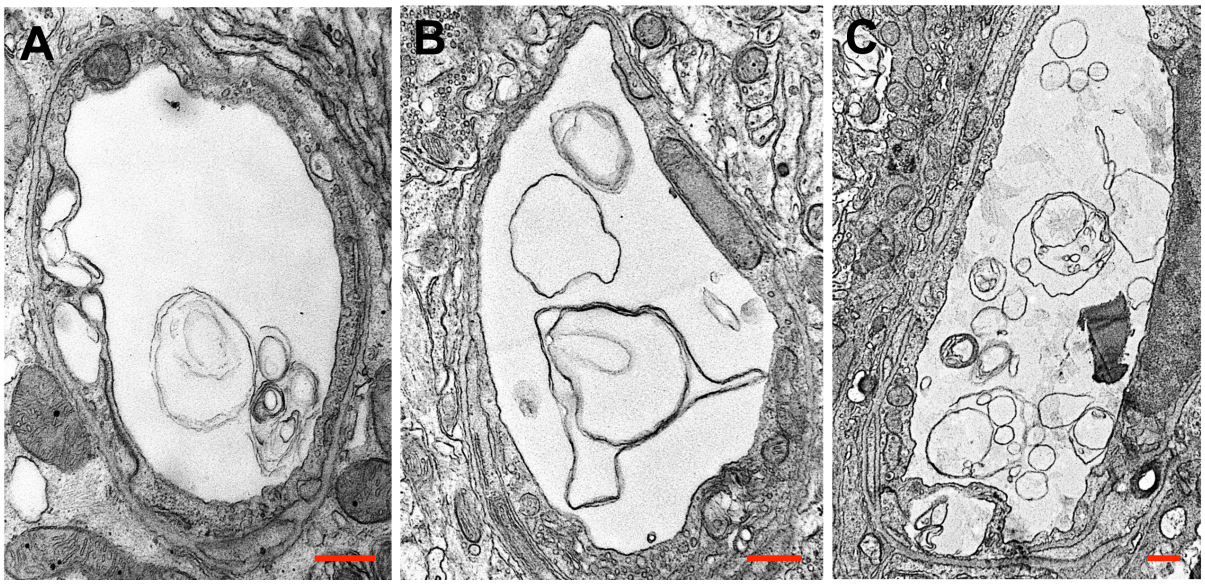

Figure 6.6. Hypertension causes buildup of ACs in the capillary lumen.

Lumenal ACs were observed in brain capillaries of hypertensive TgSwDI (A,B) and WT (C) mice. ACs were observed in the lumen of capillaries at low (A), moderate (B) and high (C) abundance in hypertensive mice of both genotypes. The presence of ACs in the capillary lumen suggests that ACs were being cleared from the brain into the circulation (scale bars = 500 nm).

It is likely that the ACs observed in the lumen of capillaries by EM (Figure 6.6) were in the process of being exocytosed by endothelial cells, since completely detached structures would have been carried away by capillary flow or perfusion. Three-dimension electron microscopy (3D-EM) revealed that ACs that appeared to be detached in the lumen were actually attached to endothelial cells at nearby points not captured in the EM image (Figure 6.7).

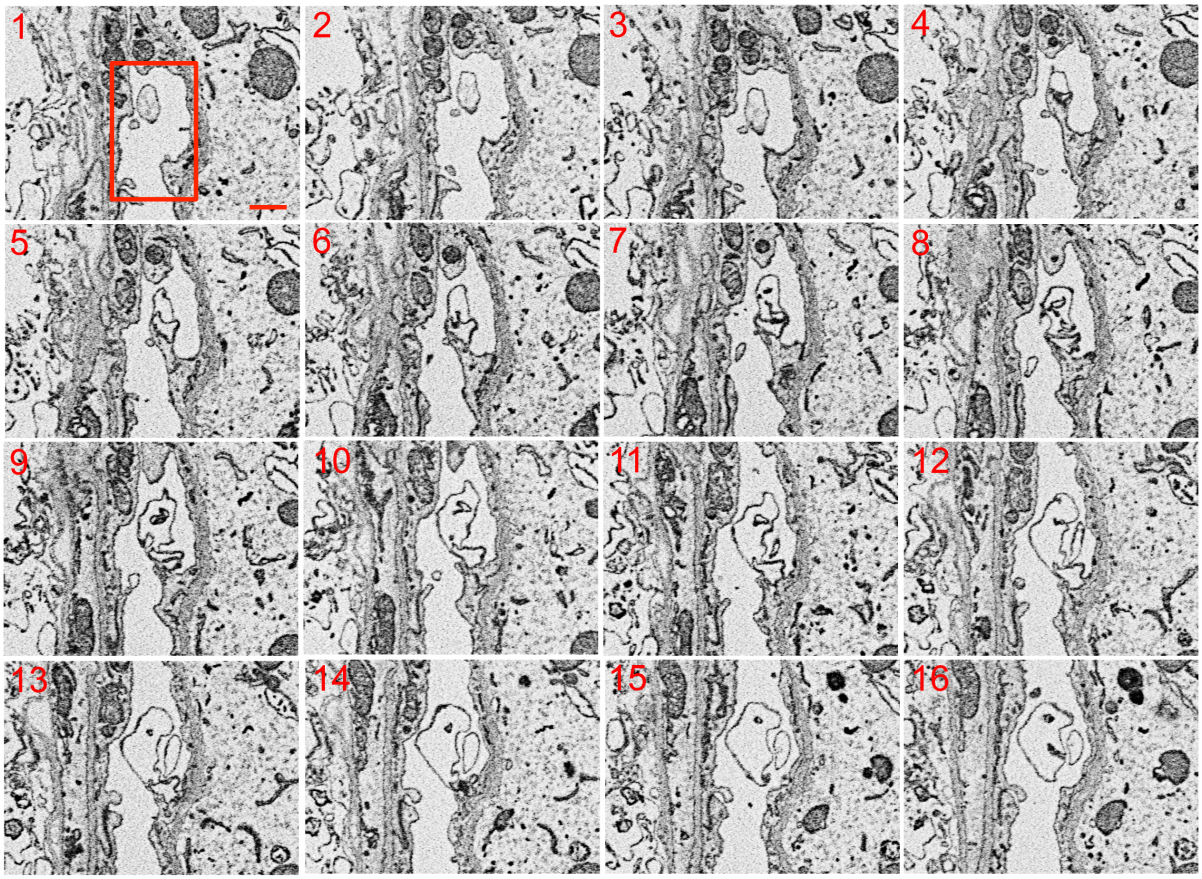

Figure 6.7. ACs are exocytosed from endothelial cells in hypertensive mice. Sequential EM images processed using 3View are presented in order of image collection from left-to-right and top-to-bottom. Early during image capture, the AC (red box) observed in the capillary lumen of a hypertensive TgSwDI mouse, appeared completely lumenal. Images captured at different points along the Z-axis (presented here at 100-nm intervals) show that the AC was attached to the nearby endothelial cell. The endothelial cell appeared to be in the process of exocytosing the AC into the capillary lumen (scale bar = 1 μm).

Though ACs were occasionally observed in astrocyte endfeet in normotensive WT mice, they were very rarely observed within the lumen of capillaries in normotensive TgSwDI or normotensive WT mice (not shown). Notably, they were never observed within tight junction structures in normotensive animals. For this reason, the ACs that appeared to disrupt the BBB seem to be a product of hypertension.

CHAPTER 7: DISCUSSION AND CONCLUSIONS

Pathological Timecourse in TgSwDI Mice

The hippocampus coordinates memory consolidation and spatial navigation and is one of the first regions in the brain to suffer damage in AD[93]. The DG receives all hippocampal inputs and passes them through the hippocampus proper (CA1-4) to the subiculum, which projects out of the hippocampus to the entorhinal cortex[94]. Thus, proper function of the DG, which receives all hippocampal inputs, and the subiculum, which sends hippocampal projections, are essential to memory consolidation and spatial navigation. Additionally, rat studies suggest that the subiculum is involved in the spread of Aβ, as lesions in this region inhibit plaque formation in other brain regions[95]. The earliest pathological changes observed in the TgSwDI mouse model occurred in the subiculum (Figure 3.2-3.5). It is unclear why this occurs, since expression of the APP transgene is not localized to particular brain regions in the TgSwDI mouse line. The cognitive deficits observed in TgSwDI mice as well as the pathological progression observed throughout the brain over time may be due in large part to the presence of early pathology in the subiculum.

Given the abundance of Aβ plaques in brains of humans with severe AD, it is unclear whether Aβ deposits are a contributor to dysfunction in the disease or merely an indication of pathological severity. Interestingly, at 2 months-of-age, TgSwDI mice exhibited dramatic microglia activation in the DS (Figure 3.3D) relative to the amyloid deposited at this age, which was undetectable (Figure 3.2A). Since the transgenic mutations in TgSwDI mice result in overproduction of Aβ, it is

reasonable to assume that Aβ production is the cause of the early microglial activation, since no activation was observed in WT mice at any age (Figure 3.3). Importantly, though no fibrillar Aβ deposits were detected in TgSwDI mice at 2 months-of-age by ThioS staining, soluble forms of Aβ may still have been present and may have resulted in the observed activation of microglia. LAMP-1 staining was also increased in TgSwDI mice at around 3 months-of-age, again prior to widespread plaque or CAA pathology. The timecourse of these changes suggests that microglial activity at 2 months-of-age was able to keep Aβ deposition low, but was overwhelmed at around 3 months-of-age when Aβ deposition was first observed in these mice (Figure 3.2B). At this age, observable increases in autophagy were also noted (Figure 3.5B). Alternatively, early soluble forms of Aβ could have fibrillized after reaching a certain threshold. It is unclear whether changes in expression of autophagy markers represent dysfunctional autophagy or simply upregulated autophagy serving to control the increasing Aβ load in the brain. It is also unclear whether fibrillar and oligomeric forms of Aβ had different effects on the microglia activation or autophagic processes observed[96, 97]. It is possible that early mechanisms acting to clear plaques observed at 3 months-of-age resulted in microvascular deposition of Aβ by 6 months-of-age, as well as a reduction in plaque size and number. It is also possible that early plaques were easily cleared, while amyloid deposited as CAA occurred later during the pathological timecourse, but persisted.

Breakdown of the BBB was observed as early as 3 months-of-age in TgSwDI homozygotes. Since Aβ deposition was not severe and was also not vascular at 3 months-of-age (Figure 3.2B), the early increases in microgliosis and autophagy may be more directly linked to loss of BBB integrity than Aβ abundance or CAA. If opening of the BBB were in fact a mechanism for removal of Aβ from the brain, as proposed in Chapter 6 (Figure 6.5, 6.7), the timescale of increased BBB permeability is consistent with the timescale of other clearance mechanisms relative to Aβ load. However, the basis for such a hypothesis is not well established and requires confirmation.

Accelerated Neuropathology in Hypertensive TgSwDI Mice

Under normal conditions, hypertension induces pathological changes within the cerebral vasculature, resulting in impaired autoregulation, microbleeds, and lacunar infarcts, as well global downstream changes, such as WMLs and atrophy[31, 98-103]. In fact, these changes within the cerebral vasculature of hypertensive individuals also occur in AD patients in the absence of hypertension[104-106]. Additionally, midlife hypertension is a significant risk factor for the development of AD later in life[16]. Hypertension may initiate vascular damage prior to the onset of AD, allowing symptoms to be more pronounced and progress more quickly after onset. Additionally, compromised vessels may be more vulnerable to the deleterious effects of Aβ. For example, since hypertension results in reduced BBB integrity (Figure 5.5), blood components may enter the brain before large-scale accumulation of Aβ occurs. These blood components may serve as a seed for Aβ deposition and

increase vascular inflammation (Figure 5.4), resulting in cellular damage and the release of toxic molecules[107].

The location, but not abundance, of Aβ deposits was altered in hypertensive TgSwDI mice, which also exhibited dramatic cognitive decline. These findings suggest that microvascular Aβ contributed more to cognitive decline than parenchymal plaques. CAA deposits were found to adhere to capillary basement membranes (Figure 5.3G), which normally bind NVU cells together. For this reason, Aβ deposited as CAA may act as a physical barrier to cell signaling at the NVU. Moreover, CAA could obstruct astrocyte endfoot binding and contribute to pericyte loss (Figure 5.8). Both astrocytes and pericytes are involved in the recruitment of blood flow during neuronal activity and damage to or interference with signaling of these cell types in hypertensive TgSwDI mice may impair neurovascular coupling.

Aβ is thought to be deposited as CAA due to failed clearance across the BBB and along perivascular spaces[108]. Since L-NAME treatment resulted in increased CAA in TgSwDI mice without an overall increase in Aβ levels, hypertension may have a detrimental effect on these Aβ clearance pathways. L-NAME inhibits eNOS and thereby prevents the production of the vasodilator NO. It could be that NO-mediated vasodilation is required for effective clearance of Aβ across the BBB or along perivascular drainage pathways. If L-NAME disrupted this process, Aβ would be preferentially deposited along capillaries, as observed in hypertensive TgSwDI mice.

The neuronal loss in hypertensive TgSwDI mice (Figure 5.9) could have resulted from the proposed reductions in blood flow as well as impaired function of NVU support cells that either degenerate (pericytes; Figure 5.8) or are chronically activated (microglia; Figure 5.4). Since brain atrophy is associated with hypertension in humans [31] and hypertensive WT mice exhibited a trend towards reduced neuron number, it is possible that the vascular changes that occur during hypertension in WT mice, such as BBB leakage (Figure 5.5), affect neuronal health. However, the changes specific to TgSwDI mice with hypertension, such as dramatically increased microgliosis (Figure 5.4) and severe CAA (Figure 5.3) likely contributed in some way. In addition to the cytotoxic effects of Aβ itself[109-111], activated microglia are known to produce cytotoxic molecules[107], which may damage neurons. Therefore, the increased microvascular Aβ deposition and microgliosis in hypertensive TgSwDI mice, but not in hypertensive WT mice, may have contributed to the neuronal loss observed in this group.

Though models of comorbid hypertension and AD are limited, the results presented here are consistent with what has been observed in other models. Ang-II infusion in APPPS1 mice results in a more rapid onset of AD pathology[112]. It is possible that long-term hypertension facilitated by the use of L-NAME exacerbated previously observed pathologies, such as cognitive decline (Figure 5.2) and early and dramatic Aβ deposition (Figure 5.3), and revealed new neuropathologies not previously observed, such as microglia activation (Figure 5.4), BBB leakage (Figure 5.5), and pericytic and neuronal loss (Figure 5.8, 5.9).

Studies linking hypertension with AD define midlife as the time between the ages of 40 and 64 years. Midlife hypertension is associated with an increased risk of developing AD, but hypertension later in life (≥65 years-of-age) does not have this association. Given that heterozygous TgSwDI mice developed AD symptoms around 6 months-of-age (Aβ deposition, microgliosis; Figures 5.3, 5.4) and cognitive decline around 10-12 months (not shown), hypertension was induced at a time point corresponding to early adulthood developmentally, to maximize the duration of hypertension before the onset of AD symptoms. Importantly, studies linking hypertension with AD examine BP prior to onset of AD symptoms. Though midlife hypertension is a significant risk factor for AD and treatment alleviates this risk[34, 36], dramatic reduction in BP often occurs at later stages of AD, after which point antihypertensive use is deleterious to cognitive function[33, 34]. Hypertension may compromise vascular integrity during midlife and lead to cellular, basement membrane and/or BBB damage. However, after the onset of AD symptoms, low BP may aggravate brain hypoperfusion already present in AD due to other types of vascular damage. Additionally, since patients exhibit low BP during moderate and severe AD stages, rather than during mild cognitive impairment, and since the association between low BP and AD becomes stronger in more severe cases of AD, it has been proposed that AD somehow causes the low BP observed in patients[35]. This may be due to loss of or damage to cell types that control blood flow or it could be a result of other changes that often occur over the course of the disease, such as weight loss and reduced activity.

Although others have shown pericyte loss in TgSwDI mice at 18 months-of-age[28], L-NAME-induced chronic hypertension caused pericyte loss significantly earlier (9-10 months-of-age; Figure 5.8). Furthermore, neuronal loss has never been reported in this transgenic model, yet hypertensive TgSwDI mice demonstrated significant neurodegeneration in a subregion of the hippocampus (Figure 5.9). Moreover, not only did hypertension result in quantifiable neuronal loss, but it did so quite early (6-7 months-of-age) relative to the few other mouse lines that exhibit this feature of AD[113]. At 6-7 months-of-age, the first indications of AD (Aβ deposition, neuroinflammation, cognitive decline) are often just becoming apparent in other AD mouse models[113-115]. These findings are notable, since neuronal loss is widely accepted as a hallmark of AD, yet does not occur in many commonly used AD models[86]. If hypertension indeed accelerates AD pathogenesis, then a reasonable hypothesis is that neuronal loss is a downstream effect of the abundant microvascular amyloid pathology observed in TgSwDI mice. Neuronal loss is often not reported in AD mice possibly due to their short lifespans relative to the time required for AD to result in neuronal loss in humans. Pairing hypertension with genetic predisposition to AD may represent a more complete model of AD than traditional AD mouse models.

The Effects of Hypertension on Autophagy in TgSwDI and WT Mice

Abnormalities of the lysosomal system have been identified in the AD brain, though these findings have only been described in neurons[116]. Given that CAA is increased

in hypertensive TgSwDI mice (Figure 5.3) without increased overall levels of Aβ or an altered ratio of Aβ40 to 42 compared to normotensive TgSwDI mice (not shown) and that lysosomal markers LAMP-1 and CATD are also increased in hypertensive TgSwDI mice, it is possible that Aβ deposited microvascularly differentially affects autophagic processes relative to Aβ deposited as plaques in the brain. This process could be due to the cell types located near CAA and the ability of these cell types to take up and degrade Aβ (Figure 1.2). Although CAA seems to increase autophagic flux in NVU cell types, the most dramatic changes in autophagic processing appear to be brought about by hypertension.

Typically when identification of autophagic structures is based on morphology alone, only vesicles containing cytoplasmic material, in most cases ribosomes or mitochondria, can be called autophagic in mammalian cells[117]. Given the lack of electron-dense material inside ACs, the supposition that they may be remnants of an autophagic process is purely speculative.

Normal AV induction, but impaired clearance would theoretically result in an abundance of membrane-bound compartments with little electron-dense material inside[116]. The ACs observed in hypertensive brains are most similar in appearance to AVs, a term which has been used to refer to autophagosomes, amphisomes and autolysosomes. Thus, AV is a general term for autophagy-related vesicular structures at an intermediate stage in autophagic flux [116]. AVs are less electron-dense than MVBs and have fewer surrounding membranes than MLBs (Figure 6.4).

However, since structures resembling AVs, MVBs and MLBs have been observed in the brains of hypertensive mice, it is possible that “AC”, as it is used here, refers to a group of structures at different points in autophagic processing.

In general, the ratio of early to late autophagic compartments is indicative of the cause of accumulation[117]. ACs in hypertensive animals appear to be at a late stage of clearance due to their lack of electron-dense components, since even late autophagic compartments typically still contain electron-dense material[117]. Accumulation of late autophagic compartments, may suggest a defect in ultimate degradation of these structures.

Autophagy is induced in heart tissue during hypertensive heart disease[118] as well as in neurons in the brains in hypertensive animals[119]. Hypertension is also known to increase levels of Aβ in WT mice due to RAGE-mediated Aβ-influx through endothelial cells[37]. Since ACs were rarely observed in normotensive TgSwDI mice, despite their high Aβ load relative to hypertensive WT mice, it is possible that the mechanism by which Aβ enters the brain is involved in production of ACs. Importantly, APP is present in membranes of organelles involved in autophagy[47] and Aβ production may be elevated during the increased autophagic flux that occurs during hypertension. Hypertension could also alter autophagic processes at the NVU by causing damage to the cell types responsible for Aβ clearance. If cells are prevented from properly degrading Aβ, this could result in the observed buildup of

ACs in hypertensive TgSwDI and WT brains (Figure 6.3, 6.5, 6.6), as well as the increased CAA in hypertensive TgSwDI mice (Figure 5.3).

Since ACs were observed in the lumen of capillaries in normotensive WT mice, albeit rarely, clearance of ACs through endothelial cell exocytosis may be a transient mechanism for the transfer of brain components to the blood. This process may play a role in cellular waste removal from the brain, supplementing clearance along perivascular drainage pathways[108]. This process could turn over rapidly in normotensive WT mice, but could be altered in hypertensive animals leading to buildup of ACs near endothelial cells.

Whether the proposed opening of the BBB for clearance of ACs would result in improved removal of cellular waste components from the brain or a dramatic infiltration of blood components into the brain and subsequent neuroinflammation is unclear. Deleterious changes involving increased BBB permeability, such as microhemorrhage and increased risk of stroke, have been observed in AD[12, 13]. However, some recent studies have shown that focused ultrasound (FUS) is effective in clearing Aβ from the brain and restoring cognitive abilities in rodent models of AD[120], due to activation of glia and transient and focal opening of the BBB to endogenous antibodies. Importantly, neither the increased BBB permeability in TgSwDI mice due to hypertension (Figure 5.5) nor the increase in microglial activation (Figure 5.4) appears to have a positive effect on cognitive function (Figure 5.2) or Aβ-load (Figure 5.3). Perhaps the presence of increased levels of Aβ within

the microvasculature impacts the infiltration of useful endogenous antibodies into the brain in TgSwDI mice. Importantly, FUS appeared to have an effect on the activation state of microglia, as they increase in size, though not in number, after FUS. The increased Iba-1 staining in hypertensive TgSwDI mice does not necessarily reflect a microglial state of increased Aβ clearance. Additionally, FUS localizes BBB permeability to specific areas rather than increasing general BBB permeability, which could have different effects on Aβ clearance.

In tissue from hypertensive TgSwDI mice with CAA, endfeet appeared to be enlarged due to abundance of ACs that collected there (Figure 6.3). Swollen astrocyte endfeet have been observed in a variety of conditions from schizophrenia to ischemia, as well as in CAA[21, 22, 121, 122]. However, since ACs are poorly defined currently, the similarity of swollen astrocyte endfeet in hypertensive TgSwDI mice compared to swollen endfeet observed in other conditions is unclear. Since astrocyte endfeet perform quite a large number of neuronal support functions at the NVU[123-125], disruption of their morphology and function could have dramatic effects on neuronal health and function. Given the close physical relationship between astrocyte endfeet and CAA, as well as the increased presence of ACs within endfeet, it is very surprising that the experimental cohort did not show disruption in astrocytic markers (not shown). Since ACs are occasionally observed in astrocyte endfeet in normotensive WT tissue, though never within tight junction structures (not shown), it is unclear whether they are part of a normal process that occurs transiently in WT brains or whether they are indicative of pathology. It is possible

that the endfeet are a common site for autophagic processes given the well-described role of astrocytes in degradation and protein clearance[9]. However, this process may be disrupted due to hypertension and thus ACs appear much more frequently near hypertensive capillaries in the brain.

Future Directions

Most of the changes observed in the hypertensive TgSwDI mice from the experimental cohort were also observed in the pilot cohort (not shown). However, differences in astrocyte markers in the hypertensive TgSwDI group in the pilot cohort (Figures 5.6, 5.7) were not recapitulated in the experimental cohort. One difference between these two cohorts that could account for this difference is that the pilot cohort contained only male mice. This was due to the fact that the females were undergoing a second round of IVF in order to generate mice for the experimental cohort. The presence of estrogen in the brains of female mice may be slightly neuroprotective[126]. If repeated analysis reveals that important astrocyte markers are normal in hypertensive TgSwDI brains from the experimental cohort, repeating the experiment using only male mice may be useful in order to investigate additional features of astrocyte pathology.

It would be interesting to examine levels of tight junction proteins in hypertensive and normotensive brains of each genotype to determine if markers of tight junctions are altered. Reduced expression of tight junction markers may contribute to the fragmentation of tight junctions observed by EM in hypertensive TgSwDI mice

(Figure 5.5) and the disrupted tight junction structures in hypertensive TgSwDI and WT mice due to the presence of ACs and the BBB leakage observed in these animals (Figure 5.5).

Previous attempts to confirm that the ACs were indeed autophagic by IEM were unsuccessful, because techniques required for ultrastructural preservation can interfere with antigenicity. This work is ongoing with different antibodies that might display stronger binding to tissue fixed for EM. It would also be useful to know if the ACs contain soluble Aβ, such as the more toxic oligomeric forms of the protein[127]. I would expect this to be the case if transcytosis of ACs were a mechanism for removal of Aβ from the brain, rather than simply evidence of dysfunctional lysosomal clearance mechanisms. The fact that levels of Aβ oligomers in plasma negatively correlate with AD severity in patients, suggests that clearance through the blood may reflect a mechanism for preserving cognitive ability and when it is disrupted, cognitive function suffers[128].

Though EM is very useful for the qualitative study of cellular phenomena, quantification of findings by EM can be more challenging than by traditional light or fluorescence microscopy. Measurement of the ratio of early to late autophagic compartments by Western blotting may provide insight into the disruption that occurs in hypertensive mice. Unfortunately, less is known about molecular markers involved in clearance of autophagic structures than formation and maturation[42]. Comparison of hypertensive and normotensive WT mice may also provide information regarding

the nature of ACs, since autophagic flux appears to occur normally in normotensive WT mice. To what extent ACs build up in astrocytes and tight junctions in hypertensive WT compared to hypertensive TgSwDI mice also remains to be determined. Finally, examination of human tissue with and without hypertension and with and without comorbid AD will be important to confirm that the findings described are relevant to humans with these conditions and not an artifact of L-NAME treatment itself.

APOE is involved in cellular uptake of Aβ as well as trafficking of Aβ to lysosomes in an isoform-dependent manner[129]. Interestingly, there is a stronger correlation for protective effect of antihypertensive drug use among APOE4 carriers[130, 131]. Antihypertensive drug use appears to abolish the risk of LOAD conferred by the APOE4 allele. This correlation could be explained by a common effect of APOE4 and hypertension on autophagy. If both risk factors disrupted autophagic processes, then their coincidence would exacerbate the effect of one or the other alone. Examining brain tissue from APOE4 individuals with and without hypertension could shed light on the interaction between these two risk factors.

Understanding the molecular pathways responsible for buildup of ACs as well as the proposed exocytosis through endothelial cells could potentially prove therapeutically useful. If AC exocytosis through endothelial cells were a mechanism for removal of cellular waste, enhancing this process may prove beneficial, especially in the case of hypertension, where the process appears to occur inefficiently. If this process

instead results in loss of BBB integrity and leakage of blood components into the brain, inhibiting it might prove more therapeutically beneficial.

REFERENCES

1. Kowalska A. Amyloid precursor protein gene mutations responsible for early-onset autosomal dominant alzheimer's disease. *Folia Neuropathol*. 2003;41:35-40

2. Potter R, Patterson BW, Elbert DL, Ovod V, Kasten T, Sigurdson W, Mawuenyega K, Blazey T, Goate A, Chott R, Yarasheski KE, Holtzman DM, Morris JC, Benzinger TL, Bateman RJ. Increased in vivo amyloid-beta42 production, exchange, and loss in presenilin mutation carriers. *Sci Transl Med*. 2013;5:189ra177

3. Isik AT. Late onset alzheimer's disease in older people. *Clin Interv Aging*. 2010;5:307-311

4. Balin BJ, Hudson AP. Etiology and pathogenesis of late-onset alzheimer's disease. *Curr Allergy Asthma Rep*. 2014;14:417

5. Grundke-Iqbal I, Iqbal K, Quinlan M, Tung YC, Zaidi MS, Wisniewski HM. Microtubule-associated protein tau. A component of alzheimer paired helical filaments. *J Biol Chem*. 1986;261:6084-6089

6. Jellinger KA, Attems J. Prevalence and pathogenic role of cerebrovascular lesions in alzheimer disease. *J Neurol Sci*. 2005;229-230:37-41

7. Qu BX, Gong Y, Moore C, Fu M, German DC, Chang LY, Rosenberg R, Diaz-Arrastia R. Beta-amyloid auto-antibodies are reduced in alzheimer's disease. *J Neuroimmunol*. 2014;274:168-173

8. Weldon DT, Rogers SD, Ghilardi JR, Finke MP, Cleary JP, O'Hare E, Esler WP, Maggio JE, Mantyh PW. Fibrillar beta-amyloid induces microglial phagocytosis, expression of inducible nitric oxide synthase, and loss of a select population of neurons in the rat cns in vivo. *J Neurosci*. 1998;18:2161-2173

9. Jones RS, Minogue AM, Connor TJ, Lynch MA. Amyloid-beta-induced astrocytic phagocytosis is mediated by cd36, cd47 and rage. *J Neuroimmune Pharmacol*. 2013;8:301-311

10. Caccamo A, Oddo S, Sugarman MC, Akbari Y, LaFerla FM. Age- and region-dependent alterations in abeta-degrading enzymes: Implications for abeta-induced disorders. *Neurobiol Aging*. 2005;26:645-654

11. Weller RO, Massey A, Kuo YM, Roher AE. Cerebral amyloid angiopathy: Accumulation of a beta in interstitial fluid drainage pathways in alzheimer's disease. *Ann N Y Acad Sci*. 2000;903:110-117

12. Yates PA, Sirisriro R, Villemagne VL, Farquharson S, Masters CL, Rowe CC. Cerebral microhemorrhage and brain beta-amyloid in aging and alzheimer disease. *Neurology*. 2011;77:48-54

13. Stemer A, Ouyang B, Lee VH, Prabhakaran S. Prevalence and risk factors for multiple simultaneous intracerebral hemorrhages. *Cerebrovasc Dis*. 2010;30:302-307

14. Thal DR, Ghebremedhin E, Orantes M, Wiestler OD. Vascular pathology in alzheimer disease: Correlation of cerebral amyloid angiopathy and arteriosclerosis/lipohyalinosis with cognitive decline. *J Neuropathol Exp Neurol*. 2003;62:1287-1301

15. Attems J, Quass M, Jellinger KA, Lintner F. Topographical distribution of cerebral amyloid angiopathy and its effect on cognitive decline are influenced by alzheimer disease pathology. *J Neurol Sci*. 2007;257:49-55

16. Kalaria RN, Ballard C. Overlap between pathology of alzheimer disease and vascular dementia. *Alzheimer Dis Assoc Disord*. 1999;13 Suppl 3:S115-123

17. Winkler EA, Sagare AP, Zlokovic BV. The pericyte: A forgotten cell type with important implications for alzheimer's disease? *Brain Pathol*. 2014;24:371-386

18. Lyros E, Bakogiannis C, Liu Y, Fassbender K. Molecular links between endothelial dysfunction and neurodegeneration in alzheimer's disease. *Curr Alzheimer Res*. 2014;11:18-26

19. Lakshmikanthan S, Zieba BJ, Ge ZD, Momotani K, Zheng X, Lund H, Artamonov MV, Maas JE, Szabo A, Zhang DX, Auchampach JA, Mattson DL, Somlyo AV, Chrzanowska-Wodnicka M. Rap1b in smooth muscle and endothelium is required for maintenance of vascular tone and normal blood pressure. *Arterioscler Thromb Vasc Biol*. 2014;34:1486-1494

20. Kalaria RN, Hedera P. Differential degeneration of the cerebral microvasculature in alzheimer's disease. *Neuroreport*. 1995;6:477-480

21. Yamashita K, Miyakawa T, Katsuragi S. Vascular changes in the brains with alzheimer's disease. *Jpn J Psychiatry Neurol*. 1991;45:79-84

22. Higuchi Y, Miyakawa T, Shimoji A, Katsuragi S. Ultrastructural changes of blood vessels in the cerebral cortex in alzheimer's disease. *Jpn J Psychiatry Neurol*. 1987;41:283-290

23. Sagare AP, Bell RD, Zhao Z, Ma Q, Winkler EA, Ramanathan A, Zlokovic BV. Pericyte loss influences alzheimer-like neurodegeneration in mice. *Nat Commun*. 2013;4:2932

24. Kalaria RN. Cerebrovascular degeneration is related to amyloid-beta protein deposition in alzheimer's disease. *Ann N Y Acad Sci*. 1997;826:263-271

25. Carrillo-Mora P, Luna R, Colin-Barenque L. Amyloid beta: Multiple mechanisms of toxicity and only some protective effects? *Oxid Med Cell Longev*. 2014;2014:795375

26. Iadecola C. Neurovascular regulation in the normal brain and in alzheimer's disease. *Nat Rev Neurosci*. 2004;5:347-360

27. Niwa K, Kazama K, Younkin L, Younkin SG, Carlson GA, Iadecola C. Cerebrovascular autoregulation is profoundly impaired in mice overexpressing amyloid precursor protein. *Am J Physiol Heart Circ Physiol*. 2002;283:H315-323

28. Park L, Koizumi K, El Jamal S, Zhou P, Previti ML, Van Nostrand WE, Carlson G, Iadecola C. Age-dependent neurovascular dysfunction and damage in a mouse model of cerebral amyloid angiopathy. *Stroke*. 2014;45:1815-1821

29. Niwa K, Kazama K, Younkin SG, Carlson GA, Iadecola C. Alterations in cerebral blood flow and glucose utilization in mice overexpressing the amyloid precursor protein. *Neurobiol Dis*. 2002;9:61-68

30. Zhou J, Yu JT, Wang HF, Meng XF, Tan CC, Wang J, Wang C, Tan L. Association between stroke and alzheimer's disease: Systematic review and meta-analysis. *J Alzheimers Dis*. 2015;43:479-489

31. Beauchet O, Celle S, Roche F, Bartha R, Montero-Odasso M, Allali G, Annweiler C. Blood pressure levels and brain volume reduction: A systematic review and meta-analysis. *J Hypertens*. 2013;31:1502-1516

32. Forette F, Seux ML, Staessen JA, Thijs L, Birkenhager WH, Babarskiene MR, Babeanu S, Bossini A, Gil-Extremera B, Girerd X, Laks T, Lilov E, Moisseyev V, Tuomilehto J, Vanhanen H, Webster J, Yodfat Y, Fagard R. Prevention of dementia in randomised double-blind placebo-controlled systolic hypertension in europe (syst-eur) trial. *Lancet*. 1998;352:1347-1351

33. Liu J, Liu S, Tanabe C, Maeda T, Zou K, Komano H. Differential effects of angiotensin ii receptor blockers on abeta generation. *Neurosci Lett*. 2014;567:51-56

34. Joas E, Backman K, Gustafson D, Ostling S, Waern M, Guo X, Skoog I. Blood pressure trajectories from midlife to late life in relation to dementia in women followed for 37 years. *Hypertension*. 2012;59:796-801

35. Guo Z, Viitanen M, Fratiglioni L, Winblad B. Low blood pressure and dementia in elderly people: The kungsholmen project. *BMJ*. 1996;312:805-808

36. Townsend KP, Obregon D, Quadros A, Patel N, Volmar C, Paris D, Mullan M. Proinflammatory and vasoactive effects of abeta in the cerebrovasculature. *Ann N Y Acad Sci*. 2002;977:65-76

37. Carnevale D, Mascio G, D'Andrea I, Fardella V, Bell RD, Branchi I, Pallante F, Zlokovic B, Yan SS, Lembo G. Hypertension induces brain beta-amyloid accumulation, cognitive impairment, and memory deterioration through activation of receptor for advanced glycation end products in brain vasculature. *Hypertension*. 2012;60:188-197

38. Walker D, Lue LF, Paul G, Patel A, Sabbagh MN. Receptor for advanced glycation endproduct modulators: A new therapeutic target in alzheimer's disease. *Expert Opin Investig Drugs*. 2015;24:393-399

39. Paris D, Humphrey J, Quadros A, Patel N, Crescentini R, Crawford F, Mullan M. Vasoactive effects of a beta in isolated human cerebrovessels and in a transgenic mouse model of alzheimer's disease: Role of inflammation. *Neurol Res*. 2003;25:642-651

40. Benbrook DM, Long A. Integration of autophagy, proteasomal degradation, unfolded protein response and apoptosis. *Exp Oncol*. 2012;34:286-297

41. Rajawat YS, Hilioti Z, Bossis I. Aging: Central role for autophagy and the lysosomal degradative system. *Ageing Res Rev*. 2009;8:199-213

42. Boland B, Kumar A, Lee S, Platt FM, Wegiel J, Yu WH, Nixon RA. Autophagy induction and autophagosome clearance in neurons: Relationship to autophagic pathology in alzheimer's disease. *J Neurosci*. 2008;28:6926-6937

43. Salminen A, Kaarniranta K, Kauppinen A, Ojala J, Haapasalo A, Soininen H, Hiltunen M. Impaired autophagy and app processing in alzheimer's disease: The potential role of beclin 1 interactome. *Prog Neurobiol*. 2013;106-107:33-54

44. Nilsson P, Loganathan K, Sekiguchi M, Matsuba Y, Hui K, Tsubuki S, Tanaka M, Iwata N, Saito T, Saido TC. Abeta secretion and plaque formation depend on autophagy. *Cell Rep*. 2013;5:61-69

45. Guglielmotto M, Monteleone D, Piras A, Valsecchi V, Tropiano M, Ariano S, Fornaro M, Vercelli A, Puyal J, Arancio O, Tabaton M, Tamagno E. Abeta1-42 monomers or oligomers have different effects on autophagy and apoptosis. *Autophagy*. 2014;10:1827-1843

46. Nixon RA, Wegiel J, Kumar A, Yu WH, Peterhoff C, Cataldo A, Cuervo AM. Extensive involvement of autophagy in alzheimer disease: An immuno-electron microscopy study. *J Neuropathol Exp Neurol*. 2005;64:113-122

47. Nixon RA. Autophagy, amyloidogenesis and alzheimer disease. *J Cell Sci*. 2007;120:4081-4091

48. Masliah E, Sisk A, Mallory M, Mucke L, Schenk D, Games D. Comparison of neurodegenerative pathology in transgenic mice overexpressing v717f beta-amyloid precursor protein and alzheimer's disease. *J Neurosci*. 1996;16:5795-5811

49. Elder GA, Gama Sosa MA, De Gasperi R. Transgenic mouse models of alzheimer's disease. *Mt Sinai J Med*. 2010;77:69-81

50. Davis J, Xu F, Deane R, Romanov G, Previti ML, Zeigler K, Zlokovic BV, Van Nostrand WE. Early-onset and robust cerebral microvascular accumulation of amyloid beta-protein in transgenic mice expressing low levels of a vasculotropic dutch/iowa mutant form of amyloid beta-protein precursor. *J Biol Chem*. 2004;279:20296-20306

51. Miao J, Vitek MP, Xu F, Previti ML, Davis J, Van Nostrand WE. Reducing cerebral microvascular amyloid-beta protein deposition diminishes regional neuroinflammation in vasculotropic mutant amyloid precursor protein transgenic mice. *J Neurosci*. 2005;25:6271-6277

52. Xu F, Grande AM, Robinson JK, Previti ML, Vasek M, Davis J, Van Nostrand WE. Early-onset subicular microvascular amyloid and neuroinflammation correlate with behavioral deficits in vasculotropic mutant amyloid beta-protein precursor transgenic mice. *Neuroscience*. 2007;146:98-107

53. Morishima-Kawashima M. Molecular mechanism of the intramembrane cleavage of the beta-carboxyl terminal fragment of amyloid precursor protein by gamma-secretase. *Front Physiol*. 2014;5:463

54. Iwatsubo T, Odaka A, Suzuki N, Mizusawa H, Nukina N, Ihara Y. Visualization of a beta 42(43) and a beta 40 in senile plaques with end-specific a beta monoclonals: Evidence that an initially deposited species is a beta 42(43). *Neuron*. 1994;13:45-53

55. Kuperstein I, Broersen K, Benilova I, Rozenski J, Jonckheere W, Debulpaep M, Vandersteen A, Segers-Nolten I, Van Der Werf K, Subramaniam V, Braeken D, Callewaert G, Bartic C, D'Hooge R, Martins IC, Rousseau F, Schymkowitz J, De Strooper B. Neurotoxicity of alzheimer's disease abeta peptides is induced by small changes in the abeta42 to abeta40 ratio. *EMBO J*. 2010;29:3408-3420

56. Swonger AK, Rech RH. Serotonergic and cholinergic involvement in habituation of activity and spontaneous alternation of rats in a y maze. *J Comp Physiol Psychol*. 1972;81:509-522

57. Barnes CA, Eppich C, Rao G. Selective improvement of aged rat short-term spatial memory by 3,4-diaminopyridine. *Neurobiol Aging*. 1989;10:337-341

58. Haroutunian V, Riccio DC. Effect of arousal conditions during reinstatement treatment upon learned fear in young rats. *Dev Psychobiol*. 1977;10:25-32

59. Porsolt RD, Bertin A, Jalfre M. Behavioral despair in mice: A primary screening test for antidepressants. *Arch Int Pharmacodyn Ther*. 1977;229:327-336

60. McDonald KL, Morphew M, Verkade P, Muller-Reichert T. Recent advances in high-pressure freezing: Equipment- and specimen-loading methods. *Methods Mol Biol*. 2007;369:143-173

61. Villacampa N, Almolda B, Gonzalez B, Castellano B. Tomato lectin histochemistry for microglial visualization. *Methods Mol Biol*. 2013;1041:261-279

62. Rowell JF, Ruff AL, Guarnieri FG, Staveley-O'Carroll K, Lin X, Tang J, August JT, Siliciano RF. Lysosome-associated membrane protein-1-mediated targeting of the hiv-1 envelope protein to an endosomal/lysosomal compartment enhances its presentation to mhc class ii-restricted t cells. *J Immunol*. 1995;155:1818-1828

63. Zurita E, Chagoyen M, Cantero M, Alonso R, Gonzalez-Neira A, Lopez-Jimenez A, Lopez-Moreno JA, Landel CP, Benitez J, Pazos F, Montoliu L. Genetic polymorphisms among c57bl/6 mouse inbred strains. *Transgenic Res*. 2011;20:481-489

64. Simon MM, Greenaway S, White JK, Fuchs H, Gailus-Durner V, Wells S, Sorg T, Wong K, Bedu E, Cartwright EJ, Dacquin R, Djebali S, Estabel J, Graw J, Ingham NJ, Jackson IJ, Lengeling A, Mandillo S, Marvel J, Meziane H, Preitner F, Puk O, Roux M, Adams DJ, Atkins S, Ayadi A, Becker L, Blake A, Brooker D, Cater H, Champy MF, Combe R, Danecek P, di Fenza A, Gates H, Gerdin AK, Golini E, Hancock JM, Hans W, Holter SM, Hough T, Jurdic P, Keane TM, Morgan H, Muller W, Neff F, Nicholson G, Pasche B, Roberson LA, Rozman J, Sanderson M, Santos L, Selloum M, Shannon C, Southwell A, Tocchini-Valentini GP, Vancollie VE, Westerberg H, Wurst W, Zi M, Yalcin B, Ramirez-Solis R, Steel KP, Mallon AM, de Angelis MH, Herault Y, Brown SD. A comparative phenotypic and genomic analysis of c57bl/6j and c57bl/6n mouse strains. *Genome Biol*. 2013;14:R82

65. Condorelli G, Morisco C, Stassi G, Notte A, Farina F, Sgaramella G, de Rienzo A, Roncarati R, Trimarco B, Lembo G. Increased cardiomyocyte apoptosis and changes in proapoptotic and antiapoptotic genes bax and bcl-2 during left ventricular adaptations to chronic pressure overload in the rat. *Circulation*. 1999;99:3071-3078

66. Kwak C, Lee SH, Kaang BK. Social isolation selectively increases anxiety in mice without affecting depression-like behavior. *Korean J Physiol Pharmacol*. 2009;13:357-360

67. Huang H, Wang L, Cao M, Marshall C, Gao J, Xiao N, Hu G, Xiao M. Isolation housing exacerbates alzheimer's disease-like pathophysiology in aged app/ps1 mice. *Int J Neuropsychopharmacol*. 2015

68. Huang HJ, Liang KC, Ke HC, Chang YY, Hsieh-Li HM. Long-term social isolation exacerbates the impairment of spatial working memory in app/ps1 transgenic mice. *Brain Res*. 2011;1371:150-160

69. Anderson JM, Gimbrone MA, Jr., Alexander RW. Angiotensin ii stimulates phosphorylation of the myosin light chain in cultured vascular smooth muscle cells. *J Biol Chem*. 1981;256:4693-4696

70. Valles P, Wysocki J, Batlle D. Angiotensin ii and renal tubular ion transport. *ScientificWorldJournal*. 2005;5:680-690

71. Antonaccio MJ, Cushman DW. Drugs inhibiting the renin - angiotensin system. *Fed Proc*. 1981;40:2275-2284

72. Hunseler C, Paneitz A, Friedrich D, Lindner U, Oberthuer A, Korber F, Schmitt K, Welzing L, Muller A, Herkenrath P, Hoppe B, Gortner L, Roth B, Kattner E, Schaible T. Angiotensin ii receptor blocker induced fetopathy: 7 cases. *Klin Padiatr*. 2011;223:10-14

73. Wakisaka Y, Chu Y, Miller JD, Rosenberg GA, Heistad DD. Spontaneous intracerebral hemorrhage during acute and chronic hypertension in mice. *J Cereb Blood Flow Metab*. 2010;30:56-69

74. Yang Y, Yu T, Lian YJ, Ma R, Yang S, Cho JY. Nitric oxide synthase inhibitors: A review of patents from 2011 to the present. *Expert Opin Ther Pat*. 2015;25:49-68

75. Barinaga M. Is nitric oxide the "retrograde messenger"? *Science*. 1991;254:1296-1297

76. Feldstein CA. Association between chronic blood pressure changes and development of alzheimer's disease. *J Alzheimers Dis*. 2012;32:753-763

77. Shah NS, Vidal JS, Masaki K, Petrovitch H, Ross GW, Tilley C, DeMattos RB, Tracy RP, White LR, Launer LJ. Midlife blood pressure, plasma beta-amyloid, and the risk for alzheimer disease: The honolulu asia aging study. *Hypertension*. 2012;59:780-786

78. Johnstone M, Gearing AJ, Miller KM. A central role for astrocytes in the inflammatory response to beta-amyloid; chemokines, cytokines and reactive oxygen species are produced. *J Neuroimmunol*. 1999;93:182-193

79. Claudio L. Ultrastructural features of the blood-brain barrier in biopsy tissue from alzheimer's disease patients. *Acta Neuropathol*. 1996;91:6-14

80. Leonardi A, Gandolfo C, Caponnetto C, Arata L, Vecchia R. The integrity of the blood-brain barrier in alzheimer's type and multi-infarct dementia evaluated by the study of albumin and igg in serum and cerebrospinal fluid. *J Neurol Sci*. 1985;67:253-261

81. Wisniewski HM, Kozlowski PB. Evidence for blood-brain barrier changes in senile dementia of the alzheimer type (sdat). *Ann N Y Acad Sci*. 1982;396:119-129

82. Brightman MW, Reese TS. Junctions between intimately apposed cell membranes in the vertebrate brain. *J Cell Biol*. 1969;40:648-677

83. Dermietzel R, Leibstein AG. The microvascular pattern and perivascular linings of the area postrema. A combined freeze-etching and ultrathin section study. *Cell Tissue Res*. 1978;186:97-110

84. Szpak GM, Lewandowska E, Wierzba-Bobrowicz T, Bertrand E, Pasennik E, Mendel T, Stepien T, Leszczynska A, Rafalowska J. Small cerebral vessel disease in familial amyloid and non-amyloid angiopathies: Fad-ps-1 (p117l) mutation and cadasil. Immunohistochemical and ultrastructural studies. *Folia Neuropathol*. 2007;45:192-204

85. German DC, Eisch AJ. Mouse models of alzheimer's disease: Insight into treatment. *Rev Neurosci*. 2004;15:353-369

86. Zahs KR, Ashe KH. 'Too much good news' - are alzheimer mouse models trying to tell us how to prevent, not cure, alzheimer's disease? *Trends Neurosci*. 2010;33:381-389

87. Novikoff AB, Beaufay H, De Duve C. Electron microscopy of lysosomerich fractions from rat liver. *J Biophys Biochem Cytol*. 1956;2:179-184

88. Cataldo AM, Petanceska S, Terio NB, Peterhoff CM, Durham R, Mercken M, Mehta PD, Buxbaum J, Haroutunian V, Nixon RA. Abeta localization in abnormal endosomes: Association with earliest abeta elevations in ad and down syndrome. *Neurobiol Aging*. 2004;25:1263-1272

89. Silva EO, Diniz JA, Lainson R, DaMatta RA, de Souza W. Ultrastructural aspects of fallisia effusa (haemosporina: Garniidae) in thrombocytes of the lizard neusticurus bicarinatus (reptilia: Teiidae). *Protist*. 2005;156:35-43

90. Kraft AW, Hu X, Yoon H, Yan P, Xiao Q, Wang Y, Gil SC, Brown J, Wilhelmsson U, Restivo JL, Cirrito JR, Holtzman DM, Kim J, Pekny M, Lee JM. Attenuating astrocyte activation accelerates plaque pathogenesis in app/ps1 mice. *FASEB J*. 2013;27:187-198

91. Nixon RA, Cataldo AM. Lysosomal system pathways: Genes to neurodegeneration in alzheimer's disease. *J Alzheimers Dis*. 2006;9:277-289

92. Tuma P, Hubbard AL. Transcytosis: Crossing cellular barriers. *Physiol Rev*. 2003;83:871-932

93. Laczo J, Vlcek K, Vyhnalek M, Vajnerova O, Ort M, Holmerova I, Tolar M, Andel R, Bojar M, Hort J. Spatial navigation testing discriminates two types of amnestic mild cognitive impairment. *Behav Brain Res*. 2009;202:252-259

94. Gorchetchnikov A, Grossberg S. Space, time and learning in the hippocampus: How fine spatial and temporal scales are expanded into population codes for behavioral control. *Neural Netw*. 2007;20:182-193

95. George S, Ronnback A, Gouras GK, Petit GH, Grueninger F, Winblad B, Graff C, Brundin P. Lesion of the subiculum reduces the spread of amyloid beta pathology to interconnected brain regions in a mouse model of alzheimer's disease. *Acta Neuropathol Commun*. 2014;2:17

96. Malmsten L, Vijayaraghavan S, Hovatta O, Marutle A, Darreh-Shori T. Fibrillar beta-amyloid 1-42 alters cytokine secretion, cholinergic signalling and neuronal differentiation. *J Cell Mol Med*. 2014;18:1874-1888

97. Lopez-Gonzalez I, Schluter A, Aso E, Garcia-Esparcia P, Ansoleaga B, F LL, Carmona M, Moreno J, Fuso A, Portero-Otin M, Pamplona R, Pujol A, Ferrer I. Neuroinflammatory signals in alzheimer disease and app/ps1 transgenic mice: Correlations with plaques, tangles, and oligomeric species. *J Neuropathol Exp Neurol*. 2015;74:319-344

98. Calcinaghi N, Wyss MT, Jolivet R, Singh A, Keller AL, Winnik S, Fritschy JM, Buck A, Matter CM, Weber B. Multimodal imaging in rats reveals impaired neurovascular coupling in sustained hypertension. *Stroke*. 2013;44:1957-1964

99. Heistad DD, Baumbach GL. Cerebral vascular changes during chronic hypertension: Good guys and bad guys. *J Hypertens Suppl*. 1992;10:S71-75

100. Romero JR, Preis SR, Beiser A, DeCarli C, Viswanathan A, Martinez-Ramirez S, Kase CS, Wolf PA, Seshadri S. Risk factors, stroke prevention treatments, and prevalence of cerebral microbleeds in the framingham heart study. *Stroke*. 2014;45:1492-1494

101. van Swieten JC, Geyskes GG, Derix MM, Peeck BM, Ramos LM, van Latum JC, van Gijn J. Hypertension in the elderly is associated with white matter lesions and cognitive decline. *Ann Neurol*. 1991;30:825-830

102. Klarenbeek P, van Oostenbrugge RJ, Rouhl RP, Knottnerus IL, Staals J. Higher ambulatory blood pressure relates to new cerebral microbleeds: 2-year follow-up study in lacunar stroke patients. *Stroke*. 2013;44:978-983

103. Kaiser D, Weise G, Moller K, Scheibe J, Posel C, Baasch S, Gawlitza M, Lobsien D, Diederich K, Minnerup J, Kranz A, Boltze J, Wagner DC. Spontaneous white matter damage, cognitive decline and neuroinflammation in middle-aged hypertensive rats: An animal model of early-stage cerebral small vessel disease. *Acta Neuropathol Commun*. 2014;2:169

104. Benedictus MR, Goos JD, Binnewijzend MA, Muller M, Barkhof F, Scheltens P, Prins ND, van der Flier WM. Specific risk factors for microbleeds and white matter hyperintensities in alzheimer's disease. *Neurobiol Aging*. 2013;34:2488-2494

105. Arai H, Kobayashi K, Ikeda K, Nagao Y, Ogihara R, Kosaka K. A computed tomography study of alzheimer's disease. *J Neurol*. 1983;229:69-77

106. Claassen JA, Diaz-Arrastia R, Martin-Cook K, Levine BD, Zhang R. Altered cerebral hemodynamics in early alzheimer disease: A pilot study using transcranial doppler. *J Alzheimers Dis*. 2009;17:621-629

107. Nakajima K, Kohsaka S. Microglia: Activation and their significance in the central nervous system. *J Biochem*. 2001;130:169-175

108. Attems J, Jellinger K, Thal DR, Van Nostrand W. Review: Sporadic cerebral amyloid angiopathy. *Neuropathol Appl Neurobiol*. 2011;37:75-93

109. Xu J, Chen S, Ahmed SH, Chen H, Ku G, Goldberg MP, Hsu CY. Amyloid-beta peptides are cytotoxic to oligodendrocytes. *J Neurosci*. 2001;21:RC118

110. Folin M, Baiguera S, Tommasini M, Guidolin D, Conconi MT, De Carlo E, Nussdorfer GG, Parnigotto PP. Effects of beta-amyloid on rat neuromicrovascular endothelial cells cultured in vitro. *Int J Mol Med*. 2005;15:929-935

111. Liu ML, Hong ST. Early phase of amyloid beta42-induced cytotoxicity in neuronal cells is associated with vacuole formation and enhancement of exocytosis. *Exp Mol Med*. 2005;37:559-566

112. Cifuentes D, Poittevin M, Dere E, Broqueres-You D, Bonnin P, Benessiano J, Pocard M, Mariani J, Kubis N, Merkulova-Rainon T, Levy BI. Hypertension accelerates the progression of alzheimer-like pathology in a mouse model of the disease. *Hypertension*. 2014

113. Eriksen JL, Janus CG. Plaques, tangles, and memory loss in mouse models of neurodegeneration. *Behav Genet*. 2007;37:79-100

114. Janus C. Search strategies used by app transgenic mice during navigation in the morris water maze. *Learn Mem*. 2004;11:337-346

115. Lovasic L, Bauschke H, Janus C. Working memory impairment in a transgenic amyloid precursor protein tgcrnd8 mouse model of alzheimer's disease. *Genes Brain Behav*. 2005;4:197-208

116. Lee S, Sato Y, Nixon RA. Lysosomal proteolysis inhibition selectively disrupts axonal transport of degradative organelles and causes an alzheimer's-like axonal dystrophy. *J Neurosci*. 2011;31:7817-7830

117. Yla-Anttila P, Vihinen H, Jokitalo E, Eskelinen EL. Monitoring autophagy by electron microscopy in mammalian cells. *Methods Enzymol*. 2009;452:143-164

118. Wang ZV, Rothermel BA, Hill JA. Autophagy in hypertensive heart disease. *J Biol Chem*. 2010;285:8509-8514

119. Jiang T, Gao L, Zhu XC, Yu JT, Shi JQ, Tan MS, Lu J, Tan L, Zhang YD. Angiotensin-(1-7) inhibits autophagy in the brain of spontaneously hypertensive rats. *Pharmacol Res*. 2013;71:61-68

120. Jordao JF, Thevenot E, Markham-Coultes K, Scarcelli T, Weng YQ, Xhima K, O'Reilly M, Huang Y, McLaurin J, Hynynen K, Aubert I. Amyloid-beta plaque reduction, endogenous antibody delivery and glial activation by brain-targeted, transcranial focused ultrasound. *Exp Neurol*. 2013;248:16-29

121. Westergaard E, Go G, Klatzo I, Spatz M. Increased permeability of cerebral vessels to horseradish peroxidase induced by ischemia in mongolian gerbils. *Acta Neuropathol*. 1976;35:307-325

122. Najjar S, Pearlman DM. Neuroinflammation and white matter pathology in schizophrenia: Systematic review. *Schizophr Res*. 2015;161:102-112

123. Jukkola P, Guerrero T, Gray V, Gu C. Astrocytes differentially respond to inflammatory autoimmune insults and imbalances of neural activity. *Acta Neuropathol Commun*. 2013;1:70

124. Carmignoto G, Gomez-Gonzalo M. The contribution of astrocyte signalling to neurovascular coupling. *Brain Res Rev*. 2010;63:138-148

125. Gandhi GK, Cruz NF, Ball KK, Dienel GA. Astrocytes are poised for lactate trafficking and release from activated brain and for supply of glucose to neurons. *J Neurochem*. 2009;111:522-536

126. Pike CJ. Estrogen modulates neuronal bcl-xl expression and beta-amyloid-induced apoptosis: Relevance to alzheimer's disease. *J Neurochem*. 1999;72:1552-1563

127. Austen BM, Paleologou KE, Ali SA, Qureshi MM, Allsop D, El-Agnaf OM. Designing peptide inhibitors for oligomerization and toxicity of alzheimer's beta-amyloid peptide. *Biochemistry*. 2008;47:1984-1992

128. Zhou L, Chan KH, Chu LW, Kwan JS, Song YQ, Chen LH, Ho PW, Cheng OY, Ho JW, Lam KS. Plasma amyloid-beta oligomers level is a biomarker for alzheimer's disease diagnosis. *Biochem Biophys Res Commun*. 2012;423:697-702

129. Li J, Kanekiyo T, Shinohara M, Zhang Y, LaDu MJ, Xu H, Bu G. Differential regulation of amyloid-beta endocytic trafficking and lysosomal degradation by apolipoprotein e isoforms. *J Biol Chem*. 2012;287:44593-44601

130. Zhu L, Fratiglioni L, Guo Z, Basun H, Corder EH, Winblad B, Viitanen M. Incidence of dementia in relation to stroke and the apolipoprotein e epsilon4 allele in the very old. Findings from a population-based longitudinal study. *Stroke*. 2000;31:53-60

131. de Frias CM, Schaie KW, Willis SL. Hypertension moderates the effect of apoe on 21-year cognitive trajectories. *Psychol Aging*. 2014;29:431-439